https://doi.org/10.57634/RCR5071

2D nanocrystals of metal oxides and hydroxides with nanosheet/nanoflake morphology in biomedicine, energy and chemistry †

Valeri P. Tolstoy, Larisa B. Gulina, Aleksandra A. Meleshko

Institute of Chemistry, Saint Petersburg State University, Universitetskii prosp. 26, Peterhof, 198504 Saint Petersburg, Russian Federation

The review addresses the structural and chemical features of 2D nanocrystals of metal oxide and hydroxides in the form of nanosheets (nanoflakes), basic methods for their synthesis and their applications. Nanocrystals with this type of morphology are characterized by high anisotropy of properties, exceptionally high proportion of surface atoms capable of interacting with the environment, relatively large number of defects in the structure, and a special quantum confined electronic subsystem. Nanosheets can be functionalized with various low-molecular-weight reagents. These features account for the unique physicochemical properties of metal oxide and hydroxide nanosheets and largely determine their practical significance. Consideration of issues of the preparative chemistry of these nanocrystals is focused on soft chemistry methods using solutions of metal salts, in particular chemical precipitation (including methods using templates), successive ionic layer deposition and reactions on the surface of bulk metals and at the solution/gas interface. Special attention is paid to the conditions of synthesis of nanosheet arrays, a sort of packages of single particles arranged in an ordered fashion on the substrate and oriented relative to the substrate. The applications of metal oxide and hydroxide nanosheets are considered. It is demonstrated that they are of considerable interest for applications in biomedicine, electrochemical energy engineering, chemical sensorics and photo- and electrocatalysis as parts of various functional nanomaterials with a unique set of physicochemical properties, including magnetic, electrophysical, electrochemical, optical, sorption and other properties. The bibliography includes 317 references.

Contents

1. Introduction

The so-called nanosheet (NS) morphology refers to nanosized 2D particles with thickness of a few nanometres or fractions of a nanometre and lateral size of hundreds or thousands of nanometres. This morphology leads to distortion of a planar NS geometry and accounts for some of their specific physicochemical features, which enable the design of functional nanomaterials with unique practically important properties. The interest in the synthesis and properties of these compounds has markedly increased in the last ~15 years after the appearance of the first publications devoted to graphene. During this period, a new

† In commemoration of the 300th anniversary of St Petersburg State University's founding.

Received 1 November 2022

research area has actually appeared in nanotechnology, dealing with the synthesis, properties and practical applications of NSs. It is noteworthy that previously, bulk compounds and their thin-layer structures were the major investigation objects.

Among the diversity of structures of this type, nanosheets of metal oxides and hydroxides occupy a special place. Analysis of the publications using the Scopus international database with the keywords nanosheets (nanoflakes) and oxide (hydroxide) excluding the word graphene showed that ~15 000 papers on the indicated topic have already been published. Furthermore, the numbers of publications were ~200 in 2010, 800 in 2015, 1500 in 2018 and ~2200 in 2021. Among the mentioned papers, there are more than 150 reviews, some of which appeared in top scientific journals such as *Chemical Reviews* (*e.g.*, Ref. 1), *Coordination Chemistry Reviews*,[2] *Advanced Materials*,[3,4] *Advanced Energy Materials*,[5] *Nanoscale*,[6] *Small*,[7] *Russian Chemical Reviews*[8,9] and in many other.

However, the authors of these reviews analyzed, most often, the conditions of synthesis of 2D nanocrystals by exfoliation from layered bulk crystals.[9–12] This approach is good for the indicated compounds, because it makes it possible to prepare relatively large volumes of NS suspensions. However, some drawbacks of this method also deserve mention, for example, it is inapplicable to compounds with crystal structures other than layered structure, the presence of organic impurities in the suspension and so on.

One more strategy for the preparation of NSs implies the use of chemical reactions involving low-dimensional species, mainly ions in metal salt solutions, *i.e.*, actually this is a bottom-up approach. In our opinion, this strategy is most appropriate for metal oxides and hydroxides, as these compounds can be obtained rather easily using solutions of reactants and conditions of soft chemistry. This approach is described in a number of reviews (*e.g.*, Refs 13, 14) that address, most often, specific aspects of the synthesis related to the manufacture of a narrow range of functional nanomaterials. As exceptions, note publications[15,16] devoted to the growth of 2D nanocrystals of a broad range of compounds in solutions using complex formation and certain soft templates based on amines and carboxylic acids.

The distinctive features of the present review are systematic presentation and integration of methods for the preparation of NSs of metal oxides and hydroxides and discussion of new approaches to their synthesis, including the synthesis of NSs at the precursor solution/gaseous reactant interface[17–19] and successive ionic layer deposition.[20–28] In addition, the review includes consideration of the structural and chemical features of these NSs with exceptionally high proportion of surface atoms with respect to the volume, which gives rise to a unique combination of electron-donor and -acceptor properties. The models and mechanisms of the formation of NS type nanocrystals in solutions and conditions of the formation of ordered NS arrays are discussed. It is important that arrays of this type on the surface of various substrates can be obtained only using the considered synthetic approaches with solutions of metal salts as precursors.

The last Sections describe the possible practical applications of this type of nanocrystals, in particular as parts of highly efficient electrodes for chemical current sources, as electro- and photoelectrocatalysts of water decomposition, highly sensitive electrochemical and conductometric sensors, sorbents for treatment of environmental objects, bactericidal materials, drug delivery systems, *etc.*

2. 2D nanomaterials containing metal oxide and hydroxide nanosheets: morphological diversity and classification

The nanosheet morphology is present for compounds consisting of sets of nanocrystals (or amorphous nanoparticles) with a thickness at about a few lattice spacings (for amorphous compounds, a few interatomic distances) with lateral dimensions of hundreds to thousands of nanometres. Nanosheets either have or do not have a decoration at the edges corresponding to the type of their crystal structure. In the latter case, most authors consider the so-called nanoflake morphology. Under real conditions, nanosheets usually change the initial planar geometry and exist as intricately curved or crumpled figures.

Before considering details of the NS synthesis, we would like to note that the graphene boom brought the understanding that the number of such compounds is very high.[29] Indeed, whereas 20 years ago bulk crystals and thin films on various substrates were mainly studied, currently quite a few samples of similar composition with a new morphology and evidently with a new set of practically useful properties can be designed (Fig. 1).

There are at least four types of nanosheets:

— nanosheets isotropic in the composition and structure;

— anisotropic (*e.g.* in the composition) nanosheets, which are actually 2D nanocomposites;

— perforated nanosheets with holes of different size and different density of arrangement on the NS plane;

— functionalized nanosheets, *i.e.*, NS surface-modified by various compounds.

The last mentioned type of materials can be subdivided into several groups characterized by functionalization of two planar sides of the nanosheet with the same or different compounds, or functionalization of only one side or edges of the nanosheet. Furthermore, both composite and perforated NS can also be functionalized. This is obviously also indicative of the exceptional diversity of these compounds.

Each of the NS types listed above can form arrays consisting of a set of nanosheets. These arrays can be formed in suspensions in various solvents, exist independently as powders of separate microparticles or be attached to the surface of a substrate. In the first approximation, several types of such arrays can be distinguished. The NS

V.P.Tolstoy. Doctor of Science (Chemistry), Professor at the Department of Solid State Chemistry, SPbSU.
E-mail: v.tolstoy@spbu.ru
Current research interests: development of new synthetic routes to inorganic compounds under soft chemistry conditions, optical spectroscopy of nanoscale compounds, electrochemical energy engineering.
L.B.Gulina. Doctor of Science (Chemistry), Senior Researcher at the same Department.
E-mail: l.gulina@spbu.ru
Current research interests: specific features of chemical reactions at the gas/liquid interface and production of practically important nanomaterials by these reactions.
A.A.Meleshko. PhD, Researcher at the same Department.
E-mail: alya_him@mail.ru
Current research interests: preparation of new biomedical nanomaterials under soft chemistry conditions.

Translation: S.P.Svitanko

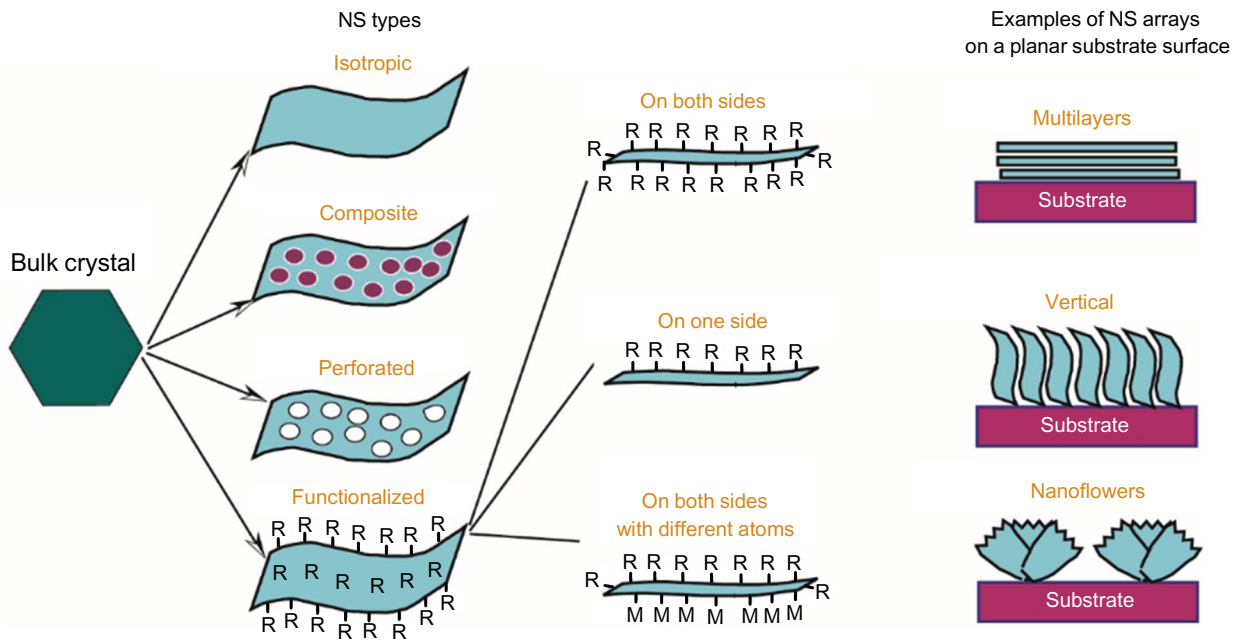

Figure 1. Main types of nanosheets and their arrays prepared on the basic of a bulk compound. M and R are atoms and chemical groups, respectively.

arrays deposited on a substrate can be classified into arrays located on the surface of nanofibres or nanorods and those located on a planar surface; furthermore, the nanosheets can be positioned along the substrate or at various angles to the substrate. In particular, these arrays can represent sets of so-called nanoflowers of various shapes with nanosheet petals, *etc*.

In this respect, it is possible to distinguish several organization levels of NSs in space; even a tentative consideration reveals at least three levels. For example, ribbons several micrometres wide consisting of NSs oriented perpendicular to the substrate can be formed, while these ribbons can be arranged to form various ordered structures such as honeycombs and other.

Thus, preliminary analysis of the formation of hypothetically possible structures containing nanosheets of metal oxides and hydroxides attests to their abundance and diversity; together with unique practically important properties of these structures, this obviously stimulates the development of preparative inorganic chemistry and solid state chemistry. Detailed description of many aspects of the synthesis of these compounds is beyond the scope of this review; therefore, we will restrict ourselves to the discussion of studies addressing the synthesis and properties of isotropic metal oxide and hydroxide nanosheets as well as to a more detailed analysis of the most recent results.

3. Structural and chemical features of 2D nanocrystals of metal oxides and hydroxides with nanosheet morphology

Unlike bulk crystals, ultrathin metal oxide nanosheets have an exceptionally large specific surface area. Indeed, a single crystal cube with a volume of 1 cm^3 has $S = 6$ cm^2. When this cube is split into separate sheets not more than 2 nm thick, the calculated surface area is $S = 10^7$ cm^2. However, this does not mean that the chemical reactivity of the material will increase by seven orders of magnitude. The two-dimensional material with exceptionally high ratio of the number of surface atoms to the number of bulk atoms is actually (by almost 100%) transformed into a specific chemical state in which nanoscale effects typical of this state are manifested.

The nanoscale thickness and extension in one direction account for the anisotropy of NSs, that is, the dependence of physical and chemical properties on the arrangement in space. Unlike bulk analogues, NSs are flexible, optically transparent and, in certain directions, they retain the mechanical strength.[30] The state of atoms on the NS surface fundamentally changes compared to their state in the bulk: they become exposed and can serve as highly reactive centres for many reactions. In addition, the NS base planes and facets are formed by atoms in different coordination states and, hence, they can differ in chemical reactivity. The whole set of above factors give rise to a considerable anisotropy of NS properties, which depend on the direction in space.

Nanosheets can carry an electrical charge; this facilitates their organization into arrays (Fig. 2 *a*,*b*). The atomic structure of the surface of nanosheets formed by transition metal oxides involves oxygen and/or cationic vacancies. It is known that these vacancies determine the unique electronic structure of NSs.[34,35] For example, Wang *et al.*[32] studied the effect of concentration of O and Mn vacancies on the electronic structure of MnO_2 nanosheets. It was found that O2p and Mn3d atomic orbitals around a Mn vacancy are hybridized (Fig. 2 *c*–*f*). The calculations showed that the electronic structure of a defect-free layer of MnO_6 octahedra corresponds to the state of a typical semiconductor, while the electronic structure of the layer with vacancies can be described as a half-metal.

A similar change in the electronic structure induced by the appearance of free dangling bonds at surface atoms was detected in the study of γ-CoOOH nanosheets.[33] A structural distortion of the CoO_{6-x} octahedron causes a change in the occupancy of 3d levels of cobalt atoms giving rise to

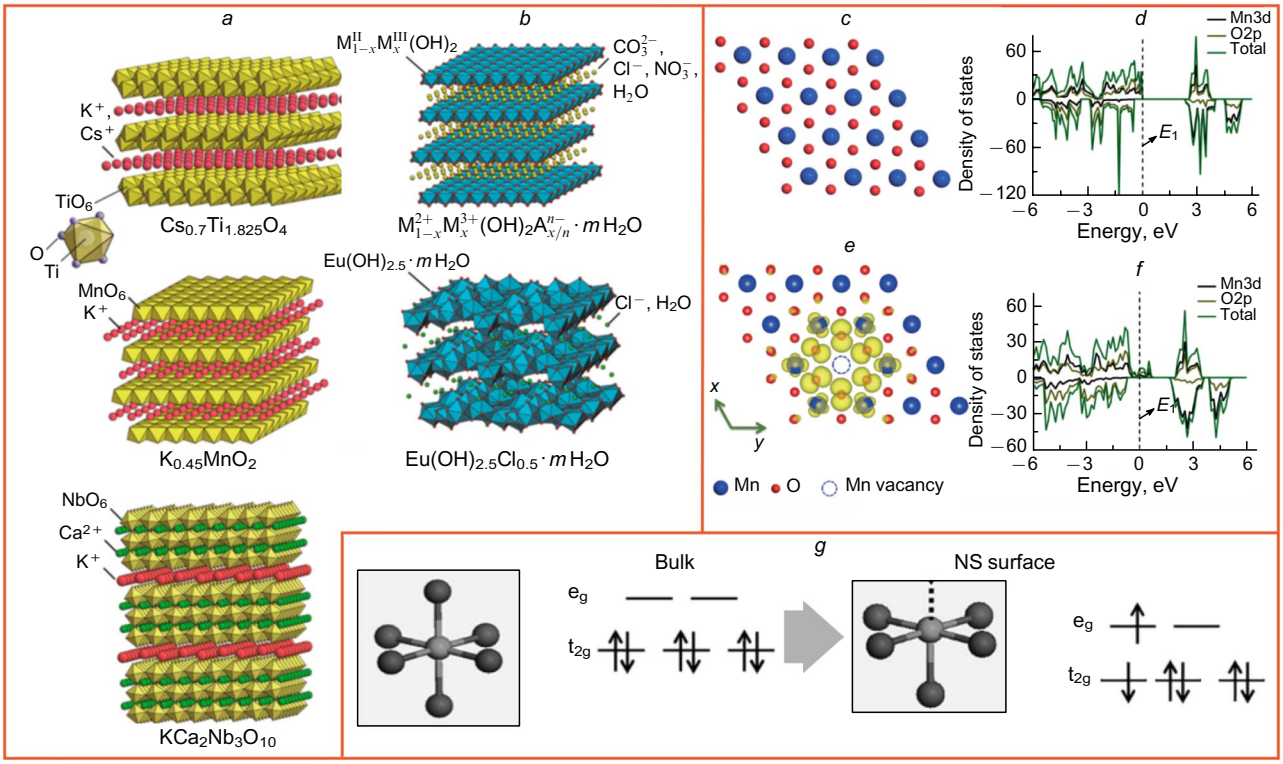

Figure 2. Illustration of structural and chemical features of 2D nanocrystals of metal oxides and hydroxides with NS morphology. (*a*) metal oxides with negatively charged NS surface: $Cs_{0.7}Ti_{1.825}O_4$ (or $K_{0.8}Ti_{1.73}Li_{0.27}O_4$), $K_{0.45}MnO_2$, $KCa_2Nb_3O_{10}$;[31] (*b*) hydroxides with positively charged NS surface: $M^{2+}_{1-x}M^{3+}_x(OH)_2A^{n-}_{x/n}\cdot m\,H_2O$ (A = CO_3^{2-}, Cl^-, NO_3^-) and $Eu(OH)_{2.5}\cdot m\,H_2O\cdot Cl^-_{0.5}$;[31] (*c*) defect-free layer of (4 × 4) MnO_6 octahedra; (*d*) calculated density of states for the defect-free layer of MnO_6 octahedra; (*e*) change in the electron density on the layer of (4 × 4) MnO_6 octahedra with a Mn vacancy;[32] (*f*) results of calculations of the density of states for a layer with a Mn vacancy; (*g*) calculated density of states for γ-CoOOH on going from the bulk state to the nanosheet.[33] Figures *a*, *b* are published with permission from ACS, Fig. *c*–*g* is published with permission from Wiley.

partially occupied antibonding e_g orbitals, along with the unoccupied t_{2g} states; this results in the formation of $t_{2g}5e_g$ configuration (Fig. 2 *g*). According to *ab initio* calculations, γ-CoOOH nanosheets and the bulk material have markedly different densities of states near the Fermi level (E_F). In the case of moderately thick NSs, almost all metal ions are exposed; this leads to increasing density of states near the Fermi level and to electron population of the band gap. Thus, nanomaterials with the same composition but different dimensionality have different densities of states due to the change in the electron distribution.[6]

The atomic thickness of ZnO nanosheets induces a strong quantum confinement effect and results in a shift of the photoluminescence maximum to shorter wavelengths (3.85 eV) in comparison with the emission maximum of a bulk crystal.[36] In addition, the spectrum exhibited a broad-band luminescence in the violet and red regions associated with interband defects.

The state of atoms on the surface of ultrathin metal oxide NSs can be described resorting to X-ray photoelectron spectroscopy (XPS). Sun *et al.*[37] synthesized ultrathin nanosheets of TiO_2, ZnO, Co_3O_4, WO_3, Fe_3O_4 and MnO_2 *via* their self-assembly in micelles in solutions of reactants in the presence of amphiphilic block copolymers and surfactants based on short-chain alcohols as structuring agents followed by crystallization induced by solvothermal treatment. The electronic structure of the resulting NSs was studied by XPS. Notably, the Ti2p, Zn2p, Co2p and W4f electron binding energy peaks were shifted by 0.5–2 eV to lower values with respect to the binding energy peaks of the corresponding bulk metal oxide crystals.

It is known that the decrease in the binding energy for the surface metal atoms may be caused by the partial reduction of ions, for example Ti^{4+} to Ti^{3+}, due to the transfer of electrons from the surrounding oxygen atoms.[38] Probably the change in the chemical state of transition metal atoms or electron transfer to them from oxygen atoms is due to the crystal structure distortion, which occurs in ultrathin oxide nanosheets. In order to confirm this hypothesis, DFT (density functional theory) calculations were carried out[37] and demonstrated that metal ions in ultrathin NSs have higher electron densities, *i.e.*, they are more reduced than the metal ions in the corresponding bulk materials. This entails either a change (bond cleavage and formation) or distortion of metal–oxygen chemical bonds; this conclusion is in good agreement with the shift of binding energy peaks in the X-ray photoelectron spectra. Hence, the crystal lattice in 2D NSs is considerably distorted in comparison with internal atomic planes of bulk crystals as a result of change, formation and cleavage of additional chemical bonds, accompanied by electron density redistribution, and much less pronounced electron transfer from metal atoms to oxygen atoms. This, in turn, results in lower oxidation states of transition metal atoms. These results attest once again to the unique chemical state of the surface atoms in the ultrathin 2D nanosheets of transition metal oxides, which is responsible for their specific physicochemical properties.

The high specific surface area and crystal lattice defects account for the increased number of active sites on the surface of metal oxide and hydroxide nanosheets in comparison with that in the bulk materials and some dispersed compounds and for the significant increase in the chemical reactivity of these materials. It is important that, owing to the chemical reactivity of the surface atoms, nanosheets can be easily modified *via* functionalization and doping to generate additional active sites [39] or *via* insertion of anions and/or molecules into the interlayer space (this is widely used, for example, in the design of layered double hydroxides).[40] Actually, these features open up prospects for the control over the NS structure and redox properties; in some cases, this may considerably improve their functional characteristics.

The specific electronic structure in combination with the large number of active sites on the NS surface provide for fast electron transfer over the surface. It is important that characteristics of this process can be tuned by varying the morphology, first of all, the thickness of nanosheets. Elakkiya *et al.*,[41] who synthesized Co_3O_4, CuO, NiO and Fe_3O_4 nanosheets *via* reduction under hydrothermal conditions, demonstrated that the number and crystal structure features of atomic layers affect the electronic structure of the NSs, thus determining their reactivity towards electrochemical oxidation of glucose in an alkaline medium. Feng *et al.*[42] developed surface modification methods by chemical functionalization, intralayer doping and lattice deformation that affected the electronic structure of 2D nanomaterials with the goal of increasing their electrical conductivity.

It is noteworthy that nanosheets exhibit their unique properties both when they exist separately in solutions and when they are attached to a solid substrate for the fabrication of thin-film nanostructures. The anisotropy of the properties of two-dimensional materials can be illustrated in relation to their ionic conductivity in different directions. The conductivity in the plane of the sheet is 4–5 times higher than that in the direction perpendicular to the plane of stacked nanosheets of layered double hydroxides (LDHs).[43] This feature and the possibility of 2D ion transport are important for a variety of applications.

Unlike rigid porous 3D materials that are characterized by slow diffusion, the nature of 2D nanomaterials dictates fast ion transport along 2D channels, which can be expanded or contracted.[44] Furthermore, as shown [45] in relation to WO_3, V_2O_5 and $LiCoO_2$, the dynamics of atoms in the 2D crystal lattice of separately existing oxide NSs differs from the dynamics of atoms in the lattices of similar bulk compounds.

To summarize, we would like to note once again that high anisotropy, exposure of atoms on the NS surface towards reactions with the environment, specific electron structure and crystal lattice dynamics and the presence of relatively large number of defects account for the unique physicochemical properties of metal oxide and hydroxide NSs and largely determine their practical significance.

4. Conditions and models of formation of metal oxides and hydroxides with nanosheet morphology in reactant solutions

For the formation of a new solid phase in a homogeneous solution, appropriate conditions are required. Crystallization is usually accompanied by the following processes: dehydration of ions that form the solid phase, formation of primary crystallization centres in supersaturated solution areas, nucleation, growth of the nuclei *via* the attachment of ions from the solution, ageing of the nuclei, their subsequent association into aggregates and, finally, separation of the solid phase.[46] The appearance of particles with NS morphology in a homogeneous supersaturated solution may be promoted by the layered crystal structure, which is characteristic of some transition metal oxides and hydroxides and layered double hydroxides. The general formula of the last-mentioned compounds is $[M^{2+}_{1-x}M^{3+}_x(OH)_2]^{q+}[(A^{n-})_{q/n}\cdot y\,H_2O]$, where M^{2+} is a doubly charged metal cation, *e.g.*, Mg^{2+}, Ca^{2+}, Cu^{2+}, Mn^{2+}, Ni^{2+} and Zn^{2+}; M^{3+} is a triply charged metal cation, *e.g.*, Al^{3+}, Cr^{3+}, Fe^{3+}, Mn^{3+} and Co^{3+}; A^{n-} is an inorganic anion such as Cl^-, CO_3^{2-}, NO_3^- and SO_4^{2-}, or organic anion; and $q = x$. The positive charge $q+$ of the $[M^{2+}_{1-x}M^{3+}_x(OH)_2]$ layers is determined by the $M^{2+}:M^{3+}$ ratio and is counterbalanced by introducing a definite number of anions into the interlayer space.[47,48]

The formation of precipitates composed of NSs in solutions is affected by quite a number of factors, including the presence of surfactants, pH, the degree of supersaturation and so on. Usually these external factors influence the relative growth rate of crystal planes, which, in turn, determines the orientation of the growing nanocrystals. Some examples of synthesis of metal oxides and hydroxides with this type of morphology (Figs 3, 4), which illustrate the most typical options of the formation of such nanocrystals, are considered below.

Dong *et al.*,[49] who studied the hydrolysis of $Fe(acac)_3$, $Co(acac)_3$, $Zn(acac)_2$, $Mn(acac)_2$ and $Ni(acac)_2$ in buffer solutions, *e.g.*, in a mixture of Na_2CO_3 and NaOH, found conditions for the formation of FeOOH, CoOOH, $Ni(OH)_2$, ZnNiOH, ZnCoOH and MnFeOH nanosheets with a thickness of 2.0–2.5 nm. In the authors opinion, nanosheets were formed upon the hydrolysis of these salts and appearance of hydroxide nuclei, which then formed nanosheets (Fig. 3 *a*). The flat planes of these NSs have a high atomic density; therefore, they grow more slowly, which accounts for the radial growth of NSs.

One of the possible conditions for the radial growth is adsorption of surfactant molecules or ions on NS facets, which may result in additional blocking or generatation of new centres. In particular, while studying the preparation of ZnO nanosheets by treating a zinc metal powder with HCl, Zhang *et al.*[51] showed that adsorption of H^+ ions on the terminal oxygen atoms of each NS gives rise to OH groups, which bind Zn^{2+} ions from the solution; this initiates particularly the radial growth of ZnO nanosheets (Fig. 3 *b*).

An approach utilizing graphene oxide (Fig. 3 *c*) as the template has been reported:[50] MnO_2 nanosheets were prepared by redox reactions between the MnO_4^- anions in a solution of $KMnO_4$ and GO. The latter is hydrophilic; therefore, all functional groups and carbon–carbon bonds participated in redox reactions; as a result, MnO_2 nanosheets appeared instead of graphene oxide NSs, and CO_2 gas was released.

Important results were reported by Yang *et al.*,[52] who monitored the growth of nanocrystals *in situ* in special cells by transmission electron microscopy (TEM) (Fig. 4 *a*). The experiments were carried out using solutions of $Co(acac)_2$ and/or $Ni(acac)_2$ in a mixture of solvents: oleylamine, oleic acid and benzyl ether. Approximately 100 nL of this solution was loaded into a cell giving a $\sim$100 nm-thick liquid layer sandwiched between two silicon nitride (SiN_x) mem-

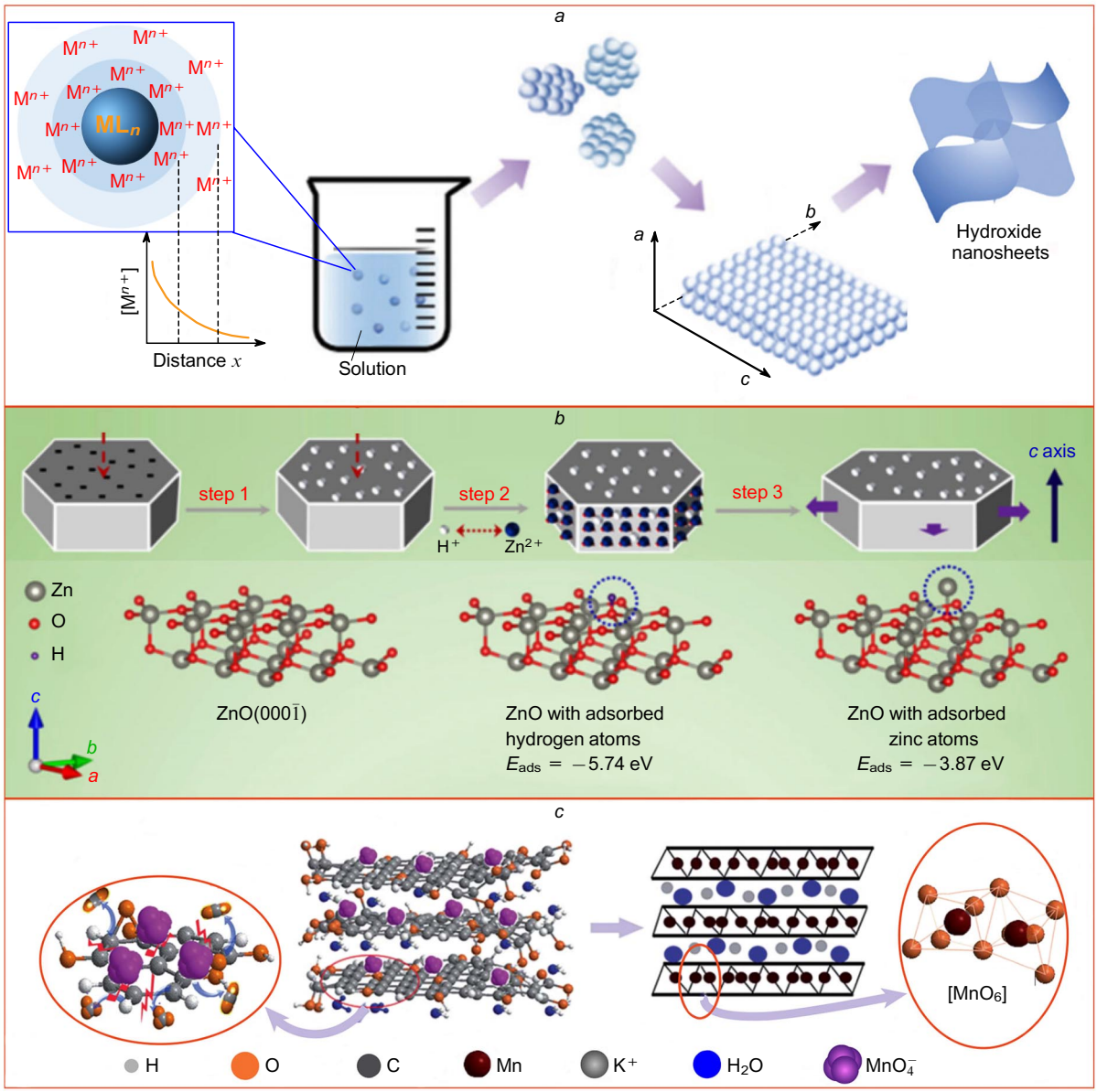

Figure 3. Schematic mechanisms of formation of metal oxide and hydroxide NSs during the synthesis in solutions of reactant mixture. (*a*, *b*) Radial growth. The first step in an acid medium is passivation of the (0001) surface by protons, which is illustrated by Fig. *b* with red vertical arrows; in the next stage, Zn^{2+} ions are attached to exposed lateral facets, with further increase in the crystal size in the *ab* plane.[49,51] (*c*) formation *via* redox reaction involving graphene oxide (GO).[50] Figures *a* and *c* are published with permission from RSC, Fig. *b* is published with permission from Springer.

branes. It was found that in a few first seconds of the reaction, 3D nanocrystals of several nanometres in size were formed in the solution, and within a few tens of seconds, they were transformed into 2D nanocrystals with NS morphology. It was assumed that this transformation takes place due to competition between the negative surface energy and the positive edge energy of the nanocrystals; furthermore, it is highly important that the overall energy is negative, because this drives the observed 3D → 2D transformation. The ratio between the surface and edge energies depends on the size of nanocrystals; it was found that this transformation becomes noticeable for particles of ~4 nm in size.

There is also a mechanism of NS formation *via* a peculiar coalescence of nanorods of the required oxides. It was found[53] that during hydrothermal treatment of a solution containing a mixture of nickel, cobalt and copper nitrates with urea and NH_4F at 150 °C, nanorods of a complex oxide of these metals precipitate in the first 5 h (Fig. 4 *b*). However, if the reaction is carried out for 8 h, these nanorods are transformed into an NS array.

Monitoring of the size and shape of nanocrystals in a TEM chamber was also used by Wang *et al.*[54] A specific feature of the approach used by the authors is that they analyzed the formation of LDH NSs on the electrode surface of an electrochemical cell to which a controlled potential was applied. In these experiments, the authors were able to study the effects of NS formation in the near-electrode electric field, *i.e.*, they simultaneously performed electrochemical measurements and observed the nanocrystal growth (Fig. 4 *c*). Nanosheets were synthesized in a solution of a mixture of di- and trivalent transition metal

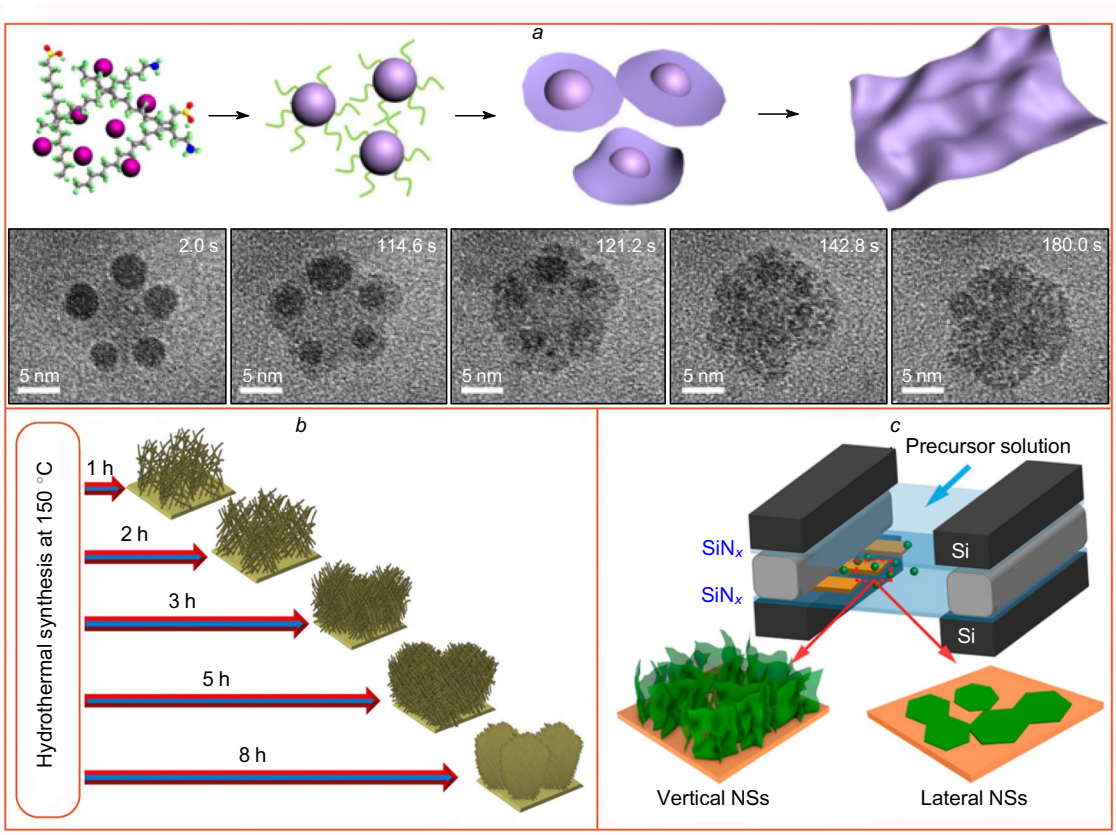

Figure 4. Mechanisms of formation of metal oxide and hydroxide NSs during the synthesis in solutions of reactant mixture. (*a*) 3D→2D growth (precursor solution → formation of nanoparticles → transformation) and micrographs of particles at different instants of the synthesis;[52] (*b*) 1D→2D growth;[53] (*c*) formation of oriented NSs on the electrode surface in an electrochemical cell; gray color designates spacers that confine the liquid-phase electrochemical cell between two thin SiN_x membranes transparent for electrons (shown in light-blue).[54] Figure *a* is published with permission from Springer Nature, Fig. *b* is published with permission from Elsevier, Fig. *c* is published with permission from ACS.

nitrates at a working electrode potential corresponding to the reduction of nitrate ions. The OH^- ions formed at the working electrode reacted with metal ions in the solution; this resulted in the growth of LDH nanosheets on the electrode surface. It was found that at a relatively low concentration of cations in the solution, nanosheets grew along the electrode surface, while at higher concentrations, the growth was perpendicular to the surface (see Fig. 4 *c*). This is due to the fact that at low salt concentrations, the amount of hydroxide ions required for NS formation is reached only in the near-surface region. Meanwhile, if the salt concentration exceeds a certain value, the contents of ions needed for hydroxide precipitation are already attained at some distance from the electrode. It is also noteworthy that the presence of an electric field between the electrodes of the electrochemical cell serve as an additional factor promoting the vertical growth of NS. It is important that the detected effect of concentration on the morphology of the growing NS layer opens up the possibility of controlled synthesis of oriented NS arrays, which are in great demand, for example, for the design of new high-performance electrodes for various electrochemical devices such as supercapacitors, sensors, *etc*.

5. Methods for the synthesis of metal oxide and hydroxide nanosheets using reactant solutions

It is evident that the use of the bottom-up strategy and solutions of salts for the preparation of metal oxide and hydroxide nanosheets is an attractive methodological approach, since it is possible to use readily available reagents and relatively low temperatures of reactions. However, there are many problems that must be solved to establish the optimal conditions for such syntheses. One challenge is to conduct a precise and reproducible synthesis of NSs with a thickness of fractions of nanometre or a few nanometres and a lateral size of 100 (or more) nanometres. These NSs have the greatest specific surface area and are of interest for practically important applications. In this respect, an important role obviously belongs to methods used to verify the morphological characteristics of ultrathin NSs such as TEM, scanning electron microscopy (SEM) and atomic force microscopy. The most significant results were obtained using these precise methods. The preparation of ordered NS arrays and the possibility of controlling not only morphological characteristics, but also the composition and crystal structure of separate NSs are also important issues.

Currently, a wide range of experiments have been performed in this field of preparative chemistry and a relatively large body of experimental data has been collected. In particular, there are data on the synthesis of metal oxide and hydroxide NSs by chemical precipitation from solutions, hydro- and solvothermal processes, microwave and template methods, electrochemical synthesis, successive ionic layer deposition, chemical reactions at the liquid/gas interface, oxidation of bulk metals, *etc*. (Fig. 5). The synthesis by hydro- and solvothermal,[55–60] microwave[61–64]

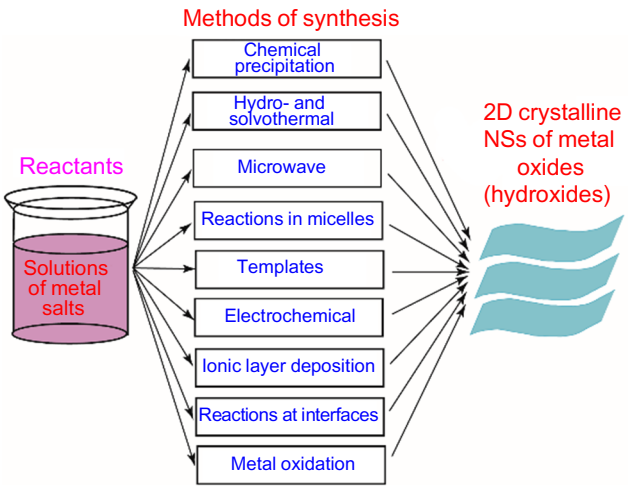

Figure 5. Methods for the synthesis of 2D nanocrystals of metal oxides and hydroxides with nanosheet morphology using solutions of metal salts.

and electrochemical[65–68] methods have been described in the literature in most detail; therefore, we restrict ourselves to the description of only some of the listed methods. A common feature of the methods considered here is that they are based entirely on the chemical approach using soft chemistry methods without physical impacts on the reactants such as electric fields in the electrochemical cell or microwave radiation.

5.1. Synthesis of nanosheets in solutions of reactant mixtures

5.1.1. Synthesis by chemical precipitation

The NS synthesis in a mixture of reactant solutions is apparently one of the simplest approaches regarding both the required equipment and the experimental procedure. The nanosheets of the ternary layered Ni-Fe-Mn hydroxide with a thickness of ~3.7 nm were synthesized by co-precipitation in an alkaline medium in the presence of oxygen at room temperature from a solution containing metal nitrates in the desired stoichiometric ratios.[69] The double hydroxide nanosheets described as $(Y_{0.98}E_{0.02})_2(OH)_5NO_3 \cdot n\,H_2O$ (where E = Pr, Sm, Eu, Tb, Dy, Ho, Er, Tm) were obtained by precipitation by NaOH from solutions of yttrium and some rare earth metal nitrates.[70] The nanosheets of $MgAlNO_3$ double layered hydroxides with the brookite structure with different Mg : Al ratios can be synthesized from metal nitrate solutions by dropwise addition of NaOH up to pH 10 followed by keeping at 60 °C for 8 h and dispersion in water under ultrasonic treatment.[71] In view of the fact that the spatial structures of α-$Co(OH)_2$ and γ-CoOOH are similar, Huang *et al.*[33] developed a two-stage process for the synthesis of γ-CoOOH nanosheets based on a phase transition. In the first stage, α-$Co(OH)_2$ sheets were synthesized by alkalization of a solution of $CoCl_2$ to pH 9. The subsequent oxidation with NaClO at room temperature yielded 1.4 nm thick γ-CoOOH nanosheets with an area of up to several hundreds of square nanometres.

Note that there are various procedures for solution mixing: adding an alkali to a salt solution or *vice versa*, fast mixing or dropwise addition, using magnetic stirring or ultrasonic treatment, and combinations of several techniques, usually aimed at separating the nucleation and ageing stages.[72] The above examples of synthesis of metal oxide and hydroxide NSs are usually performed in two steps: fast mixing of precursor solutions to induce nucleation followed by relatively long-term incubation. For example, up to 10 nm thick ZnO nanosheets with the wurtzite structure were prepared by precipitation of zinc hydroxide from an aqueous solution of $Zn(NO_3)_2$ by adding a NaOH solution up to pH > 10 with long-term stirring of the solution heated to 70 °C.[73] The possible mechanism of formation of these NSs is depicted in Fig. 6 *a*.

One of the options for conducting the ageing stage is to treat the precipitate under hydrothermal conditions. In particular, layered Ni-Fe hydroxides containing nitrate, vanadate or molybdate anions were synthesized by co-precipitation from solutions followed by hydrothermal treatment of the suspension.[76]

The precipitation in the solution bulk is associated with difficulty of determination and control of the degree of supersaturation and variability of pH and local concentrations in micro areas, which prevents accurate control of the particle size and morphology. In addition, the tendency of particles for aggregation is also a problem. The above difficulties can be avoided, for example, by using time or space constraints. For example, by using various types of continuous flow methods for reactions of solutions, it is possible to restrict the reaction time and maintain a nearly invariable concentration of reactants, thus ensuring a constant supersaturation. A review[77] describes some procedures of continuous flow synthesis of LDHs with NS morphology and composites based on them and reactor designs providing optimal characteristics of component mixing and heat and mass transfer processes.

One more way to suppress the interaction between neighbouring nanosheets is to introduce special additives into the precursor solution. These additives can form complexes with inorganic ions in the solution; the structure of the complexes can be precisely controlled by thorough selection of the composition and component ratio. This helps to obtain crystals of desired composition and morphology. This approach without the use of hydrothermal treatments or special reactors was utilized to obtain manganese oxide NSs with up to 10 nm thickness and the birnessite crystal structure.[78] The reaction was started with the preparation of a solution containing manganese(II) cations, ethylenediaminetetraacetic acid (EDTA) anions and NaOH and was continued with stirring for up to 3–5 days at room temperature. It was noted that without EDTA in the presence of air oxygen in an alkaline medium, fast formation of hydroxyl compounds of di- and trivalent manganese such as $Mn(OH)_2$ and Mn_3O_4 is possible. In the presence of EDTA anions, stable complexes with Mn^{2+} ions are formed; this inhibits fast precipitation, and manganese is oxidized to the tri- or tetravalent state. One more function of EDTA in the formation of NSs is to ensure the transport of manganese to the particle growth zone, while the specific interaction of EDTA at the (001) facets of birnessite retards the increase in the NS thickness. Tertiary and quaternary ammonium salts, water-soluble organic compounds or polymers can also be used as special additives. Most often, the crystal growth in certain directions is restricted due to the electrostatic interaction between the faces of inorganic crystal and organic surfactants.

For example, Lim *et al.*[79] obtained MnO_2 nanosheets by conducting oxidation with H_2O_2 in the presence of tetramethylammonium (TMA) hydroxide followed by removal of

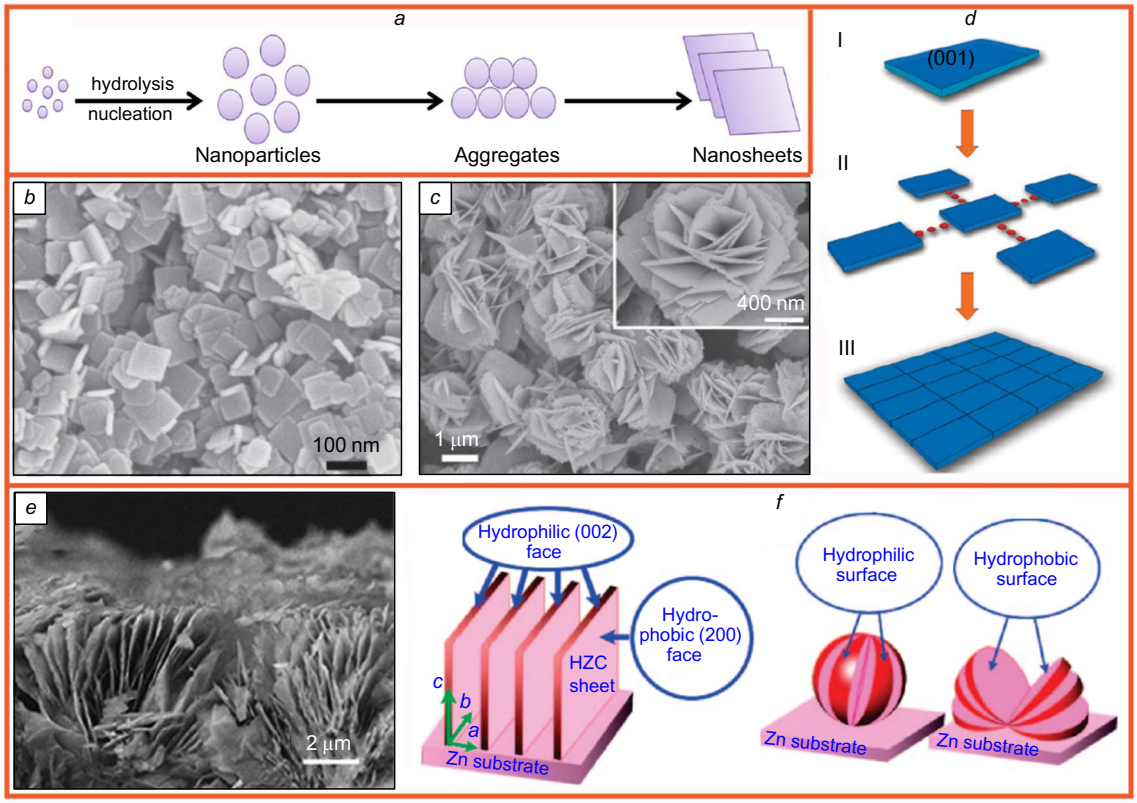

Figure 6. Examples of synthesis of metal oxide and hydroxide NSs using solutions of reactants. (*a*) mechanism of formation of ZnO nanosheets upon precipitation from a zinc nitrate solution by alkali at 70 °C;[73] (*b*–*d*) illustration of the effect of PVP addition on the TiO_2 nanosheet morphology:[74] SEM images of NSs prepared in the absence (*b*) and in the presence (*c*) of PVP at different magnifications; (*d*) formation of mosaic nanoparticles: (I) formation of single NSs with PVP macromolecules adsorbed on (001) faces; (II) coalescence of neighbouring NSs in *ab* plane; (III) formation of mosaic structures with a large area; (*e*) SEM image of arrays of vertical $Zn_5(CO_3)_2(OH)_6$ hydroxycarbonate nanosheets; (*f*) models of NS arrays obtained under various conditions (solution concentrations and times of treatment) determining the hydrophobic (hydrophilic) properties of the surface.[75] Figure *a* is published with permission from Springer, Figs *b*–*d* are published with permission from RSC, Figs *e*, *f* are published with permission from ACS.

excess reactants by dialysis. The nanosheets of Fe-Co double oxide were synthesized in solution by $NaBH_4$ reduction in the presence of cetyltrimethylammonium bromide (CTAB).[80] It was noted that owing to fast reduction, the use of $NaBH_4$ results in the formation of NSs with a higher electrocatalytic activity in the oxygen evolution reaction compared to the activity of nanoparticles of the same composition, which are formed when a hydrazine solution is used as the reduced agent. The sorption of polyvinylpyrrolidone (PVP) molecules on the (001) facets of anatase enabled the preparation of TiO_2 nanosheets.[74] The adsorbed PVP molecules not only served as links between the blocks, but also prevented them from aligning along the *c* axis (Fig. 6 *b*–*d*). In that study, like in other studies devoted to the synthesis of TiO_2 (Ref. 81) and SnO_2 (Ref. 82) nanosheets in the presence of PVP, hydrothermal treatment was used. Thus, special reagents acting as complexing agents and growth inhibitors promote the control over mass transfer and can lead to the evolution of the morphology of growing crystals, in particular, providing the formation of nanosheets of oxide and hydroxide derivatives.

In some studies, organic solvents rather than water were used to conduct the reaction. For example, in the synthesis of Ni-Co double layered hydroxides, specified metal nitrates were dispersed in an aqueous solution of ethylene glycol and then urea was added to this mixture with stirring.[83] For ageing, the solution was kept at 90 °C for 3 h.

Chemical bath deposition (CBD) is a known method for the formation of films of inorganic compounds on solid substrates from aqueous solutions. The benefits of this method include low temperature of the synthesis and scalability, which allows treatment of large areas at relatively low operating costs. It is possible to find conditions under which hydrolysis in solution would result in the deposition of the nanocrystals of some metal oxides and hydroxides on the substrate surface. Under certain conditions of synthesis (when the concentration ranges, temperature and/or light flux are appropriately chosen), it is possible to obtain films with a specified texture caused by the predominant orientation of nanocrystals.

The formation of metal oxides upon chemical deposition on the substrate may include several stages, in particular dissociation of the reactants in the solution and establishing of the equilibrium between the complex-forming agent and water; formation of ionic metal–ligand complexes $[M(L)_i]^{(n-ik)+}$, where M^{n+} is the metal cation, L^{k-} is the ligand; reaction of metal cations or charged complexes with hydroxide anions to give $M(OH)_n$; and dehydration of the obtained hydroxide. The last step often takes place during the heat treatment of freshly precipitated metal hydroxides. The overall reaction of oxide formation can be written as [84]

$$[M(L)_i]^{(n-ik)+} + \frac{n}{2}H_2O \longrightarrow MO_{n/2} + n\,H^+ + i\,L^{k-} \qquad (1)$$

It is noteworthy that according to most CBD procedures, cations or charged metal complexes should be adsorbed on the substrate surface; this makes it possible to avoid precipitation in the solution bulk. However, in practice, the formation of colloidal solutions followed by particle deposition on the substrate surface is possible.

Cao *et al.*[85] were apparently the first to observe the formation of arrays of ZnO nanosheets perpendicular to the substrate. They used an aqueous solution containing 0.1 M of $Zn(NO_3)_2 \cdot 6\,H_2O$ and 0.025–0.05 M of the dimethylaminoborane complex $Me_2NH \cdot BH_3$ (DMAB) as a reagent and single crystalline silicon wafers as substrates. The substrates were immersed into the solution and the vessel was kept for 3 h at 70 °C. The hydrolysis of DMAB in the solution was accompanied by increase in the pH, which induced the intermediate formation of $Zn(OH)_2$ molecules or $Zn(OH)_4^{2-}$ anions, which were easily dehydrated at elevated temperature. Finally, arrays of single crystalline wurtzite ZnO nanosheets with dimensions of several micrometres and a thickness of several tens of nanometres oriented normally to the substrate were formed.

Hosono *et al.*[86] used an aqueous methanol solution containing $Co(NO_3)_2 \cdot 6\,H_2O$ or $CoCl_2 \cdot 6\,H_2O$ and urea at 60 °C to obtain a sample of $Co_x^{II}Co_{x-1}^{III}(OH)_y(CO_3)_zA_c \cdot n\,H_2O$ (where A = Cl^- or NO_3^-) as ~10 nm-thick nanosheets with a hydrotalcite type structure grown perpendicular to the borosilicate glass substrate. As a result of pyrolysis at 300 °C, LDH nanosheets were converted to the oxide Co_3O_4, which retained the same morphology. A number of cobalt(II) salts — nitrate, chloride, acetate and sulfate — were used as precursors for the deposition of layered cobalt hydroxycarbonate NSs on FTO (fluorine-doped tin oxide) from solutions containing urea.[87] After the chemical deposition, the samples were calcined at 400 °C to obtain Co_3O_4 films, which served as sensor electrodes for the electrochemical determination of acetaminophen.

For CBD of TiO_2 films on glass substrates, an aqueous solution of titanium butoxide was used as the precursor.[88] The reaction, which was carried out at 80 °C for several hours, resulted in the formation of arrays of rutile NSs with a thickness of ~20 nm oriented perpendicular to the substrate. When aqueous ethanol or absolute ethanol was used as the solvent, the phase composition of the reaction products was modified towards increasing yield of anatase in the mixture with rutile.

A series of studied[89–92] describe elucidation of conditions for the chemical bath deposition of arrays of vertically oriented nanosheets using hexamethyltetramine (HMTA): Mg_3O_4nanosheets were deposited from a manganese(II) sulfate solution on titanium,[89] β-$Ni(OH)_2$ nanosheets were formed from a solution of nickel salt on the glass or steel surface[90] and CuO nanosheets were formed from a solution containing copper sulfate and ammonia.[91] More recent studies address the effect of complexing agents such as ammonia, ammonium persulfate and HMTA on the morphology and packing mode of copper oxide NSs[92] and the effect of addition of ionic liquids such as dimethylimidazolium salts, dihydroxypropylmethylimidazolium salts, *N*-(3-methyl-2-oxopropyl)pyridinium chloride[93] and surfactants such as Triton X-100, CTAB and polyethylene glycol (PEG).[94] Park *et al.*[95] studied in detail the role of the solution pH for the deposition of $Ni(OH)_2$ nanosheets and the influence of the post-treatment temperature.

Nanosheets of monoclinic $Cd(OH)_2$ with a size of several micrometres and average thickness of ~9 nm were obtained on a cadmium foil surface from a $CdCl_2$ solution upon the addition of aqueous NH_3 up to pH 12 and keeping at room temperature for 22 h.[96] The CBD method was also used to prepare nanosheets of Fe_2O_3,[97] Bi_2O_3,[98] nickel-cobalt-manganese ternary oxide[99] and ZnO/NiO composite.[100, 101]

Some researchers consider the substrate functioning also as the precursor, that is, the source of metal cations. Su *et al.*[75] carried out the oxidation of zinc surface in an aqueous solution of urea or in a water–organic solution containing acetone or dimethylformamide, apart from urea, at a temperature of 80 °C for a period from 1 to 72 h. After 24-h treatment, arrays of up to 80 nm-thick $Zn_5(CO_3)_2(OH)_6$ nanosheets were formed on the zinc plate; they were perpendicular to the zinc plate and spaced apart from one another by 50 nm to 15 μm (Fig. 6 *e*); as a result, the zinc plate acquired superhydrophilic properties. This effect was interpreted resorting to powder X-ray diffraction data; on the basis of these data, models of the NS structure were designed (see Fig. 6 *f*). In particular, it was shown that the (002) plane of zinc hydroxy carbonate contains six oxygen atoms, which provide for high concentration of the hydroxyl groups on the surface, thus making it hydrophilic. The NS sides consisting mainly of zinc atoms are relatively hydrophobic. The growth of NSs perpendicular to the substrate may be induced by the concentration gradient arising on the substrate after nucleation or by drops of water released upon dehydration and spread over the substrate surface. Su *et al.*[75] considered in detail the effect of the duration of synthesis on the morphology of the resulting films and demonstrated the possibility of controlling their hydrophobic (hydrophilic) properties.

Thus, the foregoing demonstrates that the chemical deposition from solutions on substrates is a promising method for the preparation of oriented metal oxide and hydroxide NS arrays.

5.1.2. Synthesis in a mixture of reactants using emulsions and soft templates

Using aqueous solutions of inorganic salts and liquids containing surfactants (such as fatty acid anions) as precursors for the preparation of metal oxides and hydroxides, it is possible to obtain hydrophobic nanocrystals at the interface held on the surface by the long alkyl chains of the surfactant. The use of organic solvents immiscible with water makes it possible, in some cases, to avoid the aggregation of the resulting NSs. These microemulsion methods of synthesis can be used to control the nucleation and the growth of nanocrystals. This approach is illustrated by the study[102] in which characteristics of layered Zn-Ti hydroxide nanosheets synthesized using reverse micelles were compared with the characteristics of the bulk material of the same composition obtained by co-precipitation from a homogeneous solution with subsequent hydrothermal treatment.

Nanosheets of Mg-Al LDHs containing 14, 20 or 35 layers were obtained in a microemulsion.[103] It was found that the thickness of these NSs depends on the concentration ratio between the oleylamine and water in the synthesis. Ding *et al.*[104] prepared ZnO nanosheets by photopolymerization of a two-phase liquid containing an aqueous solution of $Zn(NO_3)_2$, cyclohexane and surfactants, Triton X-100 and hexanol (Fig. 7 *a*). An emulsion approach of this type

can also be used for the solvo- or hydrothermal synthesis, as shown in relation to the synthesis of TiO_2,[106] SnO_2,[107] Co_3O_4 (Ref. 108) and other nanosheets.

When solutions of immiscible liquids in emulsions are used, particles of definite shape appear. The emulsion can actually be considered as a sort of soft template for the preparation of nanostructured compounds. Among these templates, sodium carboxymethylcellulose (CMC), an environmentally safe polysaccharide derivative with carboxyl and hydroxyl functional side groups, proved to be promising for the synthesis of ultrathin NSs of various compounds, including transition metal oxides and hydroxides.[105] The carboxyl and hydroxyl side groups of CMC promote the formation of bonds with inorganic cations (first of all, *via* electrostatic attraction). As a result of self-assembly, the hydrated inorganic oligomers get inside the CMC matrix, which results in the formation of a 2D structure of inorganic oxide and hydroxide compounds upon a gentle hydrothermal or solvothermal treatment in an alkaline medium (Fig. 7 *b*). According to a typical protocol, CMC were dissolved in deionized water, and inorganic metal salts were added with vigorous stirring. After the self-assembly processes, an ammonia solution was added dropwise to the stirred reaction mixture. Heating to 80 °C induced crystallization of inorganic oxides and/or hydroxides with NS morphology, which was formed due to the use of CMC as a template. According to this strategy, 0.85–1.70 nm-thick nanosheets of metal hydroxides [$Ni(OH)_2$, $Co(OH)_2$, $Cd(OH)_2$ and $Mg(OH)_2$] and oxides (ZnO and Mn_3O_4), LDHs of transition metals (Ni-Co, Ni-Fe, Co-Fe), and Ni-Co-Fe three-component layered hydroxide were successfully synthesized.

SiO_2 nanosheets were prepared in the water–cyclohexane two-phase system in the presence of CTAB using micelles as a soft template.[109] The effects of addition of various alcohols, temperature and duration of the reaction on the morphology and specific surface area of the materials were studied; the optimal conditions for the preparation of 3.7 nm-thick NSs with a specific surface area of 1420 $m^2\ g^{-1}$ were determined. In order to ensure the formation of 2D morphology, Lutz *et al.*[110] performed template synthesis using amphiphilic proteins the secondary structure of which allowed the preparation of SiO_2 nanosheets with a thickness of 2.1 nm. Polymer templates of various composition have also been used for this purpose.[111, 112]

Copper oxide nanosheets were obtained using sodium dodecyl sulfate (anionic surfactant) as the template.[113] The surfactant anions and Cu^{2+} cations formed a lamellar mesophase in an aqueous ethanol solution due the electrostatic interaction. The addition of alkali induced crystallization of CuO as 0.8 nm-thick nanosheets with the tenorite structure, with the solution structure remaining invariable.

5.1.3. Template synthesis using nanosheets of carbon compounds as substrates and surfactants

When metal oxides and hydroxides with NS morphology are prepared by template synthesis using 2D substrates, the substrates are normally removed by dissolution or thermal destruction at the final stage. For example, graphene oxide nanosheet can serve as such substrate. Lu *et al.*[114] chose GO sheets with dimensions of 4 μm and thickness of 0.9 nm as the template to obtain SiO_2 nanosheets, which were deposited on the substrate surface by the sol–gel process using tetraethoxysilane as the precursor. The thickness of the resulting GO@SiO_2 structures was 3.7 nm. The template was removed by heating the sample at 500 °C in air. After this treatment, the sample was white-coloured and represented a set of SiO_2 nanosheets. Since partial agglomeration of NSs may take place during heat treatment, a relatively low annealing temperature was chosen to avoid the nanosheet sintering. The resulting oxide material was used in the next stage to obtain silicon NSs *via* reduction.

A similar procedure was used to obtain Co_3O_4 nanosheets.[115] According to TEM examination, the nanosheets

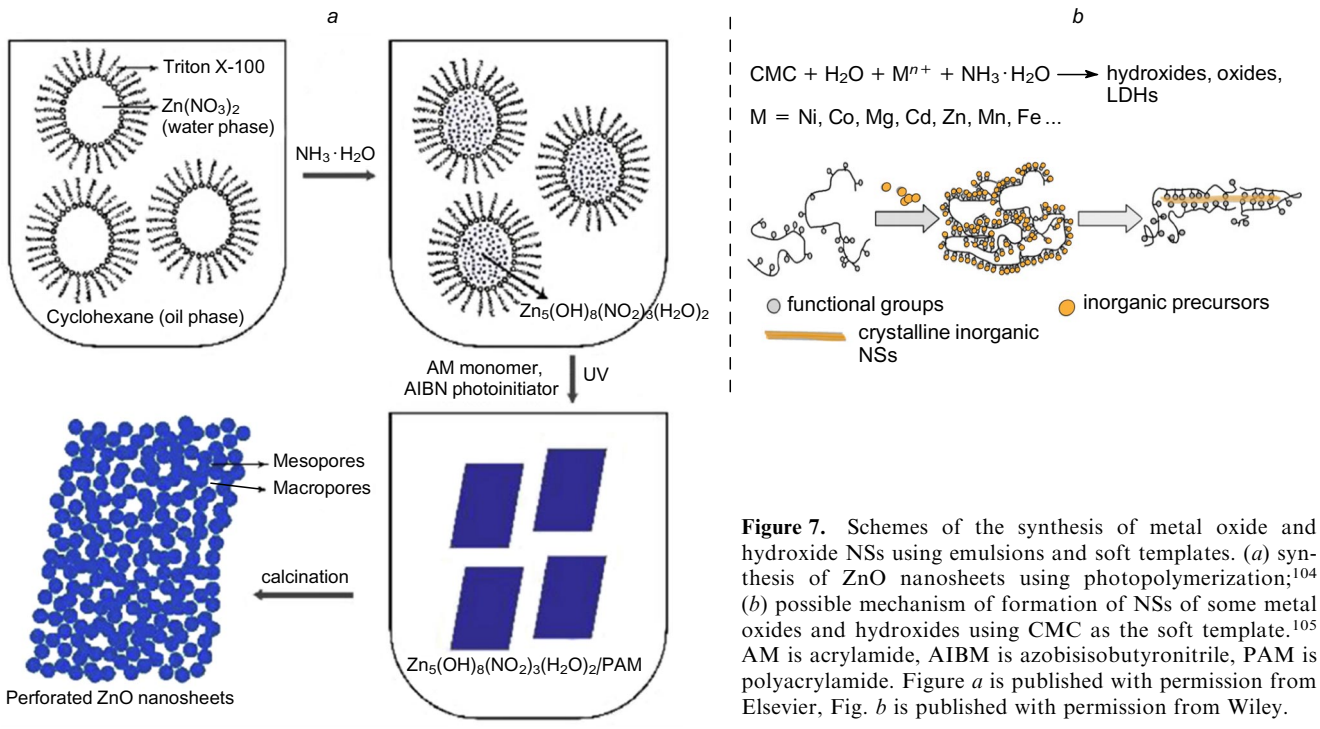

Figure 7. Schemes of the synthesis of metal oxide and hydroxide NSs using emulsions and soft templates. (*a*) synthesis of ZnO nanosheets using photopolymerization;[104] (*b*) possible mechanism of formation of NSs of some metal oxides and hydroxides using CMC as the soft template.[105] AM is acrylamide, AIBM is azobisisobutyronitrile, PAM is polyacrylamide. Figure *a* is published with permission from Elsevier, Fig. *b* is published with permission from Wiley.

obtained in this way were not single crystals, but were composed of 5–10 nm nanoparticles arranged predominantly along the (*h*00) plane. This polycrystalline structure of NSs provided a porous structure and improved characteristics of the biosensor based on them. Zhang *et al.*[116] studied the effect of the solution pH on the morphology of Co_3O_4nanosheets. The porous Co_3O_4 nanosheets synthesized by the same procedure demonstrated good capacity characteristics for accumulation of alkali metal ions.[117]

Takenaka *et al.*[118] prepared TiO_2 and ZrO_2 nanosheets using GO as the template and cyclohexane solutions of $Ti(OC_4H_9)_4$ and $Zr(OC_4H_9)_4$, respectively, as the precursors. The prepared suspensions were subjected to the solvothermal treatment at 180 °C to form metal oxide/reduced graphene oxide composites. Graphene oxide was removed by calcining the composite at 450–650 °C. The synthesized TiO_2 and ZrO_2 nanosheets in the free state were 3.2 to 4.2 nm thick. Wang *et al.*[119] observed the formation of the porous structure of oxide NSs upon the calcination of the TiO_2/GO composite for removal of the template as a result of decomposition of the organic components and release of gaseous CO_2.

The Nb_2O_5 nanosheets possessing a porous structure (to provide fast ion transport) were synthesized[120] by ultrasound-induced deposition from a solution of niobium oxalate on the GO surface followed by hydrothermal and final thermal treatment at 750 °C in air.

A similar approach was used[121] to prepare nanosheets of transition metal double oxides, $ZnMn_2O_4$, $ZnCo_2O_4$, $NiCo_2O_4$ and $CoFe_2O_4$. It was shown that nanoparticles of the desired composition can serve as the precursors for NSs. Peng *et al.*[122] used surfactants, particularly, Pluronic copolymers with different molecular weights (1100, 4400, 12600) in ethylene glycol as template substrates, apart from GO, to generate an ordered porous structure of $ZnFe_2O_4$ nanosheets. It was shown that the pore size in NSs depends on the molecular weight of the polymer. It is important that nanocrystalline $ZnFe_2O_4$ particles of 6 nm, pre-synthesized by precipitation under hydrothermal conditions, served as the NS precursors. In another study,[123] the template synthesis of $NiCo_2O_4$ spinel nanosheets on the GO surface was performed using the zeolite-like nickel cobalt imidazolate metal-organic frameworks (ZIF-67 MOFs) as the precursors.

In some cases, it is not necessary to remove the template for the preparation of composite nanomaterials. For example, composite nanosheets based on a metal oxide and a conductive component have improved electrochemical properties compared to those of pure metal oxides. In another study,[124] graphene oxide NSs acting as the substrate were placed into a solution of nickel acetate, kept for 48 h and thoroughly washed with distilled water. Then the samples were heated at 500 °C in air for 4 h and used to prepare an electrochemical sensor for urea. The NiO : C ratio in the prepared material was 1 : 2.

Yang *et al.*[125] used negatively charged GO as the template, which adsorbed Ni^{2+} cations from a solution due to electrostatic attraction forces. In the presence of excess $NaBH_4$ in the solution, Ni^{2+} ions adsorbed on the GO surface were bound to the BH_4^- anions and GO was reduced to graphene. This resulted in the formation of Ni-B oxide/G/Ni-B oxide 2D-on-2D three-layer hybrid heterostructures with a thickness of ~6.5 nm. Since the Ni-B oxide nanosheets were deposited on both sides of the template, the thickness of each sheet was estimated as 3.2 nm. In view of the conductivity of graphene and the porous structure of oxidized NSs, the resulting 2D nanomaterial is promising for electrochemical applications, for example, as a catalyst for water splitting.

In the opinion of Xu *et al.*,[126] graphite-like carbon nitride (g-C_3N_4) nanosheets have an advantage over other 2D templates, because they can decompose directly during the hydrothermal synthesis. Nanosheets of In_2O_3, CeO_2 and Co_3O_4 were obtained using g-C_3N_4 template. Urea, which served as a reactant, decomposed during the synthesis thus generating a weakly alkaline medium needed to precipitate the hydroxide.

The range of possible templates for NS preparation is not limited to planar substrates; the results of application of templates of diverse shapes and sizes have been published. It is important that by using template materials with relatively low decomposition temperature, it is possible to reduce the temperature of template removal. For example, when polystyrene (PS) nanospheres are used as templates, ultrasonic treatment of a dispersion containing the template, Ni^{2+} ions and urea, results in the deposition of $Ni_2CO_3(OH)_2$ nanosheets, which are converted to ~10 nm-thick NiO NSs after calcination at only 300 °C. The possible mechanism of formation of these NSs is depicted in Fig. 8 *a*.[127]

Wang *et al.*[130] used SiO_2 as the template for the preparation of $CoMoO_4$ nanosheets. When the synthesis was conducted under solvothermal conditions, NS formation and template removal took place simultaneously, *i.e.*, the process was not multistage, unlike most processes of template synthesis.

Kong *et al.*[128] obtained CuO nanosheets with a thickness of up to 10 nm by mere addition of H_2O_2 to an aqueous dispersion of Cu_2O crystals with a size of 95 nm. The scheme of the synthesis of CuO nanosheets using cubic Cu_2O nanocrystals as the template is shown in Fig. 8 *b*.

A similar approach was used[129] to obtain nanotubes formed by CuO nanosheets (Fig. 8 *c*). In the first stage, a solution of $CuCl_2$ was reduced with hydrazine in the presence of surfactants, which gave 1D copper structures (nanowires). In the next stage, the nanowires were placed into a 5% solution of H_2O_2 and subjected to ultrasonic treatment. The chemical reaction first gave one-dimensional Cu@CuO core–shell structures and then hollow tubes composed of monoclinic CuO nanosheets appeared, as confirmed, among other data, by electron microscopic examination (Fig. 8 *d*–*f*).

The ZIF-67 metal-organic framework with the nanocube morphology was used as the template[131] to obtain nanoboxes composed of numerous ultrathin $CoWO_4$–$Co(OH)_2$ nanosheets. The replacement of the methylimidazole ligands in MOF by WO_4^{2-} ions took place in a solution of sodium tungstate; due to alkalinity of this solution, some of Co^{2+} ions in MOF reacted with OH^- to give $Co(OH)_2$, which finally afforded the heterophase $CoWO_4$–$Co(OH)_2$ nanosheets, which assembled into a hollow cubic structure. The electrocatalytic properties of these hierarchical structures towards the oxygen evolution reaction are due both to their morphology (namely, the large number of active sites on the exposed surfaces of ultrathin NSs) and to the synergistic effect in the heterophase product, in which the interfaces promoted accelerated charge transfer from $CoWO_4$ to $Co(OH)_2$.

Thus, the template approach provides successful synthesis of metal oxide and hydroxide NSs. Most of the studies in this field are devoted to the application of

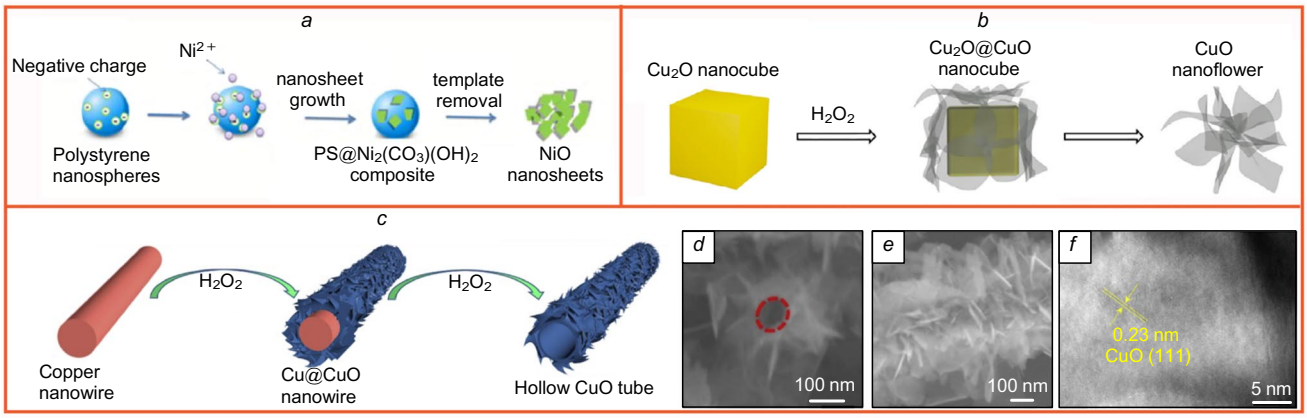

Figure 8. Illustration of application of various types of templates for the preparation of metal oxide NSs. Scheme of the synthesis of NiO nanosheets using polystyrene nanospheres as a template (*a*);[127] CuO nanosheets using cubic Cu_2O nanocrystals as a template (*b*);[128] CuO nanosheets using copper nanowire as a template (*c*);[129] (*d*, *e*) SEM images of CuO nanosheets; (*f*) high-resolution TEM images of CuO nanosheets.[129] Figure *a* is published with permission from RSC, Figs *b*–*f* are published with permission from Elsevier.

graphene oxide NSs as a hard template. The intermediate composite materials obtained by deposition on the GO surface from a solution are subjected in the next stage to high-temperature treatment in air to remove the template matrix. As a rule, the thermal destruction of the template is accompanied by the formation of a porous NS structure. This can be avoided by using template materials with relatively low decomposition temperature (*e.g.*, g-C_3N_4 and polymer matrices) or by using chemical degradation of the template, which was demonstrated in relation to Cu or Cu_2O substrates in the preparation of CuO nanosheets. In the bath deposition, cationic and anionic surfactants, polymers and natural products can serve as soft templates. On the one hand, these materials contribute to creation of soft or green chemistry conditions for the synthesis. However, on the other hand, there is the risk that the reaction product is contaminated with organic components, which can be removed only at elevated temperature. Nevertheless, the presented examples demonstrate the extensive potential for selecting and optimizing the experimental conditions for the template synthesis of nanosheets.

5.2. Synthesis by the reactions of metal surface with solutions of oxidants

The oxidation of valve metals gives rise to continuous oxide films on their surface, which protect them from corrosion. However, treatment of magnesium or cobalt metal in deionized water at room temperature affords hydroxide films composed of 2D nanocrystals with NS morphology — $Mg(OH)_2$ and $Co(OH)_2$, respectively. It was shown[132] that treatment of magnesium gives rise to a ~15 nm-thick nanosheet film with a lateral dimension of ~400 nm, while treatment of cobalt affords a film composed of nanosheets with dimensions of up to 120 nm and thickness of ~10 nm vertically aligned on the substrate/environment interface. The formation of hydroxide NSs on the surface of magnesium and magnesium-based alloys on treatment with solutions of various metal salts was considered in detail by, for example, Ishizaki *et al.*[133] The formation of nanocrystals with NS morphology was also observed in a study of the WO_3 layer formed on the tungsten surface on treatment with a KOH solution.[134] It was shown that under these conditions 30–50 nm-thick alloys with planar dimensions of up to 10 μm are formed on the surface. Bouali *et al.*,[135] who studied corrosion of aluminium alloys in zinc nitrate solutions, reported the formation of an array of Zn-Al LDH nanoflakes arranged perpendicularly to the surface.

The formation of nanosheets of the hybrid compound of $Ni(OH)_2$ with MnO_2 was observed[136] upon treatment of nickel foam with an aqueous solution of $KMnO_4$ at room temperature. Under these conditions, the following reaction took place on the surface

$$3Ni + 2MnO_4^- + 4H_2O \longrightarrow 2MnO_2 + 3Ni(OH)_2 + 2OH^- \quad (2)$$

to give nanocrystals of α-$Ni(OH)_2$ and MnO_2 as 2–7 nm-thick nanosheets with planar dimensions of >100 nm with a ramsdellite type structure. It was noted that these NSs consisted of alternating blocks of nano-sized single crystals of each component.

An original method for the preparation of hafnium, aluminium, gallium, and other metal oxide NSs was proposed by Zavabeti *et al.*[137] The authors noted the formation of ultrathin (of atomic thickness) layers of oxides on the surface of liquid gallium on contact with air in a thin layer of adsorbed water. Under these conditions, a Ga_2O_3 layer was formed on the surface of pure gallium, while on the surface of gallium alloys with other metals, layers of their oxides or double metal oxides with gallium were formed. According to the results of thermodynamic calculations, on the surface of a gallium alloy with hafnium, aluminium or gadolinium, the oxide of one of these metals was mainly formed. In order to obtain oxides of these elements as nanosheets on the substrate surface, the authors used two procedures: one consisted in the transfer of the oxide by mechanical touching a liquid alloy droplet with a solid substrate, while the other one was based on the preparation of a nanosheet suspension upon injection of air into the interface between liquid gallium or its alloy and water. The conditions of the synthesis of Ga_2O_3, HfO_2 and Gd_2O_3 nanosheets with thickness of 2.8, 0.6 and 0.5 nm, respectively, were considered as examples; the lateral dimensions of Gd_2O_3 particles exceeded several micrometres. Other procedures for the preparation of gallium oxide layers include spin coating of a liquid metal droplet on the substrate surface or dragging a gallium droplet located at the tip of a pipette over the surface.[138]

SnO nanosheets with a thickness of 0.7 nm on a silica layer overlying a silicon layer were fabricated by pressing the substrates to molten tin droplets heated to 300 °C.[139] At temperatures of ~1000 °C, arrays of vertically aligned oriented Cr_2O_3 and $(Fe, Mn)_3O_4$ nanosheets were formed on the surface of alloys of these metals upon oxidation with steam.[140]

Vimalanathan *et al.*[141] studied the formation of Ga_2O_3 nanosheets at the liquid gallium/organic solvent interface *in situ* in a special reactor with a variable inclination angle. A recent review[142] is devoted to the preparation of 2D materials using liquid metals.

Nanosheets can be produced *via* galvanic exchange reactions, that is, redox reactions between cations in NSs and cations in solution. On treatment of a suspension of MnO_2 nanosheets with an aqueous solution containing Fe^{2+} or Sn^{2+} cations, the cations were inserted into NSs.[79] Depending on the reaction temperature (25 or 90 °C), the Fe^{2+} or Sn^{2+} ions were concentrated in the gap between the negatively charged layers, or uniform galvanic exchange of manganese cations with substituting ions took place. Depending on the reaction conditions, the iron content may vary from 7 to 44 mol.%, and the tin content is 7 to 29 mol.%. Fang *et al.*[143] first synthesized NSs with the birnessite structure on the nickel foam surface by hydrothermal oxidation of Mn^{2+} cations. Then the samples were immersed into a $FeSO_4$ solution for 30 s. The galvanic exchange on the NS surface resulted in mixed Mn-Ni-Fe oxyhydroxide, which can serve as an electrode and act as an alternative to electrocatalysts based on noble metal compounds in water oxidation.

In conclusion, mention should be made of the study by Hou *et al.*,[144] who proposed a reagent-free procedure for the synthesis of ZnO nanosheets on the cathode, which represented an ITO layer on glass. A zinc plate was used in this experiment as the anode and deionized water served as the solvent. The distance between the cathode and the anode varied from a few millimetres to 1 cm. When a voltage was applied, the zinc surface was oxidized to form ZnO quantum dots with $Zn(OH)_2^+$ functional groups. The positive charge of these groups promoted the quantum dot detachment from the anode and migration towards the cathode to form ~1 nm-thick ZnO nanosheets oriented mainly perpendicular to the electrode surface with a lateral dimension of up to several micrometres.[144]

Thus, NSs of a number of metal oxides and hydroxides can be prepared using chemical reactions that take place in solutions and on solid substrate surfaces. The one-step synthesis or a certain synthetic step can be assisted by ultrasonic, microwave, hydro- or solvothermal treatment, or by a combination of these techniques, which offers new opportunities for the design of materials. The advantages of these treatment techniques include high degree of reactant mixing, uniform composition of reaction products, relatively low energy expenditure (in comparison, for example, with high-temperature synthetic procedures), easy operations and control, high productivity and scalability. In the optimization of synthesis conditions, it is necessary to thoroughly select the solvents, complexing agents, surfactants, inhibitors, templates, substrates, *etc.*

5.3. Synthesis using reactions at the solution/gas interface

5.3.1. Self-assembly processes

Nanocrystals with NS morphology for a number of metal oxides and hydroxides can be obtained on the surface of solutions of metal salts by chemical reactions that proceed at the solution/air interface. Masuda and Kato[145] used a $Zn(NO_3)_2$ solution containing ethylenediamine (EDA) and found conditions for the formation of arrays of oriented ZnO nanosheets at the liquid/air interface. For the formation on an oxide film on the solution surface, the mixture was heated to 60 °C and kept at this temperature without stirring for 6 h. During this period, EDA decomposed and pH of the solution increased; hydrolysis of the zinc complex with EDA took place, and the hydroxide anions reacted with Zn^{2+} cations to give hydrated $Zn(OH)_2$ species. On subsequent heating, dehydration occurred, and a hydrophobic zinc oxide film appeared on the solution surface. In the next stage, as the solution was cooled without stirring during 42 h, a ~5 μm-thick film consisting of zinc oxide NSs formed at the interface, with NSs being mainly perpendicular to the interface. This film can be transferred to the surfaces of various solid substrates such as polyethylene terephthalate.

Nanoflowers made of 2D crystals of zinc oxide can be formed[146] on the surface of a solution containing a zinc salt as the precursor and hexamethylenetetramine (HMTA) as the source of ammonia by the reaction

$$(CH_2)_6N_4 + 6\,H_2O \longrightarrow 6\,HCHO + 4\,NH_3 \qquad (3)$$

To increase the NS hydrophobicity, polyethyleneimine, a surfactant promoting the assembly of nanoflowers at the interface, was added to the solution.

In some publications, the procedure used to prepare NSs at the liquid/gas interface using special surfactants [*e.g.*, CoO,[147] ZnO[148–150] and $Ni(OH)_2$[151]] is called ionic layer epitaxy (ILE). For example, ZnO nanosheets were prepared[149] using an aqueous solution of $Zn(NO_3)_2$ and HMTA. A chloroform solution of sodium oleyl sulfate (surfactant) was added dropwise onto the aqueous solution surface. After a few minutes, the solvent was evaporated from the surface to leave a monolayer of aligned surfactant anions; the zinc cations were bound to the anions to form an electrical double layer (Fig. 9). For HMTA decomposition, the vessel with the solution was placed into a convection oven heated to 60 °C. As pH of the solution increased, wurtzite NSs with a thickness of up to 3 nm and lateral dimensions of up to several micrometres were formed. Under these conditions of synthesis, the surfactant film on the liquid surface acted as the soft template for the ZnO layer that formed at its lower surface. It was shown that electrostatic and covalent interactions between ions of the solution and functional groups of the monolayer promote the growth of NS crystals with a thickness depending on the density of surfactant molecules on the solution surface.

Cobalt(II) oxide nanosheets with a thickness of up to 3 nm and a surface area of up to 1 cm^2 were synthesized by the same procedure.[147] The formation conditions of these nanosheets of inorganic compounds have been described in detail,[152] and the possible applications of oxide and hydroxide NSs have been covered in a review.[153]

In most studies, the transfer of NSs from the solution surface to the substrate is performed by the Langmuir–Blodgett (LB) technology; both single and repeated transfer operations are carried out.[154] The LB technology for the preparation of thin films is based on the formation of a floating monolayer on the surface of water (or another liquid) and the subsequent transfer of the monolayer to the substrate. As a rule, special compression barriers are used to form a dense, continuous monolayer. The formed mono-

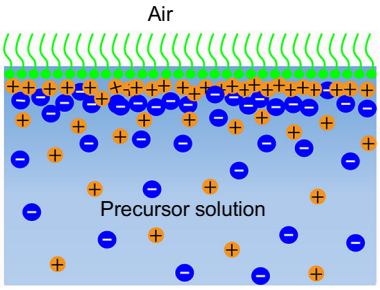

Figure 9. Scheme of formation of metal oxide and hydroxide NSs by the reaction of cations from the solution with a surfactant monolayer at the solution/air interface. The Figure was created by the authors using published data.[147]

layer can be transferred to the surface of a solid substrate using various immersion and lifting techniques.

The formation of nanosheets on the surface of aqueous suspensions and applications of functional materials based on them are considered in detail, for example, in a review by Ma and Sasaki.[155]

5.3.2. Reactions at the liquid/gas interface

The chemical reactions that take place at the interface between the metal salt solution and a gaseous reactant resulting in the formation of nanosized crystals were studied for the first time by Yu *et al.*[156] The authors investigated the reactions of a solution containing $CaCl_2$ and a hydrophilic PEG–polymethacrylic acid block copolymer with gaseous CO_2. As a result of this reaction, a nanocomposite layer with spherulite morphology composed of $CaCO_3$ nanocrystals and the polymer was formed on the solution surface. It was noted that these nanocrystals appeared in a thin layer on the solution surface during the diffusion of CO_2 molecules into the solution bulk; therefore, this method of synthesis was defined as the gas–liquid diffusion method. Despite the diversity of types of organic compounds that can be used for this polymer-controlled crystallization,[157] no nanocrystalline nanosheets of inorganic oxides were obtained in these experiments.

A similar approach to the synthesis was used in a number of other studies such as a study of ZnO preparation by the reaction of dissolved $Zn(NO_3)_2$ with ammonia gas.[158] The authors demonstrated that keeping an open vessel with a solution of this salt in concentration of 0.05 mol L^{-1} in a desiccator together with an open vessel with a 0.28% aqueous solution of ammonia for 24 h resulted in the formation of a partially hydrophobic layer on the solution surface; the layer consisted of wurtzite ZnO nanocrystals with a size from fractions of micrometre to a few micrometres oriented inside the solution. A similar procedure was used by Oaki *et al.*[159] for the synthesis of α-$Co(OH)_2$ 2D nanocrystals in the presence of polyacrylic acid (PAA); the nanocrystals were formed both in the solution bulk and on the surface.

The conditions of synthesis of nanosized α-FeOOH and γ-FeOOH crystals with NS morphology by this procedure were found in 2013 by Liu *et al.*[160] In the synthesis of α-FeOOH, the vessel with a solution of $FeSO_4$ and PAA was placed into a desiccator together with a vessel containing 2.5% aqueous NH_3. When these solutions were kept in the desiccator for several days, a FeOOH layer consisting of nanoparticles differing in shape and crystal structure and mainly pointing into the solution bulk appeared on the surface of the $FeSO_4$ solution. It was found that PAA concentration had a significant effect on the morphology and crystal structure of the nanoparticles. Lower PAA concentrations resulted in nanosheets with the α-FeOOH crystal structure, while an increase in the PAA content resulted in γ-FeOOH nanocrystals as fibres or nanorods.

Also in 2013, while studying the formation of H_xMnO_2 nanocrystals with the birnessite structure at the solution/gas interface, Tolstoy and Gulina [19] found for the first time the conditions for NS synthesis without the use of organic components. Arrays of H_xMnO_2 nanosheets were obtained [18, 19, 161] using an aqueous solution containing manganese and sodium acetates and ozone gas as reactants. A solution containing the salts in 1 : 2 concentration ratio was poured into a vessel with a volume of several cubic centimetres, which was placed in a flow chemical reactor. Then an air–ozone mixture was fed to the reactor for 1–15 min; during this period, a thin light brown layer appeared on the surface of the manganese(II) salt solution. In order to remove the excess of the reactant solution, this layer was transferred onto the surface of pure distilled water, kept for 15–20 min, transferred in a similar way onto a single-crystalline silicon plate, dried and studied by optical and electron microscopy, electron probe microanalysis, X-ray diffraction, *etc*. Conclusions about the morphology of thin layers synthesized in this way can be drawn, for example, on the basis of micrographs shown in Fig. 10, in which one can see numerous ultrathin (3–8 nm thick) NSs mainly perpendicular to the planar layer. Since the layer of a solid grows on the planar surface of an aqueous solution and NSs are perpendicular to the interface, the authors suggested that this type of NS orientation along the diffusion direction of ozone molecules is related to the experimental conditions where the reactants were supplied to the interface (the reaction zone) from different sides.

It is important that by varying the reaction conditions between manganese(II) cations and ozone molecules at the interface, it is possible to change the thickness of the formed layer, and when the manganese salt concentration is below 0.005 mol L^{-1} and the treatment time is several seconds,

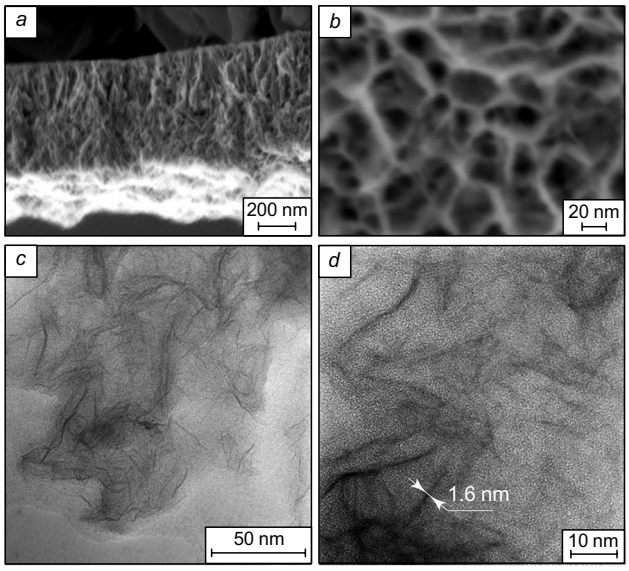

Figure 10. Electron micrographs of a manganese(III, IV) oxide layer formed on the surface of a solution of $Mn(OAc)_2$ and NaOAc salts after treatment with ozone for 10 min. SEM images: side view (*a*) and view of the layer surface from the solution (*b*); (*c*, *d*) TEM images (at different magnifications) of the manganese(III, IV) oxide layer synthesized on the surface of $Mn(OAc)_2$ solution after treatment with ozone for 5 s.[162]

horizontally lying manganese(III, IV) oxide NSs with a thickness <1 nm can be obtained on the solution surface. It is known [163] that the minimum period along the *c* axis for the birnessite structure is 7.1 Å, but this value substantially increases when water molecules or some ions are incorporated into the interlayer space. In the TEM images shown in Fig. 10 *c*,*d*, it is possible to distinguish a planar layer that contains a sort of graphene-like folds with a thickness equal to twice the layer thickness.

A similar methodological approach was used in a series of studies devoted to the fabrication of thin layers of the following compounds: As_2S_3 by decomposition of thioarsenate anions of soluble Na_3AsS_4 salt *via* the reaction with gas-phase HCl molecules;[164] LaF_3 by the reaction of La^{3+} cations present in solution with HF gas;[165] FeOOH by the reaction of the surface of an aqueous $FeCl_2$ solution with ammonia gas;[166] and Ag on the planar surface of a silver acetate solution on treatment with N_2H_4 gas.[167] Some of the layers consisted of nanocrystals with NS morphology perpendicular to the interface. For example, LaF_3 nanoparticles had a thickness from 3 to 20 nm and were packed into ordered crystal arrays;[168] 7–9 nm-thick silver arrays formed hierarchical structures with nanoflower morphology.[169] Figures 11 *a*,*b* show the SEM and TEM images of an FeOOH layer consisting of arrays of up to 10 nm-thick NSs with the lepidocrocite structure. The TEM images of a layer formed on the surface of an aqueous solution of $CoCl_2$ upon the reaction with ozone as ~45 nm-thick arrays of nanosheets mainly perpendicular to the interface are shown in Fig. 11 *c*,*d*. Gulina *et al.*[170] reported the synthesis and study of the gradient CeO_2 layer consisting of fluorite type NSs. Note that, after the removal of excess reactants, the layers of the above compositions, being transferred to the surface of solid substrates, rolled-up to form microscrolls during air drying;[171] these microscrolls exhibit new practically important properties caused by their morphology and hold promise for the development of new materials.

Analysis of the experimental data attests to the following model for the formation of metal oxide and hydroxide nanosheets upon reactions of a gaseous reagent (oxygen, ozone, ammonia) with the surface of an aqueous solution of a metal salt capable of forming a poorly soluble compound

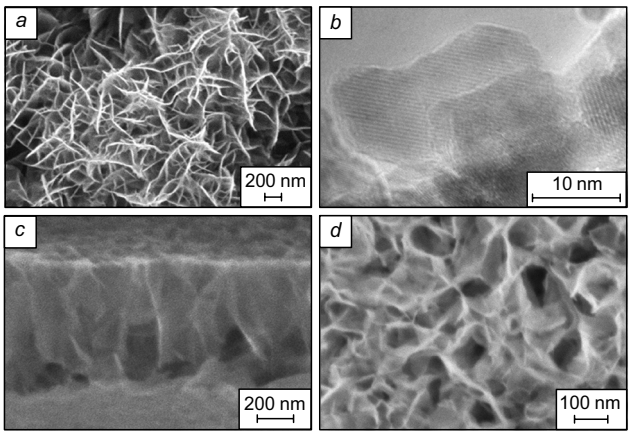

Figure 11. Electron micrographs of arrays of metal oxide and hydroxide nanosheets: SEM (*a*) and TEM images (*b*) of an FeOOH layer formed on the surface of a $FeCl_2$ solution upon treatment with NH_3 gas; (*c*, *d*) SEM images of a layer based on cobalt(II, III) oxide formed on the surface of a $CoCl_2$ solution on treatment with O_3 gas.[162]

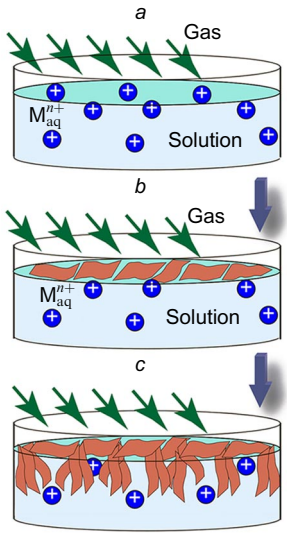

Figure 12. Scheme of the formation of a metal oxide and hydroxide NS layer with predominant orientation by the reaction at the precursor solution/gaseous reactant interface. (*a*, *b*, *c*) stages of the layer formation; for explanation, see text. The Figure was created by the authors using published data.[162]

upon separate supply of reactants to the interface. In the first stage (Fig. 12 *a*), the thin near-surface film of the solution absorbs some amount of the gaseous compound. This may lead to a local change in the pH (for example, when ammonia is absorbed), which induces hydrolysis to give a poorly soluble hydroxide. When ozone is used as the reagent, cations in the solution are oxidized to give metal oxides and hydroxides in a higher oxidation state compared to the dissolved metal ions. In this case, the solution surface acts as a sort of template, which holds crystals due to the surface tension forces and promotes the formation of NSs floating freely on the solution surface (Fig. 12 *b*). In some cases, it is possible to select synthesis conditions in such a way that horizontally aligned nanocrystals form a continuous thin film;[167] in this case, the reaction stops due to restricted access of the reactants. In most cases, a non-continuous network composed of horizontally aligned NSs is formed on the solution surface, and the reaction continues towards the solution bulk through free gaps on the surface. This gives rise to NSs that are mainly perpendicular to the interface (Fig. 12 *c*).

Most often, the layer formed from 2D nanocrystals is 200–800 nm thick, but for some compounds the thickness may reach 1–2 μm. A characteristic feature of the layer formed under these conditions is the presence of stresses caused by composition and structure gradients across the layer. These are mainly packing density and crystal orientation gradients. There is also a gradient of molecular water content, because one side of the layer faces the solution, while the other side, which faces air, can give off water molecules and, due to partial drying, it can become denser. Additionally, it is necessary to take into account the influence of atmospheric gases, first of all, the oxidative action of air oxygen; in some cases, this can give rise to a composition gradient across the layer thickness, which is manifested, for example, as different average oxidation states of metal cations. The last-mentioned factor plays a crucial role for the synthesis of transition metal oxides and hydroxides in different oxidation states, *e.g.*, manganese(II–IV), iron(II, III), cobalt(II, III), cerium(III, IV) and other hydroxyl compounds. Due to the presence of the above-mentioned internal stresses, drying of these layers induces their transformation into rolled-up multiwalled scrolls.

Interesting results were reported by Tolstoy *et al.*,[17, 172] who proposed treating the surface of a drop of an aqueous solution of a metal salt with a gaseous reagent. Ozone treatment of the surface of a 8–20 μL drop of a manganese acetate solution resulted in the formation of the surface network of intricately curved 1–2 μm-wide ribbons, some of which formed a honeycomb network with ~2–3 μm cells (Fig. 13 *a*). Typically, these cells were nearly hexagonal and, more rarely, pentagonal. In the common network structure, these shapes alternated and formed a continuous conjugated sequence similar to the carbon cage network present in fullerenes. It is also important that this ordered network is mainly preserved after the drop is dried.

A SEM examination of the microstructures that were retained on the surface of single-crystalline silicon after drying of the drop showed (Fig. 13 *b–d*) that the ribbons consisted of arrays of nanosheets with a thickness of up to 10 nm, which were mainly perpendicular to the solution/air interface, like in larger solution volumes with a planar surface. According to Tolstoy *et al.*,[17] the thickness of such ribbons ranges from 500 to 900 nm, which corresponds to the surface area of ~0.5 μm^2 for each nanosheet. According to powder X-ray diffraction data, the synthesized solid has the birnessite structure.

Tolstoy *et al.*[17] proposed a hypothesis interpreting the observed formation of ordered networks of poorly soluble compound on the surface of a drop of an aqueous solution on treatment with a gaseous reagent. Probably, in line with the classical views, the first stage of reaction results in the formation of hydrophobic nuclei of manganese oxide nanocrystals, which have equal sizes and charges and are held on the drop by the surface tension forces (Fig. 13 *e*). Due to electrostatic forces, the nuclei are repelled from one another and are located on the surface as far as possible from one another. In the next stage, the crystals grow towards the solution bulk and along the drop surface, while the reactants diffuse to the reaction zone and react near the interface. According to the results of Brune *et al.*,[173] under conditions of diffusion-limited crystallization, periodic structures resembling spherulites or fractal crystals are often formed. The formation of these nanocrystals is also facilitated by the convection currents present in the drop during its partial drying in contact with air, which stir the $Mn(OAc)_2$ solution and lead to averaging of the solution concentration throughout the drop bulk. However, the small drop does not contain a sufficient amount of hydrated manganese ions to form a continuous layer; therefore, in view of the significant surface curvature, the formation of an ordered network of oxide NS arrays on the surface can be observed.

Thus, the processes taking place at the liquid/gas interface during the formation of metal oxide and hydroxide nanosheets include numerous reactions: self-assembly, deposition, hydrolysis, solid phase nucleation, crystallization and diffusion of reactants and reaction products. The morphology, composition and structure of the products are significantly affected not only by characteristics of the multicomponent solution, but also by the vapour pressure of the reactants in the gas mixture. Meanwhile, in the synthesis at the liquid/gas interface, it is possible to use unique non-equilibrium conditions that can hardly be implemented in other systems, namely:

— the solution surface acts in phase transfer reactions as a soft template substrate, which, unlike a hard template, does not need to be subsequently removed;

— in many cases, the use of organic additives can be avoided, which makes the multistage product purification unnecessary;

— it is possible to control the morphology of NSs and the layer formed from NS arrays by controlling the rates of reactant diffusion to the reaction zone;

— the synthesis is carried out under soft chemistry conditions without the use of high-temperature treatments or intricate equipment.

5.4. Synthesis by successive ionic layer deposition

The successive ionic layer deposition method is based on the layer-by-layer synthesis of nanomaterials; its distinctive feature is the use of aqueous solutions of metal salts or polyelectrolytes as the reactants.[174–177] Successive ionic layer deposition (SILD)[174] is also called successive ionic layer adsorption and reaction (SILAR)[178, 179] or layer-by-layer (LbL) method.[180] According to this technique, nanomaterials are obtained by alternating treatment of the

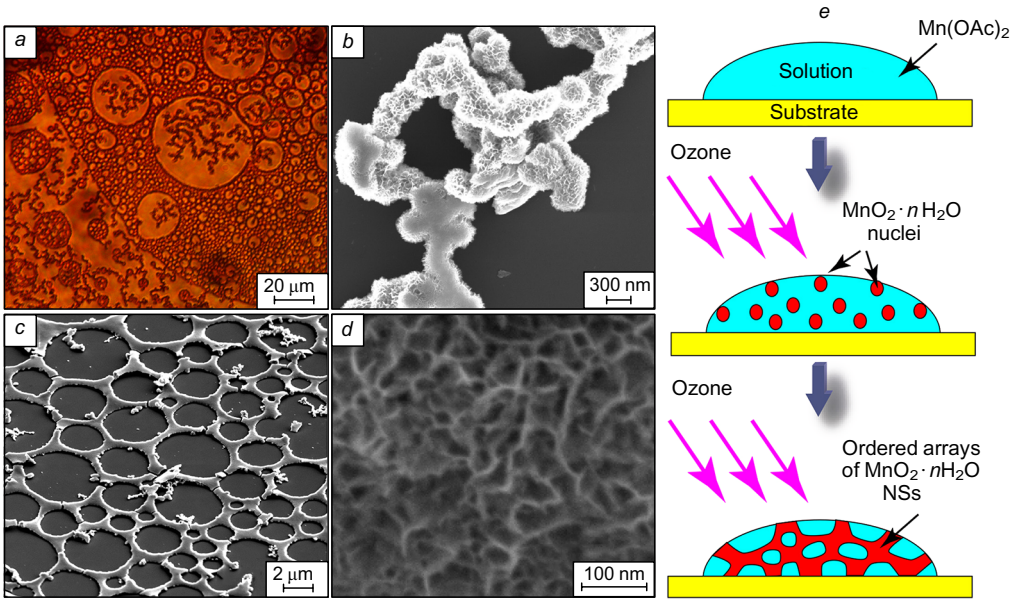

Figure 13. Formation of an ordered network of $MnO_2 \cdot n\,H_2O$ nanosheets on the surface of a droplet of an aqueous solution of $Mn(OAc)_2$ upon treatment with O_3 gas for 10 min. (*a*) optical photograph; (*b–d*) SEM images at different magnifications; (*e*) model of formation of an ordered network of NS arrays on the droplet surface. The images were taken from authors archive to Refs 17 and 172.

substrate with salt solutions and solvents; this results in successive adsorption of cations and anions, which react to form a layer of poorly soluble compound. The treatment conditions are chosen in such a way that the layer obtained after the first cycle serves as a reactive substrate for the next deposition cycle; hence, thickness of the layer increases with increasing number of cycles.

It was noted above that SILD can be used to prepare layers of diverse compounds, including slightly soluble oxides,[181] hydroxides,[21, 24] chalcogenides[182] and fluorides[183] of some transition and noble metals,[184] polymers[185, 186] and hybrid organic-inorganic compounds;[187] among these compounds, there are quite a few 2D nanocrystalline nanosheets.

For example, it was found[28] that the use of aqueous solutions of $Co(NO_3)_2$ and $Na(AlOH)_4$ as reactants results in a nanolayer composed of single 3–5 nm-thick NSs being formed on the solid substrate surface; the nanosheets represent the $Co_2Al(OH)_{7-2x}(CO_3)_x \cdot n\,H_2O$ nanocrystals with a hexagonal crystal structure similar to hydrotalcite. The authors of the cited study believe that on treatment of a polycrystalline nickel foam substrate with a $Co(NO_3)_2$ solution, Co^{2+}_{aq} cations are adsorbed on the surface and, during the subsequent treatment with a $NaAlOH_4$ solution, they react with the $Al(OH)^-_4$ anions to form nuclei of $Co_2Al(OH)_{7-2x}(CO_3)_x \cdot n\,H_2O$ nanocrystals; this is followed by the adsorption of these anions on the substrate and on the mentioned nanocrystal surfaces. The compounds obtained in the first and each subsequent ion deposition cycles serve as template substrates for the next layer. Thus, the layer buildup process is reproduced from one cycle to another.

This synthesis could be expected to give ultrathin NSs on the surface arranged tangentially with respect to the surface and wrapping around the surface roughnesses. However, it turned out that in the sample formed after 50 ion deposition cycles, the nanocrystals were mainly perpendicular to the substrate and formed a sort of arrays. This result was explained in terms of the model of formation of a layer of randomly oriented $Zn_xFe(OH)SO_4 \cdot n\,H_2O$ nanosheets shown in Fig. 14;[20, 188] the model considers the appearance of likely charged ions on the surface of each sheet in each adsorption stage and the consequent appearance of mutual repulsion forces and spatial bending of NSs. When treatment is repeated many times, this results in the formation of arrays of oriented NSs. This model is validated, in particular, by the SEM images of the $Na_xMnO_2 \cdot n\,H_2O$ nanosheets on the silicon surface (Fig. 15)[189] for several samples synthesized using solutions of $Mn(OAc)_2$ and NaClO with different numbers of ionic layer deposition cycles. The NS formation already starts in the fifth cycle (see Fig. 15 *a*) and then, with increasing

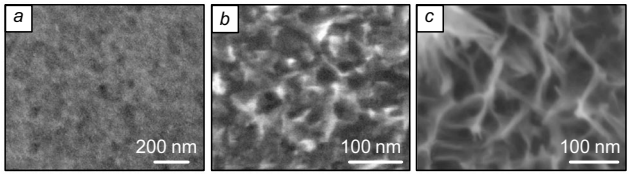

Figure 15. Electron micrographs of the $Na_xMnO_2 \cdot n\,H_2O$ layers synthesized on the silicon single crystal surface by 5 (*a*), 10 (*b*) and 30 (*c*) ionic layer deposition cycles using solutions of $Mn(OAc)_2$ and NaClO. The images were taken from authors archive to Ref. 189.

number of cycles, the density of arrangement of NSs increases (see Fig. 15 *b*,*c*) and they are actually aligned perpendicular to the substrate surface. However, it cannot be ruled out that the NS orientation on the surface changes during air drying of the sample after the synthesis and during evacuation in the scanning electron microscope chamber. Evidently, additional mechanical forces changing the planar geometry of nanosheets can arise in these stages due to the structural and chemical inhomogeneity of NS surface.

A similar effect was described in a study[24] devoted to the SILD synthesis of other inorganic compounds with a layered crystal structure, *e.g.*, nanocrystals of zinc(II) and cobalt(III) LDHs with a hydrotalcite-like crystal lattice. Solutions of cobalt acetate and a mixture of $Zn(NH_3)_4SO_4$ and $K_2S_2O_8$ were used in the synthesis. The authors suggested that after treatment with a solution of the cobalt(II) salt, doubly charged cobalt cations are adsorbed on the substrate surface, while after treatment with a solution of salt mixture, Co^{II} is oxidized to Co^{III} and the $Zn(OH)^{2-}_4$ anions are adsorbed; as a result, $ZnCo^{III}OH$ nanocrystals representing nanosheets with a thickness of 6–9 nm appear on the surface. A TEM examination of these samples showed that NSs consist of single nanocrystals with certain gaps between them, which gives rise to a sort of NS-based holey structures. This leads to increasing specific surface area, which in turn accounts for high capacitance of the electrodes of supercapacitor hybrid batteries based on these materials. In a later study[190] devoted to the synthesis of Zn^{II}-doped MnO_2 nanocrystals using solutions of $Mn(OAc)_2$ and a $ZnSO_4$/NaClO mixture, the formation of arrays of manganese oxide NSs perpendicular to the substrate was also noted.

An original approach to the synthesis of Co^{II}-Co^{III} LDH nanocrystals was proposed by Tolstoy *et al.*,[22] who carried out successive alternating treatment of the substrate with $Co(OAc)_2$ and $NaBH_4$ solutions according to the ionic layer deposition procedure. Under these conditions, during

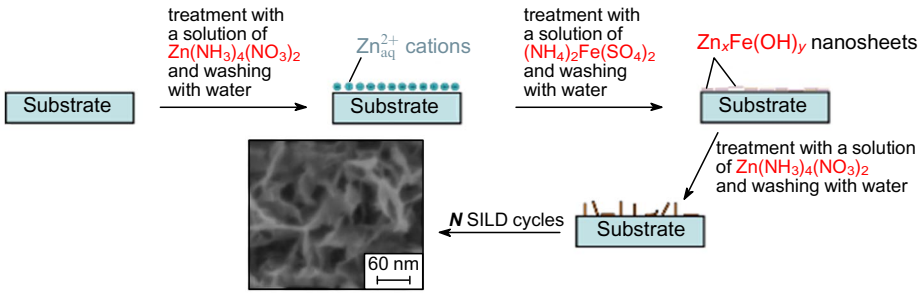

Figure 14. Scheme of the formation of $Zn_xFe(OH)SO_4 \cdot n\,H_2O$ nanosheets on the substrate surface during the ionic layer deposition synthesis involving solutions of $(NH_4)_2Fe(SO_4)_2$ and $Zn(NH_3)_4(NO_3)_2$. The Figure was created by the authors using published data.[20, 188]

treatment with cobalt acetate solution, Co^{II} cations were adsorbed on the surface, while on treatment with $NaBH_4$ solution, these ions were reduced to Co^0. It could be expected that multiple treatment cycles would result in a layer of cobalt metal on the surface. However, as shown by experiments, this did not take place, because during washing with water to remove excess reactant in each stage of the synthesis, the obtained ultrathin layer of Co^0 atoms was oxidized with air oxygen; finally this gave nanocrystals of Co^{II}-Co^{III} LDH as <3 nm-thick nanosheets.

It was shown [191–194] that the successive multiple treatments with solutions of $Bi(NO_3)_3$ and NaHal (Hal = Cl, Br, I) give rise to BiOHal nanosheets on the substrate surface (Fig. 16 *a*), with their thickness being 10–25 nm and the lateral size being up to 1 μm. If a mixture of aqueous solutions of $CuSO_4$ and $Na_2S_2O_3$ and a solution of KSCN are used,[195] arrays of CuSCN nanosheets consisting of 20–30 nm thick nanocrystals with lateral dimensions of up to 3–6 μm are formed (Fig. 16 *b*). It is important that the former of the mentioned nanocrystals exhibit semiconductor properties promising for photovoltaics, while the latter are effective field electron emitters.

The formation of nanocrystals with nanosheet morphology by SILD method was also observed [26] in the synthesis of $NiO_x \cdot n\,H_2O$ layers on the nickel foam surface. The authors used aqueous solutions of $Ni(NO_3)_2$ and $K_2S_2O_8$. In the first stage of the synthesis, Ni^{II} cations were adsorbed on the surface; the excess of these cations was removed by washing of the samples with water. The subsequent treatment with a solution of $K_2S_2O_8$ was accompanied by oxidation of the adsorbed cations to Ni^{III} and then the substrate was washed from the excess of the salt. This sequence of operations formed one SILD cycle; to obtain a practically significant capacitance for a supercapacitor electrode, this cycle was repeated for up to 100 times. Finally, this gave arrays of $NiO_x \cdot n\,H_2O$ nanosheets with a thickness of 6–12 nm oriented perpendicular to the substrate surface. Study of these layers by X-ray diffraction revealed two crystal polymorphs: cubic NiO and orthorhombic γ-NiOOH. The formation of the former type of nanocrystals is attributable to the instability of nanocrystals of the latter type during storage in air.

The formation of nanocrystals with nanosheet morphology in the SILD synthesis was explained by assuming that during growth of the nanocrysrals in an excess of each reactant, selective adsorption of counter-ions can take place on particular nanocrystal facets, resulting in suppression of the adsorption of oppositely charged ions. In this case, it becomes clear why nanocrystalline nanosheets are formed upon this type of synthesis for compounds that have no layered crystal structure, in particular the formation of monoclinic CuO nanosheets as a result of multiple successive treatments of the surface of a copper foil with $Cu(OAc)_2$ and NaOH solutions [196] and the formation of $ZnCo_2O_4$ nanoflakes with the spinel structure upon treatment with solutions of Co^{II} and Zn^{II} ammonia complexes and H_2O_2.[197] Lobinsky and Popkov [198] obtained 6–8 nm-thick Co-Cr LDH nanosheets amorphous to X-rays on a solid substrate by the SILD process. It is important that NSs of this type also form arrays and most of them are perpendicular to the substrate surface.

Thus, it was demonstrated that arrays of oriented nanosheets of oxides and hydroxides of some metals can be obtained relatively easily by soft chemistry methods (actually at room temperature); NSs are arranged on the substrate surface in an ordered fashion and are in close (in particular ohmic) contact with the substrate. While evaluating the potential of possible practical application of these materials, note that this potential has not been fully

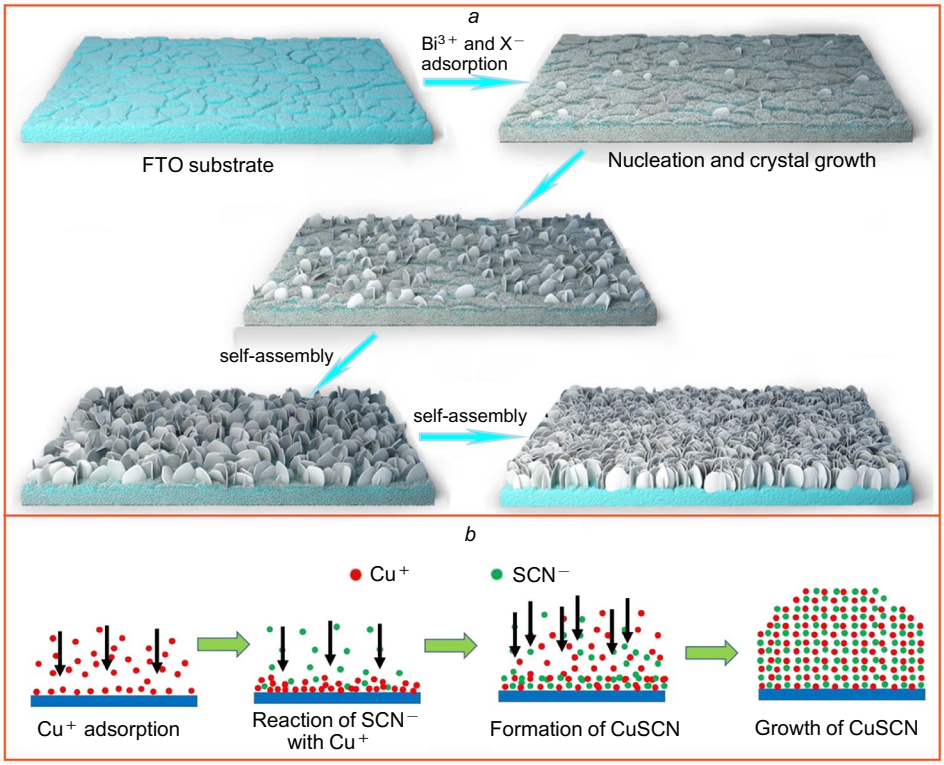

Figure 16. Models of formation of NS arrays on the FTO surface during the surface ionic layer deposition synthesis. (*a*) BiOHal nanosheets (Hal = Cl, Br, I);[194] (*b*) CuSCN nanosheets.[195] Figure *a* is published with permission from Elsevier, Fig. *b* is published with permission from RSC.

implemented as yet, since the layers desctibed in the publications were obtained after several tens of ionic layer deposition cycles, *i.e.*, the number of cycles was meant to reach a thickness required to study the materials by modern physical methods. Meanwhile, the layers that can be obtained as a result of only a few SILD cycles and also objects composed of layers of different composition were left out of consideration. In this respect, this method of synthesis has a great potential for further development.

6. Practically important results of application of nanosheets of metal oxides and hydroxides as parts of functional nanomaterials

The diverse and unique characteristics of NSs and their arrays such as high surface area to volume ratio, the presence of numerous flat interfaces, local charges and structural defects at the interfaces, pronounced anisotropy of properties and the possibility of fine tuning of functional behaviour largely determine the potential applications of metal oxide and hydroxide NSs; furthermore, there is a particular, most efficient application for each type of NSs (Fig. 17 *a*).

In our opinion, the attention paid by the scientific community to 2D materials based on nanocrystals with NS morphology and their practical applications is reflected by the number of relevant papers. Analysis of the data retrieved from the Scopus database using keywords nanosheets (nanoflakes) and oxide (hydroxide), and also the keywords characteristic of each area (*e.g.*, photocatalyst excluding the word graphene) showed that the most popular field is the design of electrodes for new supercapacitors on the basis of nanosheets of metal oxides and hydroxides: currently, there are >2000 publications on this subject (Fig. 17 *b*). Other popular areas include the design of electrodes for water electrolysis units ($\sim$2000 papers), metal ion batteries of various types ($\sim$1600 papers), conductometric gas and electrochemical sensors ($\sim$1500 papers) and photocatalysts ($\sim$1000 papers). Generally, if the studies of electrochemical current sources, production of hydrogen and oxygen by water electrolysis and photocatalysis are assigned to the field of energy engineering, then it can be stated with a high degree of certainty that particularly energy engineering attracts most attention, because there are totally $\sim$7000 publications in related subjects. This conclusion is one more proof of the high practical significance of the studies of 2D materials based on crystals with nanosheet morphology, because it is obvious that the progress in their development can make a significant contribution to solution of many problems, including environmental problems (creation of a carbon-free energy production).

While evaluating the significance of published studies, it is necessary to pay attention to comparative characteristics of the conditions of synthesis of 2D structures; in this respect, we would like to note once again that many of synthetic protocols refer to soft chemistry processes, which enable the preparation of nanomaterials actually at room temperature. It is highly important that most of the active elements of the devices based on 2D nanomaterials (supercapacitors, batteries, electrochemical sensors, air and water purification systems, *etc.*) also function at room temperature (or near room temperature). This attests to the possibility of designing highly efficient functional nanomaterials with low resource consumption and with a minimum impact on the environment.

Before we consider in detail the properties of NSs of various metal oxides and hydroxides applied in each of the fields mentioned above, we would like to note publications in other relevant areas that have not yet received much attention. Some recent reviews are devoted to practical use of metal oxide and hydroxide NSs as substrates for the epitaxial growth of other thin-layer structures,[199] active elements of photoelectrochemical sensors,[200] magnetic materials,[201, 202] dielectric nanomaterials,[203] materials for nanoelectronics,[10] polymeric membranes with improved filtration characteristics,[204] *etc.*

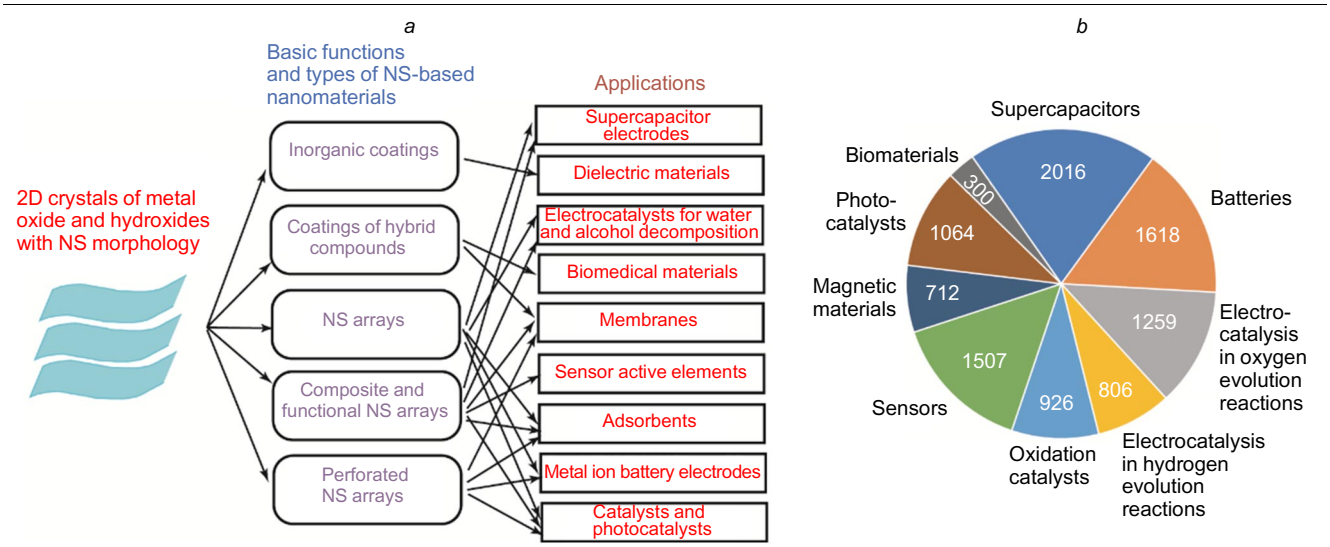

Figure 17. Scheme illustrating the diversity of nanomaterials that can be obtained using 2D nanocrystals with NS morphology and their practical applications (*a*) and distribution chart of the number of publications by subject based on the Scopus database (*b*). For explanation of the procedure used for the search of original publications, see the text; the numerals in the chart are the numbers of articles on each of the subjects.

6.1. Biomedical applications of metal oxide and hydroxide nanosheets

In recent years, 2D materials have been widely used in biomedicine as drug carriers, active elements of biosensors, antibacterial agents, active compounds for biodiagnosis, *etc*. The unique properties of these materials account for their applications for the treatment and diagnosis of cancer, *e.g.*, using photodynamic and photothermal effects, for the treatment of ischemic stroke, for bone tissue repair, *etc*. In addition, they are in demand for environmental protection: 2D crystals are used as parts of gas sensors, waste water treatment materials, sorbents for the absorption of toxic metal traces, CO_2 molecules and other compounds (Fig. 18). There are quite a few publications, including reviews, devoted to various aspects of the application of these 2D materials. Recent publications dealing with the biomedical and environmental applications of metal oxide and hydroxide NSs are considered below, with the focus being placed on the unique properties of the ordered arrays of nanosheets.

Much attention is paid to the cytotoxicity of nanomaterials. Tsukanov *et al.*[205] proposed models for the assessment of toxicity of a number of nanomaterials and confirmed that nanosheets of some layered double hydroxides, graphene, graphene oxide and boron nitride can be safely used for biomedical purposes.

6.1.1. Antibacterial materials

The antibacterial activity of metal oxide and hydroxide NSs is based on several mechanisms of action. One mechanism is related to reactive oxygen species (ROS), which cause oxidative stress and inhibit bacterial metabolism. The contact of the surface of some metal oxides with water under light irradiation induces the generation of ROS. Metal oxide and hydroxide nanopartcicles are able to efficiently generate ROS such as hydrogen peroxide (H_2O_2), superoxide anion (O_2^-) and free radicals such as $OH^{\bullet}$ (Ref. 206). Decomposition of water to give ROS may be associated not only with structural features of NSs (In particular, high activity and surface defects), but also with their photocatalytic properties, which are manifested in some metal oxides and hydroxides on irradiation. Yet another mechanism of antibacterial action is the damage or destabilization of the bacterial cell membrane as a result of direct contact with the nanoparticle. In addition, some nanomaterials based on metal oxides and hydroxides possess oxidase- or peroxidase-like antibacterial activity. The mechanisms of this action are similar to the action mechanisms of peroxidase enzymes, which decompose hydrogen peroxide to form hydroxyl radicals, or oxidase enzymes, which exhibit catalytic activity in the absence of H_2O_2. Some materials based on iron oxides with appropriate characteristics of the photothermal transformation show antibacterial effect under the action of near-IR radiation.[207] A specific morphology, first of all, large highly active surface, makes metal oxide and hydroxide NSs applicable as antibacterial agents.

A review by Mei *et al.*[208] summarizes the results of recent studies of antibacterial agents based on 2D materials, including transition metal dichalcogenides, oxides, carbides and nitrides and nanomaterials based on black phosphorus. Primary attention is devoted to the dominating mechanisms of their antibacterial action. In particular, photocatalytic antibacterial activity manifested under the action of visible light is described for NSs of TiO_2, $Fe_3O_4-TiO_2$ and boron-doped BiOBr; the photothermal effect is established for $MoO_{3-x}-Ag$ nanosheets; and antibacterial action induced by contact with a bacterial cell and release of ROS is inherent in RuO_2.[209] Mention should be made of the synthesis of nano-knife arrays of MnO_2 nanosheets with high activity against Gram-positive and Gram-negative bacteria. It was shown[210] that vertically aligned nanosheets have a higher antibacterial activity than randomly oriented NSs, probably due to damage of the bacterial cell membrane by their sharp edges. Pachaiappan *et al.*[211] surveyed the publications devoted to the antibacterial activity of nanocomposites based on metals and metal oxides; the antibacterial activity of ZnO and TiO_2 nanosheets was specially noted. A number of reviews[212–214] discuss the application potential of materials based on MnO_2 and Mg-Al LDH nanosheets as delivery systems for antibacterial drugs.

In addition to the above reviews, note interesting results indicating the applicability of metal oxide and hydroxide NSs as bactericidal agents. Yan *et al.*[215] studied the mechanisms of antibacterial action of arrays of δ-MnO_2 nanosheets doped with magnesium, sodium and potassium. Due to the synergistic effect of the NS morphology and compo-

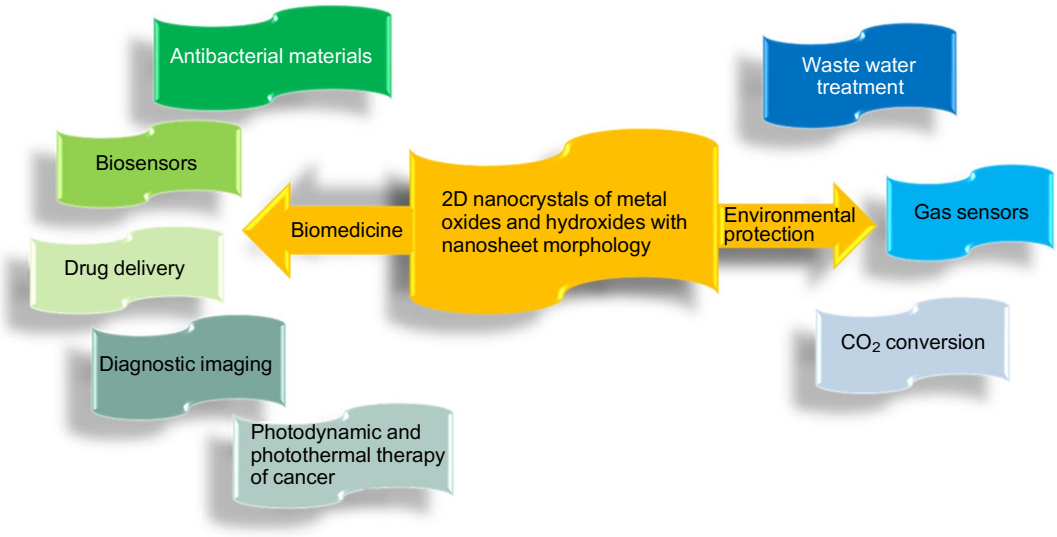

Figure 18. Biomedical and environmental applications of 2D nanocrystals of metal oxides and hydroxides with NS morphology.

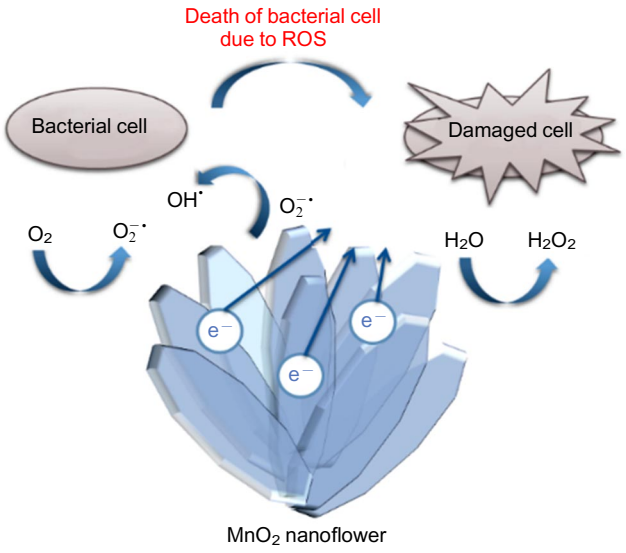

Figure 19. Scheme of antibacterial action of δ-MnO_2 nanosheets. The Figure was created by the authors using published data.[215]

sition, which promoted the generation of free electrons for the formation of ROS, the bacteria were killed even without an external source of light (Fig. 19).

Wang *et al.*,[216] who studied the antibacterial action of arrays of magnesium hydroxide nanoflakes, proposed a mechano-bactericidal description of the direct contact between the $Mg(OH)_2$ nanoflakes and *S. aureus* and *E. coli*. Upon the mechanical contact with NSs, the cell membrane is stretched under the action of surface tension forces; the sharp edges of NSs induce destruction of the bacterial cell membrane. Furthermore, the membrane stretching is accompanied by increasing intracellular level of ROS, which leads to the loss of bacterial viability. Thus, significant deformation of a cell leads to its destruction. It is important that a material based on $Mg(OH)_2$ nanoflakes is biocompatible, and this opens up prospects for its use in bone engineering for the design of biomedical implants. One more benefit of nanoflakes is their ability to create a topography mimicking the natural environment for optimization of adhesion and proliferation of new cells.

Considering characteristics of the materials based on highly ordered arrays of oriented Mg-Fe hydroxide nanosheets (obtained under hydrothermal conditions), Zhang *et al.*[217] noted good prospects for the application of these materials as biomedical implants. In addition to the capability for the photothermal energy conversion under the action of near-IR radiation, the arrays of Mg-Fe LDH nanosheets have a high ion exchange capacity, which allows trapping of active anions (such as Cl^-), and possess a good corrosion resistance.

Considering arrays of MgO nanosheets, Pavithra *et al.*[218] drew the conclusion about the synergistic effect involved in several putative mechanisms of their antibacterial activity. Positively charged magnesium oxide species can contact with the negatively charged cell wall *via* electrostatic attraction; the mechanical deformation and release of Mg^{2+} ions may damage the cell membrane integrity; the subsequent generation of ROS (H_2O_2) induces the oxidative stress, triggers a cascade of reactions involving protein molecules and retards or interrupts the bacterial cell metabolism.

Chen *et al.*[219] noted that nanosheets of Co-V double oxides, which possess oxidase- and peroxidase-like enzymatic activity in combination with high concentration of surface active sites, are promising antibacterial materials.

The optimal reactions conditions to prepare Zn-Al LDH were determined by studying the patterns of oxidation of Al/AlN/Zn composite nanoparticles in water at various temperatures.[220] The obtained nanocomposite was an agglomerate consisting of pseudoboehmite NSs, ZnO and Zn-Al hydroxide plates, together with residual zinc as nanosized inclusions. The antimicrobial activity of the AlOOH/Zn/ZnO/Zn-Al hydroxide nanocomposite in the polymer matrix was demonstrated in relation to Gram-positive and Gram-negative bacteria.

A study of the antibacterial properties of nanocomposites based on zinc and aluminium hydroxides showed, in particular, that the oxidation of Al/Zn bimetallic nanoparticles in a water–ethanol mixture affords porous composites containing boehmite NSs and hexagonal plates enriched with zinc oxide.[221] These composites showed a high antibacterial activity caused, first of all, by the release of Zn^{II} ions into the solution, and the most pronounced antimicrobial action was found for the composites that contained simultaneously AlOOH, Al, ZnO and Zn. In such composites, boehmite NSs ensured the structural stability and electrostatic interaction with bacterial membranes.

An antibacterial effect against the *B. cereus* and *K. Pneumonia* strains was found for Fe_3O_4@Mg-Al hydroxide–ibuprofen and Fe_3O_4@Mg-Al hydroxide–diclofenac composite nanostructures prepared by Yousefi *et al.*[222] The Fe_3O_4 nanospheres coated by Mg-Al LDH nanosheets are able to transport antibiotics inserted into the interlayer space of nanosheets; therefore, these systems can be considered as new drug nanocarriers.

6.1.2. Biosensors

The use of biomarkers plays a key role in early diagnosis of diseases. The electrochemical analytic methods possess high sensitivity; they are convenient for use and cost effective. Metal oxides and hydroxides show a high catalytic activity towards the electrochemical oxidation of glucose. Apart from glucose sensors, these materials are used to develop biosensors for the detection of alkaline phosphatase, glutathione, H_2O_2, H_2S, cancer antigen, *etc.*

Quite a number of reviews on the application of 2D materials in biosensorics and bioelectronics have been published in recent years. However, these publications are focused on materials based on graphene and graphene oxide, MXenes‡ and layered transition metal dichalcogenides. Below we consider examples of application of metal oxide and hydroxide NSs in bioelectronics and biosensorics. According to Chen *et al.*, [223] the most promising materials for this purpose are TiO_2, MnO_2, Nb_6O_{17}, TaO_3, MoO_3 and V_2O_5 nanosheets. It was noted that MoO_3 nanosheets can be used in the electrochemical transistors needed to develop neural interfaces. Murali *et al.*[214] noted the potential applicability of MnO_2 nanosheets in systems for fluorescence detection of glutathione and applicability of Ni-Al and Mg-Al LDH nanoshets in glucose and lactate biosensors, respectively, and to detect small biomolecules. Wang and Liu[224] considered the possibility of using MnO_2, ZnO,

‡ MXenes are layered 2D materials, transition metal carbides, carbonitrides and nitrides, discovered in 2011.

TiO_2, CoOOH and $SnNb_2O_6$ nanosheets as photoelectrochemical biosensors. A review [225] presents classification of modern biosensors, including those designed using metal oxides: CuO is used for glucose sensors, ZnO serves for the detection of cortisol, MoO_3 is applied for determination of bovine serum albumin; and $Na_2Ti_3O_7$ is used to determine Hg^{2+}. The use of arrays of $NiCo_2O_4$ nanoflakes as active elements for glucose, H_2O_2 and urea sensors was discussed by Kumar;[226] the applications of ZnO nanosheets, nanodiscs, nanoflowers and other nanostructures as parts of electrochemical sensors for medical diagnosis are addessed in a a review by Napi *et al.*;[227] and the potential biomedical applications of MnO_2 nanosheets have been considered in a number of studies.[228–230]

New publications dealing with biosensors based on metal oxide and hydroxide NS arrays that have not been discussed previously are analyzed below in more detail. The arrays of Ni-Co and Ni-Fe LDH nanosheets have found use as electrodes for the electrochemical glucose sensors. For example, Shen *et al.*[231] proposed a new electrochemical nonenzymatic glucose sensor consisting of an array of Ni-Co hydroxide nanosheets and gold nanoparticles on copper foam (Ni-Co hydroxide@Au/Cu), which was obtained by galvanic replacement and electrodeposition. Owing to the synergistic effect of three factors — 3D architecture of the copper foam substrate and high electrocatalytic capacities of Au nanoparticles and arrays of Ni-Co hydroxide nanosheets — the Ni-Co hydroxide@Au/Cu electrode shows an electrocatalytic activity towards glucose oxidation in a NaOH solution.

Zhao *et al.*[232] developed an electrode based on hierarchical Ni-Co hydroxide/*CCCH*/CuF nanostructures, where *CCCH* (cobalt copper carbonate hydroxide) is copper-doped cobalt hydroxy carbonate. The material also included arrays of Ni-Co hydroxide nanosheets synthesized by the hydrothermal procedure on the surface of *CCCH* nanorods grown on a CuF substrate. The resulting glucose sensor had high sensitivity, a wide linear range of determination, short response and recovery times, stability, and good reproducibility of results. The cobalt carbonate nanorods synthesized on the surface of carbon fibres under hydrothermal conditions [233] served as the template for the directed growth of arrays of Ni-Fe hydroxide nanosheets. The glucose sensor based on these hierarchical structures had a high electrochemical efficiency towards catalytic oxidation over a large NS surface area and high ion and electron transfer rates. The arrays of Ni-Fe hydroxide nanosheets perpendicular to the substrate, obtained by co-precipitation on an Mxene surface, were used [234] to develop a colorimetric sensor possessing a peroxidase-like activity for the detection of glutathione.

The following structures are applicable for the design of active materials for electrochemical biosensors: arrays of porous $NiMn_2O_4$ nanosheets synthesized [235] on nickel foam by hydrothermal treatment and subsequent high-temperature treatment for glucose determination; arrays of CuO/ZnO nanoflakes self-assembled into nanoflowers for nimesulide detection;[236] $WO_3 \cdot H_2O$ nanosheets obtained by hydrothermal synthesis in combination with nitrogen-doped graphene for the photoelectrochemical detection of the *E. coli* pathogen;[237] and TiO_2/BiOI-based nanocomposites for the enzymatic determination of glucose.[238]

The last-mentioned example will be considered in more detail. Photochemically active TiO_2 nanosheets were formed on an FTO substrate under hydrothermal conditions. To enhance the separation of electron–hole pairs, BiOI was grown on the TiO_2 (101) plane under solvothermal conditions. Then the prepared electrode surface was treated with glucose oxidase (GOx), nafion and chitosan solutions (Fig. 20). Upon light irradiation of the system formed in this way, electrons were generated on the TiO_2 (001) and BiOI facets. They were collected on the TiO_2 (101) facets and transported to the external circuit through the FTO substrate (*i.e.*, they transmitted an electric signal), while the holes generated upon irradiation were transferred to the TiO_2 (001) and BiOI facets and were involved in the enzymatic H_2O_2 decomposition.

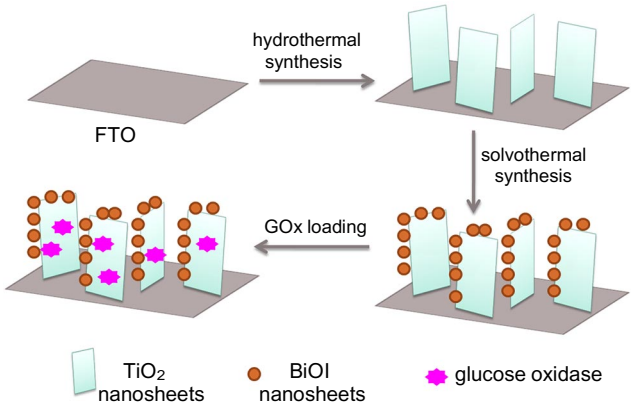

Figure 20. Scheme of fabrication of an electrode based on TiO_2/BiOI/GOx nanosheets. The Figure was created by the authors using published data.[238]

6.1.3. Cancer therapy

The use of 2D materials in the cancer therapy develops along several lines. Owing to their unique properties such as biocompatibility, large surface area and the presence of surface functional groups, metal oxide and hydroxide NSs are promising as drug delivery materials, because the negatively charged species of anticancer drugs can be adsorbed on the positively charged surfaces or embedded in the interlayer spaces of 2D structure. Apart from anticancer drug delovery, these structures can be used as carriers for small interfering RNA for gene therapy.

Considering the photothermal activity, materials based on metal oxides and hydroxides can be used in the cancer therapy for thermal ablation of tumour cells under the action of radiation. As is known, the photothermal therapy (PTT) is based on the fact that cancer cells are killed when the tumour temperature reaches 41–47 °C.[239] However, the application of PTT is limited not only by the penetration depth of the exciting radiation, but also by the thermal damage of the surrounding healthy tissues; therefore, various methods are combined in the cancer therapy to attain the synergistic effect, for example, PTT can be combined with photodynamic therapy (PDT). The latter method is based on the use of photosensitizers, that is, photosensitive materials that absorb light at a definite wavelength and generate ROS upon excitation. The photocatalytic activity is inherent in some metal oxides and hydroxides; for example, some compounds are known to act as anticancer agents and generate ROS by themselves. In addition, two-dimensional NSs with a high surface area to volume ratio may function as nanocarriers for drug delivery to the tumour.

Unlike the normal cell medium, tumour cells are characterized by high concentrations of ROS and glutathione and by lower pH values and reduced concentration of oxygen. High level of ROS may result in a damage of cell membrane, DNA and protein molecules and in reduced concentration of antioxidants. The excess formation of ROS taking place after an ischemic stroke accelerates the neuron death. An important feature of some materials, including those based on metal LDHs is the ability to scavenge ROS, which normalizes the medium.

Combination of unique structural and chemical features of nanosheets (see above) and the possibility of intercalation of rare earth elements with fluorescence and magnetic properties into the interlayer space of the 2D materials brings about prospects for the use of these materials for cancer diagnosis by imaging procedures. The interest in the use of metal oxide and hydroxide NSs in theranostics, which combines diagnostics and therapy, is steadily growing. In the last three years, ~10 reviews on the application of 2D nanomaterials for cancer diagnosis and therapy were published. Examples of application of metal oxide and hydroxide NSs for this purpose were reported.[240–245] Note, in particular, that Fe-Al, Mn-Al and Ni-Ti LDHs have been used in the tumour therapy; this is based on their ability to increase the pH level in the microenvironment of the tumour, which is characterized by higher acidity. The decomposition of alkaline LDHs in the acid medium around the tumour leads to normalization of the pH level. Apart from this, Mn-Fe, Mn-Al and Zn-Al LDH nanosheets, including those doped with gadolinium or ytterbium, and MnO_2 and MoO_3 nanosheets are used for bioimaging in the cancer diagnosis and in drug delivery systems. Nanosheets of MnO_2 can serve as photothermal agents and nanocarriers for photosensitizers in targeted PTT and PDT processes. Manganese dioxide can react with hydrogen peroxide and other ROS in the acidic microenvironment of the tumour to give oxygen and thus to eliminate hypoxia. The nanosheets of Ca-Al LDHs can act as anticancer agents as they generate ROS. A nanocomposite based on $Co_2(OH)_2CO_3$ nanosheets with CeO_2 nanoparticles has a peroxidase activity; hence, it can be used for sensitive immunoassay and cancer marker tests.

Ranathunge *et al.*[246] developed a material for the targeted delivery of the anticancer drug doxorubicin based on the array of magnesium oxide NSs. The therapeutic effect was attained by slow diffusion of the drug and the magnesium ions that are released in the damaged area upon MgO dissolution in an acid medium. Magnesium oxide nanosheets tend to retain the drug in the channels and cavities between the sheets. The layered morphology ensures strong binding and safe transport of molecules to the cancer cells where they are slowly released at a constant rate to maintain the required concentration of the drug.

Nanosheets of $CoO-Co_3O_4$ mixed oxides obtained by green chemistry methods[247] showed antitumour activity and no toxic effect; hence, they can be considered not only as a drug but also as a drug delivery agent.

Shen *et al.*[248] developed a procedure for the preparation of highly defective ultrathin NSs of Co-Mo and Ni-Mo LDHs by hydrothermal synthesis followed by acid treatment. The large number of defects accounts for higher activity of the Co-Mo hydroxide nanosheets on exposure to laser radiation used to generate ROS in comparison with other materials with similar composition. These layered double hydroxides are promising as highly active inorganic photosensitizers for PDT.

Dai *et al.*[249] reported a new multilayer nanomaterial based on arrays of Ti_7O_{13} nanosheets, which can efficiently induce the formation of ROS under the action of X-ray radiation. The resulting nanomaterial had a large specific surface area; therefore, when it was used as a nanocarrier for drug delivery, high loading of the drug was attained. When doxorubicin was delivered using this material, sustained drug release was observed. Thus, arrays of titanium oxide NSs are applicable for the therapy of cancer; they can be used to efficiently combine chemotherapy, radiation therapy and PDT.

The ZnO nanosheets obtained[250] using the aqueous extract of *C. formosum* leaves were active against Gram-negative and Gram-positive bacteria; they inhibited the growth of non-melanoma cancer cells, but had no toxic action on normal cells. The mechanism of activity of ZnO nanosheets hypothesized by the authors is based on the generation of ROS, oxidative stress, inflammation and the subsequent death of cancer cells.

Ji *et al.*[251] synthesized ultrathin biocompatible MgO and Fe_2O_3 nanosheets sandwiched between two identical layers of SiO_2 and Al_2O_3 tetrahedra, which were functionalized with PEG. The obtained material showed a high photothermal efficiency, which makes it suitable as a PTT and PDT agent. It addition, it can strongly modulate the tumour microenvironment by catalyzing H_2O_2 towards the production of O_2 and decomposition of glutathione; this is expected to mitigate hypoxia and reduce the antioxidant properties of the tumour. Functionalized MgO and Fe_2O_3 nanosheets also demonstrated high efficiency in photoacoustic, photothermal and fluorescence imaging.

It is known that in the case of ischaemia reperfusion, potent neuroprotective agents are needed to prevent ROS-induced damage to nerve cells. Wang *et al.*[252] proposed a new agent based on nanosheets of gadolinium-containing Mg-Al LDH. These NSs performed a dual function, acting as both a contrast agent in magnetic resonance imaging examinations and a drug carrier for atorvastatin and ferritin. The prepared biocompatible material not only had a neuroprotective effect, but was also able to scavenge ROS.

Thus, metal oxides and hydroxides are promising for biomedical applications owing to their morphology and unique properties. However, it is important to remember that the efficiency of particles as drug delivery agents depends not only on their size and shape, but also on many other factors (in particular, the chemical composition and charge of the surface and the potential difference).[253] In view of this fact, the design of biomedical products based on metal oxide and hydroxide nanosheets is a challenging multiparametric problem.

6.2. Environmental protection

6.2.1. Conductometric gas sensors

Conductometric gas sensors are widely used for monitoring ambient air quality, determining the composition of exhaust gases, food and cosmetics, for medical diagnosis, for detecting flammable, explosive and toxic gases, *etc*. Metal oxides such as ZnO, In_2O_3, SnO_2 and WO_3 proved to be most in demand for the manufacture of high-efficiency semiconductor gas sensors, as they possess certain benefits, which provide for not only high sensitivity, but also easy manufacture and relatively low cost of the devices. In recent years, NSs and NS arrays of metal oxides and hydroxides

have been actively studied as sensing materials. A lot of examples of this type are described in reviews,[254–257] particularly, arrays of porous ultrathin WO_3 nanosheets were used to detect NO_2 and SO_2; chromium-doped WO_3 nanosheets were found to be suitable for determination of formaldehyde; MoO_3 particles demonstrated hypersensitivity to trimethylamine; ultrathin porous In_2O_3 nanosheets with uniform mesopores showed ultrahigh response to NO_x, O_3 and formaldehyde; porous arrays of Co_3O_4 nanosheets used in a sensor improved characteristics in determination of NH_3 gas; cadmium-doped Co_3O_4 nanosheets promoted NO_2 adsorption and improved the sensor performance, owing to their high electron conductivity and increased concentration of oxygen vacancies; CuO nanosheets deposited on alumina tubes were used to manufacture gas sensors for H_2S detection; SnO_2/ZnO heteronanostructures with NS morphology were used to determine H_2S; nitrogen-doped NiO nanosheets showed enhanced response to NO_2; single-crystalline In_2O_3 nanosheets proved to be promising for the detection of NO_2 and NO; ZnO nanosheets had a high sensitivity to ethanol, butanol, acetone and formaldehyde; and a system based on CdO/ZnO/Yb_2O_3 oxide nanosheets was used to detect ethanol.

Among new studies that were not discussed in the above reviews, the following deserve attention. Zhao *et al.*[258] considered a chemoresistive SO_2 sensor based on the array of $CuSnO_2$ nanosheets. These ultrathin (< 10 nm thick) nanosheets oriented perpendicular to the substrate have a cross-linked structure, while the free space between them provides ideal conditions for gas adsorption–desorption during the measurements. An SO_2 sensor based on Zn-Cr layered double hydroxide NSs was described by Shinde *et al.*[259] Excellent sensing properties of the material were attributed to accelerated diffusion of SO_2 molecules, large number of surface active sites and good transport characteristics caused by mesoporous structure and large surface area. Han *et al.*[260] demonstrated a strategy of particle surface functionalization for WS_2 powder in which WO_3 nanosheets were aligned on the WS_2 nanopowder surface by sonochemical treatment. The WS_2-WO_3 hybrid structures obtained in this way showed excellent gas sensing characteristics towards NO_2 caused by their hierarchical structure, and high stability to environmental impacts. Zhang *et al.*[261] reported a nanocomposite based on arrays of MoO_2 and MoO_3 nanosheets and MXenes; this nanocomposite was suitable for determining low concentrations of ethanol at room temperature. When heterojunctions appeared between MoO_2 and MoO_3 nanosheets, the sensor response was markedly enhanced, and good electrical conductivity and large specific surface area of MXenes provided for the formation of adsorption active sites and reaction centres.

Nanoflowers assembled by porous MoO_3 nanosheets showed excellent performance in the detection of H_2S.[262] Liu *et al.*[263] deposited indium-doped NiO nanosheets on the surface of the montmorillonite clay mineral. The manufactured gas sensor showed high reproducibility of the analytical results and stability of properties due to hybridization with montmorillonite and surface doping, resulting in increasing number of structural defects and increasing electrical conductivity of NiO. Nanoflowers formed by ultrathin Cu-Zn-Al hydroxide nanosheets demonstrated high selectivity and durability of properties when used as NO_2 sensor at room temperature.[264]

6.2.2. Sorbents for waste water treatment and carbon dioxide capture

In recent years, several approaches to purification of domestic waste water have been developed, including methods based on physicochemical (adsorption, filtration, *etc.*), chemical (oxidation, catalysis, *etc.*) and biological processes. Naseem and Durrani[265] surveyed the possible applications of various metal oxide nanoparticles as materials for contaminated water treatment. In particular, ZnO nanosheets were used as effective photocatalysts, and CuO and NiO nanosheets were employed as adsorbents for waste water treatment. Ściezyńska *et al.*[266] focused attention on the use of the most promising 2D materials such as MXenes, Bi_2WO_6 and MOF structures as catalysts for degradation of non-biodegradable compounds in waste water treatment systems. The Bi_2WO_6 nanosheet arrays were modified by adding Cu_2ZnSnS_4 co-catalyst for increasing the photocatalytic activity of the material and for its more effective use for the degradation of organic contaminants under irradiation with visible light. The arrays of Cu^{II}-doped Bi_2WO_6 nanosheets showed better catalytic characteristics in the degradation of norfloxacin compared to undoped Bi_2WO_6.

A new organic-inorganic hybrid nanomaterial based on MnO_2 nanosheets has been developed to be used as a sorbent for simultaneous removal of toxic As^V oxyanions and Pb^{II} cations from water.[267] The obtained material has a very high adsorption capacity and excellent regeneration and recirculation characteristics. Good adsorption properties towards the dye azorubine were found for the nanohybrid based on mesoporous Ni-Zn hydroxide nanoflakes obtained by hydrothermal synthesis.[268] An economical bifunctional adsorbent consisting of Ni-Fe LDH nanoflakes and montmorillonite was also obtained by the hydrothermal method[269] for the simultaneous removal of the anionic dye methyl orange and the cationic dye methylene blue from waste water.

Li *et al.*[270] reported the solvothermal synthesis of structures of Bi_2WO_6 nanosheets vertically grown on the surface of Ta_3N_5 nanofibres. The results of photocatalytic experiments demonstrated that the Bi_2WO_6/Ta_3N_5 system is highly stable and promising as a photocatalyst for the decomposition of toxic antibiotics under the action of visible light; hence, the material can be applicable for the removal of pharmaceutical pollutants from waste water. The material consisting of Fe-Ni LDH and MOF nanosheets obtained by the hydrothermal method proved to be a promising photocatalyst for the degradation of antibiotics;[271] the possibility of using this material for waste water treatment to remove pharmaceutical pollutants is considered.

The increase in the amount of carbon dioxide emissions leads to inevitable global energy and environmental crises.[272] The capture, conversion and storage of CO_2 are challenging tasks that must be solved to preserve the climate. A few papers are devoted to the use of metal oxides and hydroxides in this field. Photocatalysts based on ZnCr LDH nanoflakes collectively grown on $Ti_3C_2T_x$ nanosheets [where T_x is the intercalated tetramethylammonium hydroxide $(CH_3)_4NOH$] were reported by Zhou *et al.*[273] The substrate acts as a co-catalyst by increasing the light absorption intensity, photoinduced electron separation and electron migration efficiency. As a result, the Zn-Cr-hydroxide/$Ti_3C_2T_x$ composite provides enhanced character-

istics of the photocatalytic reduction of CO_2 on exposure to solar light. Zhou *et al.*[274] synthesized NSs in the $Ni-MgO-Al_2O_3$ system for integrated capture and methanation of CO_2. In the first stage, CO_2 is deposited on these nanosheets owing to their dual adsorption and catalytic activity, while in the second stage, hydrogen treatment of the resulting system at high temperature affords methane. Adsorbed CO_2 can directly participate in the reduction, which makes it possible to avoid the energy expenditure for its desorption, which is involved in traditional methods for CO_2 capture, storage and utilization.

Nanoflowers assembled by Ni-Al LDH nanosheets showed a high adsorption capacity in CO_2 capture and also demonstrated a catalytic activity towards CO_2 conversion; therefore, they can be used as a dual-function material providing tandem capture and utilization of carbon dioxide.[275]

6.3. Energy conversion and conservation

The devices for energy conservation and conversion making use of metal oxide and hydroxide NSs include electrochemical devices, first of all, supercapacitors, batteries, electrolytic cells of various types and photoelectric converters. Reviews [276, 277] consider NS-based hybrid supercapacitors and analyze the problems related to the use of layered materials in energy devices, respectively. The key processes taking place on electrodes of some of these devices, namely, supercapacitors and batteries of various types are sketched in Fig. 21.[278] Examples of some metal oxide and hydroxide NS compositions promising for the fabrication of energy storage and conversion devices, their structural and chemical features and preparation methods are summarized in Table 1.

6.3.1. Electrodes of supercapcitors

Supercapacitors are electrochemical energy storage devices in which quasi-reversible charge–discharge processes take place.[283] Upon charging, regions of accumulated charges are formed near the cathode and anode; the sign of the charge is determined by the adsorption of cations or anions from the electrolyte solution. The charge magnitude depends, in particular, on the specific surface area; therefore, it is believed that deposition of NSs on the bulk metal electrodes would increase the capacitance of the supercapacitor.[2] There are two-layer (classical) supercapacitors and pseudo-supercapacitors; in the latter case, energy generation takes place also due to redox reactions on the electrode surface.[5] In addition, in some of these devices, energy is accumulated as a result of partial ion diffusion into the electrode material, for example, lithium ions into niobium oxide (see Fig. 21). The device in which the major contribution to the energy generation is made by both these processes and intercalated ions occupy actually the whole electroactive volume of the electrode are classified as batteries (Fig. 21 *d*). There are also battery–supercapacitor hybrid devices,[284] which usually contain two types of electrodes: one to store energy as a conventional supercapacitor and the other as a metal ion battery.

The assignment of particular devices to one or another type may be based on their current–voltage characteristics

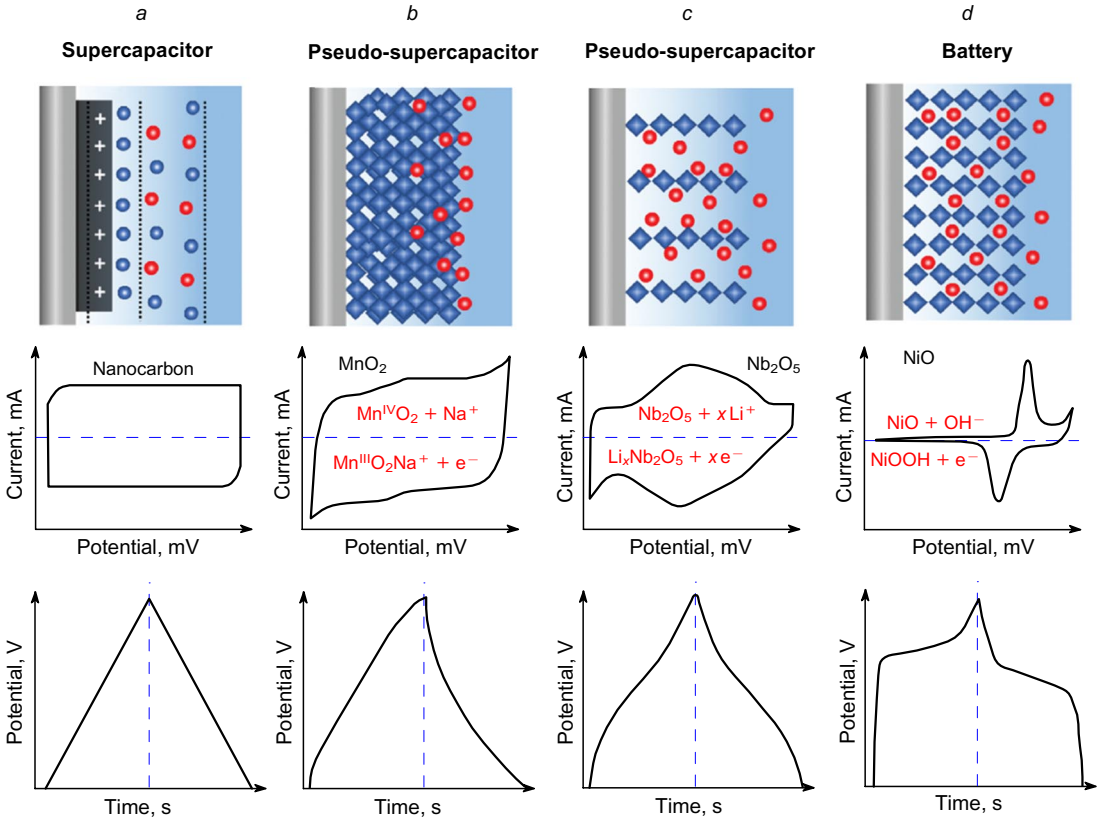

Figure 21. Schemes of processes involving electrodes of two-layer supercapacitor (*a*), pseudo-supercapacitor with electrodes participating in redox reactions (*b*) and ion intercalation reactions (*c*) and a battery with ion intercalation and redox reactions taking place on the electrodes (*d*). The second and third rows below the pictures shows typical current–voltage and charge–discharge curves for each of the devices.[278] Published with permission from Wiley.

Table 1. Compositions, structural and chemical features and preparation methods of materials based on nanosheets promising as electrodes in energy engineering devices.

Nanosheet composition	Synthesis		Nanosheets		Attained characteristics	Ref.
	method	*T*, °C	morphology	thickness, nm		
Fe-Substituted MnO_2	Galvanic reaction in a suspension of MnO_2 nanosheets in a $FeSO_4$ solution	90	–	3–4	At a current density of 200 mA g^{-1}, the specific capacity was 574 mA h g^{-1} after 35 charge–discharge cycles [a]	79
Fe_2O_3, Co_3O_4, Mn_2O_3, $ZnMn_2O_4$, $ZnCo_2O_4$, $NiCo_2O_4$, $CoFe_2O_4$	Solvothermal synthesis in the presence of GO template and ethylene glycol and heat treatment	170 [b] 400 [c]	Perforated nanosheets	20	$ZnMn_2O_4$ nanosheets showed high stability during cycling as anodes of Li ion batteries and $NiCo_2O_4$ were stable as anodes of Na ion batteries	121
$ZnFe_2O_4$	Reprecipitation from a solution in the presence of GO template, Pluronic copolymers, and ethylene glycol and heat treatment	400 [c]	Perforated nanosheets	7–11	At a current density of 3.2 A g^{-1}, the specific capacitance was 420 μA h g^{-1} after 1000 charge–discharge cycles [a]	122
CuO	Precipitation from a solution on the surface of a copper wire under the action of H_2O_2	–	Nanotubes formed by NS arrays	–	At a current density of 100 mA g^{-1}, the specific capacity was 420 mA h g^{-1} after 60 charge–discharge cycles [a]	129
$CoMoO_4$	Hydrothermal synthesis from a solution of $CoNO_3$ and Na_2MoO_4 in the presence of NH_4F, PVP and SiO_2 nanospheres as the template	180	Hollow NS nanostructures	6	At a current density of 500 mA g^{-1}, the specific capacity was 1066 mA h g^{-1} after 200 charge–discharge cycles [a]	130
$Ni(OH)_2$/MnO_2	Oxidation of nickel foam in a solution of $KMnO_4$ at room temperature away from light		Hybrid NSs	2–7	At a current density of 5 A g^{-1}, the specific capacitance was 2937 F g^{-1}, and stability was 92% after 25 000 charge–discharge cycles	136
Co_3O_4/Co-Ni hydroxide	Hydrothermal synthesis from a solution of $Co(NO_3)_2$, $Ni(NO_3)_2$ and HMTA on the foam nickel surface	–	Arrays of oriented NSs	–	At a current density of 0.5 A g^{-1}, the specific capacitance was 2677 F g^{-1}	279
α-$Ni(OH)_2$	Hydrothermal synthesis from a solution of $Ni(NO_3)_2$ and urea on the foam nickel surface	–	Nanoflowers		At a current density of 3 A g^{-1}, the specific capacitance was 2814 F g^{-1}	280
	Microwave synthesis from solutions of $Ni(NO_3)_2$ and urea and ethylene glycol and heat treatment	300	–	1.52	At a current density of 1 A g^{-1}, the specific capacitance was 4172 F g^{-1}; at a current density of 16 A g^{-1}, the specific capacitance was 2680 F g^{-1}	281
CuO	Precipitation from a solution of $CuCl_2$ on treatment with LiOH and hydrothermal treatment	180		50	At a current density of 134 mA g^{-1}, the specific capacity was 841 mA h g^{-1} after 100 charge–discharge cycles [a]	282

Note. In Ref. 121, data for some materials with different composition were obtained; in Ref. 122, polymers with various molecular weights were used for the synthesis. [a] Material with these characteristics is promising for the use in Li ion batteries. [b] Synthesis temperature. [c] Heat treatment temperature.

and charge–discharge curves (see Fig. 21). As compared with batteries, classical (two-layer) supercapacitors have higher power and lower specific capacitance, relatively short charge and discharge times and relatively high cycling stability, even over up to several hundreds of thousands (or more) cycles. The specific capacity of hybrid devices is close to that of batteries, that is, the charge and discharge times are long.

Studies considering metal oxide and hydroxide nanosheets as active elements of electrodes make a significant contribution to the development of highly efficient pseudo-supercapacitors and hybrid devices. Many of NS features are in demand for the design of these devices, such as high specific surface area, large number of defects, the presence of metal cations that can change their oxidation state, *etc*. It is also important that the devices themselves operate, most often, at room temperature; naturally, the synthesis of NS arrays on the electrode surface is also performed at room temperature without the subsequent high-temperature treatment of samples. As a result, it is possible to attain the

highest specific surface area of the electroactive layers of the electrodes.

The practical relevance of supercapacitors is one of the reasons for the enhanced attention they have attracted in recent years.[283] Below we consider some of the studies in which, in our opinion, the most significant results were obtained. First, attention is attracted by the studies devoted to the application of nanosheets of nickel and cobalt oxides and hydroxides as electrode materials for supercapacitors.[285] The choice of these compounds is caused by the fact that they are poorly soluble in aqueous electrolytes with high pH (up to pH 13–14), which is used most often in experiments. Oxyhydroxides of these elements with cations in both lower (2+) and higher (3+) oxidation states are poorly soluble and, therefore, they can be used to fabricate electrodes with a pseudocapacitance effect.

Among the most significant publications in this area is the study by Zhu *et al.*, [281] who showed that supercapacitor electrodes with a specific capacitance of 4172 F g^{-1} at a charge and discharge current of 1 A g^{-1} can be manufactured from the $Ni(OH)_2$ nanosheets with a thickness of <2 nm and lateral dimensions of several micrometres obtained by the microwave method. Characteristics of these electrodes virtually do not change after 2000 charge–discharge cycles. Using the hydrothermal method, Yi *et al.*[280] synthesized NSs of a similar composition with a thickness of a few nanometres and the lateral size of up to 8 μm on a nickel foam surface; the fabricated electrode had a specific capacitance of 2814 F g^{-1} at a current of 3 A g^{-1}. The conditions for the synthesis of Ni-Co LDH nanosheets on the surface of Co_3O_4 2D nanocrystals were described by Zhou *et al.*,[279] who studied the electrochemical properties of these NSs used in electrodes. It was shown that the specific capacitance of the supercapacitor with these electrodes is 2677 F g^{-1} at a current of 0.5 A g^{-1}; they showed high stability during multiple charge–discharge cycles.

Highly promising results were obtained in a study of electrode application of nanosheets prepared by SILD process. In particular, a new method for the synthesis of Co^{II}-Co^{III} LDH NSs was proposed, and they were used to fabricate a supercapacitor with a specific capacitance of 2260 F g^{-1} at 1 A g^{-1} current.[22] According to Lobinsky and Tolstoy,[24] the specific charge of a hybrid capacitor with electrodes based on Zn-Co hydroxide was $\sim$270 mA h g^{-1} at 1 A g^{-1} current, and this value actually did not change after 1000 charge–discharge cycles. In addition, it was shown in the cited studies that the electrochemical characteristics of the electrodes can be optimized; for this purpose, it is necessary to analyze the properties of a series of thin-layer NS structures obtained with different numbers of SILD cycles and to choose the best ones among these structures.

An additional option for the fabrication of highly efficient electrodes is to use composite materials comprising metal nanosheets of both oxides and hydroxides and other substances, including carbon.[283] It is supposed that metal oxides and hydroxides in such a composite would provide for high specific capacitance of the electrode, while other NSs would ensure high conductivity of the layer.[286]

Metal oxide and hydroxide NSs can be used to obtain highly efficient flexible supercapacitors with polymer-based electrodes,[277] which are promising for practical use in so-called wearable electronics.

6.3.2. Electrodes of metal ion batteries

Currently, extensive studies are carried out on the advancement of LIBs and on replacement of LIBs by other metal ion batteries. Among the latter, most attention is perhaps attracted by Zn, Na, Mg, Al and K ion batteries,[287, 288] which have low cost, accessibility of raw material and relatively high expected values of specific capacity (*e.g.*, for Zn ion batteries, it can exceed 800 mA h g^{-1}).[289] Components of these devices are environmentally safe and provide the possibility of designing fairly efficient batteries with aqueous electrolytes.[287, 290] Despite the achievements, there are still a lot of challenges that are to be solved to obtain a commercially competitive product. One of such challenges is to design a cathode material that would withstand both numerous charge–discharge cycles (*i.e.*, metal cation intercalation–deintercalation into the electrode) and extension of the working temperature range with characteristics remaining stable.[291]

It is important that transition metal oxides and hydroxides can be parts of the cathode when aqueous electrolytes are used. Among the diverse compounds of this type, the requirements imposed on cathodes are met, best of all, by compounds with stable crystal structure containing channels for cation diffusion and with high electron conductivity needed for charge compensation on deintercalation. In this respect, attention of researchers has been attracted by layered cobalt, manganese and vanadium oxide crystals and some transition metal phosphate crystals.[278] However, these compounds do not possess high electronic conductivity, which brings about the problem of designing NS arrays that satisfy the above requirements or fabricating composites based on other 2D nanomaterials such as MXenes and carbon compounds such as graphene. It is also evident that porosity of the material is also important for attaining the optimal electrochemical characteristics of the cathodes.

In the context of this review, we will focus on the development of cathodes using particularly NS arrays. Note first of all that these materials substantially differ in morphology from the starting bulk layered materials and were found to show new properties when used for energy storage. First of all, this is due to the fact that the predominant mechanism in this case is adsorption of cations on the NS surface rather than intercalation. This feature accounts for the absence of the plateau in the voltage–capacity curves, characteristic of batteries with electrodes based on layered crystals. It is important that this effect is retained even if the NSs have been restacked, that is, they are first obtained from a bulk crystal and then restacked to form an array. Wang *et al.*[292] prepared layered materials based on Li-Mn oxide by flocculation of MnO_2 nanosheets with lithium ions to form a lamellar structure similar to the $K_{0.45}MnO_2$ structure.[293] It is evident that some disorientation in the NS stacking is retained in the restacked nanosheets. The slope of the voltage–capacity dependence for the restacked Li-Mn oxide was nearly constant for all Li^+ insertion–extraction cycles. This leads to an important conclusion: nanosheets retain their unique properties in the restacked materials; therefore, other new properties differing from the properties of the corresponding bulk crystals can be expected.

Apart from the large specific surface area and more free ion movement, an additional reason for using these NSs for the design of highly efficient batteries is suppression of the change in the electrode volume during the charge–dis-

charge processes. The whole set of the listed features accounts for the electrochemical characteristics that are in demand for many applications. However, it should be borne in mind that the anisotropy of the physical properties of NSs may impair the capacitive performance. For example, a considerable planar distortion of NSs may slow down the ion diffusion kinetics. It was noted above that the rate of ion transport is the highest along the NS plane and side channels. It is important that bent or crumpled NSs become porous when deposited on a substrate; therefore the character of ion transport to the collector changes. Perhaps, this is one of the reasons why experiments with artificially build metal oxide and hydroxide nanosheet structures related to the use of these structures as electrodes for hybrid supercapacitors have not yet got proper attention.

6.3.3. Photocatalysts

Due to the increasing role of energy and resource-saving technologies, the development of renewable energy production acquires an important role. Solar light is converted to electrical current as a result of stimulating photochemical reactions. Large surface areas, the possibility of element doping and functionalization and also unique electrophysical and optical properties of NSs are favourable for their use as, for example, highly efficient photocatalysts and photoelectrocatalysts. Among reactions involving NSs, close attention is paid to the photoelectrochemical water splitting, because it is related to the solution of a global energy problem, namely, harvesting and storage of solar energy. Apart from known photoactive materials such as TiO_2, ZnO, Fe_2O_3, WO_3, $KTaO_3$ and $SrTiO_3$, layered double hydroxides also showed good performance characteristics as light-sensitive catalysts for electrochemical water splitting. The photocatalytic properties of Mg-Al, Ni-Ga, Co-Al, Zn-Al and Ni-Al hydroxides in the oxygen evolution reaction were compared on the basis of theoretical views and experimental data.[294]

Metal oxides and hydroxide nanosheets hold great promise as efficient photoelectrodes for splitting of water molecules. A comparison of the properties of a planar photoelectrode and a 2D nanostructured analogues revealed a number of advantages for the latter:[295]

— improved light absorption due to expansion of the absorption wavelength range and enhancement of interaction with matter *via* multiple reflection – scattering at the interface;

— nanosize effect consisting in a change in the band gap width with a decrease in the NS thickness; as the semiconductor thickness decreases, the conduction band edge shifts towards the hydrogen reduction potential, or valence band edge shifts towards the oxygen oxidation potential, or both phenomena take place;

— the possibility of separating the directions of light absorption and charge carrier collection;

— the ability to generate the internal static electric field in the crystal structure with alternating positively and negatively charged layers promotes the separation of photogenerated charge pairs (electrons and holes);

— the possibility of preferential irradiation of one particular facet of 2D nanocrystal with atom arrangement favourable for the separation of charge pairs, as compared with the irradiation of randomly oriented faces of a polycrystalline planar photoelectrode;

— large surface area and structural disorder reduce the resistance at the interface, which, despite the enhanced surface recombination, generally facilitates charge transfer across this interface.

A review by Haque *et al.*[296] addresses the most promising approaches to the search for photoelectrocatalysts possessing the highest efficiency for solar energy conversion and conservation; this search is performed, in particular, among metal oxides and hydroxides that are formed as NS arrays oriented perpendicular to the substrate. This morphological detail provides great opportunities for surface functionalization. This was demonstrated[297] in relation to the $TiO_2/Au/TiO_2$ photocatalyst, which was functionalized by introducing additional gold nanoparticles between TiO_2 nanosheets.

One more option for increasing the efficiency of photocatalysts, for example for water splitting, is to decrease the NS thickness down to one or several atomic layers; this enables successful control over the physical and chemical properties of these nanosheets.[295] Particular attention is paid to aligning of NSs on solid substrates, which is needed to maximize the benefits of the NS morphology. Ke *et al.*[298] surveyed the prospects of using 2D nanomaterials finctionalized with carbon components for the photoelectrochemical water splitting. Comparative characteristics of 2D materials regarding their use as photo- and electrocatalysts were reported by Qian *et al.*[299] It was noted that under the action of light with energy equal to or greater than the band gap energy, electrons in a photocatalytically active semiconductor are excited and can migrate from the valence band to the conduction band, thus giving rise to holes. Some of the photogenerated electrons and holes move towards the semiconductor surface, while the other recombine with release of energy as heat or photons. Depending on the chemical potentials of photoexcitons, various redox reactions involving particles on the semiconductor surface can take place.

Transition metal oxides such as TiO_2 and ZnO are widely used as disinfectants and photocatalysts in decomposition reactions of water or organic pollutants. However, wide band gaps of these oxides (3.2 – 3.4 eV) restrict light absorption to only UV region. In addition, they are characterized by low charge carrier mobility and high rate of electron – hole recombination, which deteriorate the photocatalytic characteristics. Oxides such as WO_3, MoO_3 and V_2O_5 have rather narrow band gaps (2.6 – 3.0 eV) and good electron transfer characteristics. Their photocatalytic efficiency is reduced due to fast charge recombination and low-energy position of the conduction band, resulting in the inefficient use of photoinduced electrons. A similar behaviour is characteristic of other transition metal oxides with a narrow band gap, *e.g.*, CuO and Fe_2O_3.

Unlike the listed bulk materials, nanosheets of metal oxides and hydroxides possess a number of advantages when used as photocatalysts. The large surface area ensures large number and accessibility of active sites for redox reactions with adsorbed components. The charge migration across the catalyst/electrolyte and catalyst/collector interfaces occurs more easily in these compounds than in bulk catalysts, which results in decreasing interfacial charge transfer resistance and in better kinetics of the photocatalytic process. In addition, significant surface defects and structural disorder of 2D materials affect the charge transfer at the interfaces. The effect of morphology and size factor on the photocatalytic characteristics can be illustrated by the data presented in Table 2. The advantages of metal oxide and hydroxide NSs over bulk materi-

Table 2. Compositions, structural and chemical features, preparation methods and examples of reactions involving photocatalysts based on metal oxide and hydroxide nanosheets.

Nanosheet composition	Synthesis		NS thickness, nm	Photocatalytic reaction	Reference samples	Ref.
	method	T, °C				
TiO_2 (anatase)	Hydrothermal synthesis from a solution of TiF_4 in the presence of surfactants and heat treatment	600 [a]	2	CO_2 reduction and H_2 evolution reactions from a methanol solution under irradiation with a Xe lamp	TiO_2 cuboid (anatase)	300
WO_3	Electrochemical oxidation of W electrode in a $NaNO_3$ solution	–	4 – 5	CO_2 reduction to CH_4 in the presence of H_2O under visible light irradiation (> 420 nm)	Commercial WO_3	301
	Hydrothermal synthesis from a $PbWO_4$ dispersion in the presence of HNO_3	–	25 [b]	Decomposition of rhodamine RhB under irradiation with a Xe lamp with UV filter (> 400 nm)	Commercial WO_3	302
CuO	Oxidation of the copper foil surface in a $(NH_4)_2S_2O_8$/NaOH solution	–	10 – 30	Decomposition of methyl orange under UV irradiation	CuO nanoparticles and nanowires	303
ZnO	Hydrothermal synthesis of a $Zn(MeCOO)_2$ solution in the presence of a surfactant	–	See [b]	Decomposition of rhodamine RhB under irradiation with a Hg lamp	Powdered nanoflowers	304
	Sol – gel synthesis from a solution of $Zn(NO_3)_2$, citric acid and NaOH followed by hydrothermal treatment	–	30	Decomposition of reactive blue14 (KGL) under irradiation with a Hg lamp	Commercial ZnO	305
α-MoO_3	Precipitation from a $(NH_4)_6Mo_7O_{24}$ solution in the presence of organic acid surfactants at 90 °C and heat treatment	500 [a]	20 – 40	Decomposition of rhodamine RhB and methylene blue under solar light irradiation	α-MoO_3 nanorods	306
V_2O_5	Sol – gel synthesis from $VO(OC_2H_5)_3$ in acetylacetone in the presence of surfactant and subsequent heat treatment	500 [a]	See [c]	H_2 evolution from an aqueous methanol solution under irradiation with a Xe lamp with a UV filter (> 400 nm)	Commercial V_2O_5	307

[a] Heat treatment temperature. [b] Nanoflowers. [c] Mesoporous nanosheets NS.

als of the same composition were demonstrated in relation to decomposition of organic dyes or reduction of CO_2 to CH_4 in the presence of H_2O under the action of light.[300 – 307]

It is important that the two-dimensional planar configuration enables the predominant irradiation of facets with a definite arrangement of atoms favourable for the separation of the generated charge pairs. For instance, 2 nm-thick TiO_2 nanosheets with anatase structure have 95% of exposed (100) facets, which are considered to be the most active for photocatalytic reactions. In hydrogen evolution and CO_2 reduction reactions, TiO_2 nanosheets were five times as active as the control TiO_2 cuboids, which have ~53% of exposed (100) facets.[300] The morphology and crystal structure account for the electronic structure of NSs appropriate for photocatalysis and a high surface area with a large number of active sites.

It is known that the width of the band gap and the position of the energy levels of semiconductors depend on their morphology and, in the case of NSs, primarily on their thickness. For example, WO_3 nanosheets with a thickness of 4 – 5 nm have a band gap of 2.79 eV, which is somewhat greater than that in commercial WO_3 (2.63 eV).[301] It is even more important that the conduction band edge of NSs is located at −0.42 eV, in a more negative region than the potential of the reaction

$$CO_2 + 8\,e^- + 8\,H^+ \longrightarrow CH_4 + 2\,H_2O \quad (4)$$

In the opinion of Chen *et al.*,[301] considering this fact, it is possible to estimate the probability of reduction of CO_2 to CH_4 in the presence of H_2O

$$CO_2 + H_2O \longrightarrow CH_4 + O_2 \quad (5)$$

which does not take place when commercial WO_3 with a more positive potential of the conduction band edge (0.05 eV) is used as the catalyst. The role of quantum size effect and morphology for the photocatalytic properties was discussed in relation to CuO nanoparticles with a thickness of 10 – 30 nm synthesized on the surface of a Cu substrate from a solution.[303] The band gap is greater for CuO nanosheet (2.25 eV) than for bulk CuO (1.4 eV) or CuO nanowire (1.85 eV). The photocatalytic activity of the samples with different morphology was estimated from the kinetics of decomposition of methyl orange in solution at room temperature under UV irradiation. It was found that dye decomposition is more than 2 times faster in the presence of the nanosheet photocatalysts. The authors attributed this result to more efficient separation of the photogenerated

electron – hole pairs on the NS surface compared to that on the surface of other types of particles.

It is also noteworthy that the presence of pores that enhance the specific surface area was mentioned [307] as an additional factor increasing the photocatalytic activity of the material. In the authors opinion, the mesoporous structure of V_2O_5 nanosheets promotes more efficient light absorption as a result of multiple light scattering inside the pores.

6.3.4. Electrodes for water electrolysis units

Hydrogen and oxygen production by water electrolysis, which has been a relevant issue for a relatively long time, became especially important in recent years as successful development of this area would enable the solution of some problems of hydrogen energy production and, as a consequence, provide for a decrease in the environmental impact. This is evidenced by the sharp increase in the number of publications on this subject. According to the Scopus database, the search for keywords water and electrolysis gives ~600 relevant papers in 2010, 900 papers in 2015 and >2300 papers in 2021. In our opinion, this interest is due, on the one hand, to the wish to produce hydrogen by this process on a larger industrial scale and, on the other hand, to the fact that new electrocatalysts that reduce the energy costs of electrolysis have recently been proposed. Another important goal is to develop a system for solar energy conversion and storage using solar cells combined with water electrolyzer. In the authors opinion, this design could serve for the production of environmentally benign and renewable fuel for vehicles.

Most often, electrolysis is carried out in either highly acidic or highly alkaline medium, and electrocatalysts are used for oxygen (OER) and hydrogen (HER) evolution reactions. It is clear that development of bifunctional electrocatalysts is of particular importance, because partial dissolution of electrocatalysts and their mutual influence always take place in an electrolyzer in the harsh electrolytic medium. It was found that OER makes the greatest contribution to the overpotential during water electrolysis. This is understandable in view of the fact that decomposition of a water molecule on an electrode to give an oxygen molecules requires an electrocatalytic process accompanied by transfer of four electrons.[308]

Electrocatalysts containing noble metals are most efficient for water electrolysis in acid medium, for example, $Cu_xIrO_y \cdot n\,H_2O$ may serve as an electrocatalyst for OER.[309] In the alkaline region, the most significant results were obtained using electrocatalysts based on Ni-Fe LDH NSs;[310] nanosheets of this composition attract the most attention, as they do not contain noble or toxic elements and generate minimum overpotential on the electrodes. The latter is due to the fact that a local concentration of dissolved molecular oxygen, exceeding the oxygen concentration in the electrolyte bulk, is generated in the electrolyte-filled gaps between the nanosheets. This gives rise to oxygen bubbles at a lower electrode potential. In addition, NSs impart superaerophobic properties to the electrode surface and facilitate the detachment of bubbles from the surface. Additional factors determining the interest in the use of electrocatalysts based on Ni-Fe hydroxide nanosheets is a simpler process design and easier scaling up.

For water electrolysis in an alkaline medium, the electrocatalyst is most often deposited on the surface of a nickel electrode, in particular nickel foam electrode; therefore, the features of synthesis of Ni-Fe hydroxide nanosheets have been studied in most detail exactly for nickel substrates. Currently, virtually all known procedures of synthesis have been tested, including hydrothermal, solvothermal, microwave, chemical precipitation, electrochemical, *etc*. The results have been summarized in reviews.[47, 310]

A few examples that make it possible to evaluate the influence of various types of modification of structural and chemical characteristics of Ni-Fe hydroxide nanosheets on

Table 3. Methods of synthesis, structural and chemical features and overpotentials in OER in an alkaline region on electrodes based on NiFeOH nanosheets.

No	Composition	Preparation method	NS dimensions and morphology	Overpotential (mV) at a current density of 10 mA cm^{-2}	Ref.
1	NiFeOH with a defective crystal structure	Hydrothermal synthesis followed by treatment with a $NaBH_4$ solution	NS array with lateral dimensions of 300 – 400 nm	200	311
2	$Ni_6Fe_2(SO_4)(OH)_{16} \cdot 7\,H_2O$	Hydrothermal synthesis	Nanosheets with a thickness of 3 – 5 nm	212	312
3	NiFeVOH	Hydrothermal synthesis	NS array with lateral dimensions of 400 – 600 nm	192	313
4	$NiFe^{II}Fe^{III}OH$	Chemical precipitation in a solution of a mixture of $FeCl_2$, $Fe(NO_3)_3$, $Ni(NO_3)_2$, NaOH and Na_2SO_3	Nanosheets with a thickness of 2.4 nm	195	314
5	NiFeOH doped with Mn^{2+} ions	Hydrothermal synthesis	NS array with lateral dimensions of 200 – 300 nm	190	315
6	NiFeOH and GO composite	Chemical precipitation	NS array with lateral dimensions of 200 – 500 nm	195	316
7	NiFeOH	Nickel corrosion in a solution of a mixture of $FeCl_3$, $NiCl_2$ and NaCl	Perforated NSs with a thickness of 4 – 20 nm	177	317

OER overpotential, which is a practically significant parameter of their electrocatalytic properties, are given in Table 3. In order to decrease the overpotential when conducting OER, many researchers generated oxygen defects in the crystal structure of NSs, introduced various anions into the interlayer space of the Ni-Fe hydroxide, changed the concentration ratio of nickel and iron atoms in the hydroxide, added other transition metals and so on.

In particular, Xiong *et al.*[311] generated these defects by treating NSs prepared by the hydrothermal method with a $NaBH_4$ solution; this resulted in the removal of some oxygen atoms and gave rise to a unique defective crystal structure. As a result, the overpotential decreased to 200 mV (line 1 in Table 3). The intercalation of SO_4^{2-} anions into the layered structure of double hydroxides has a less pronounced effect on the electrocatalytic properties (see line 2 in Table 3). In this case, the overpotential is 212 mV.[312] Meanwhile, replacement of some of the Ni^{2+} and Fe^{3+} cations in the basal plane with other cations, *e.g.*, Fe^{2+}, V^{4+} or Mn^{2+}, induces more significant changes in the electrocatalytic activity. Indeed, after the introduction of Fe^{2+}cations, the overpotential decreases to 192 mV; after the introduction of V^{3+} cations, it decreases to 195 mV, and Mn^{2+} cations decrease the overpotential to 190 mV. In a number of studies,[312–315] these changes were attributed to increasing lability of electron transitions in the structure, which results in increasing electrical conductivity of the electrocatalyst layer.

The electrical conductivity of this layer can also be increased by insertion of nano-sized particles with a higher conductivity, including carbon particles. A nanocomposite layer consisting of Ni-Fe hydroxide and graphene was obtained by chemical precipitation method; the overpotential was found to be 195 mV.[316] A more pronounced decrease in the overpotential can be attained by preparing the electrocatalyst layer by the procedure proposed by Li *et al.*[317] The greatest decrease in the overpotential (down to 177 mV) was found for perforated NSs. In this case, the specific surface area sharply increases, numerous defects are formed in the crystal structure, and a relatively large number of terminal chemical bonds appear on the basal planes.

Thus, for obtaining practically significant results, thorough investigations in the NS design are required. This is indicated by the above-considered experimental data on the design of highly active electrocatalysts based on metal oxide and hydroxide NSs for water splitting reactions.

7. Conclusion

In relation to metal oxide and hydroxide nanosheets, we demonstrated that a high diversity of building blocks promising for the development of new functional nanomaterials have appeared in the last two decades. These blocks comprise four types of NSs of the indicated compounds: isotropic, anisotropic in the composition or crystal structure, functionalized and perforated. In view of the dependence of NS properties on the morphology and size, it can be stated that even among these types of NSs there are many representatives that significantly differ in properties. It is important that the synthesis in solutions using templates and surfactants may give metal oxide and hydroxide nanosheests with not only layered structure, but also with another crystal or amorphous structure.

Mention should be made of numerous ways to design such NSs and diverse modes of NS packing to form arrays, which may be formed by nanosheets of either a single type or different types. In this respect, it is not surprising that increasing number of new nanomaterials based on metal oxide and hydroxide NSs, exhibiting unique and practically important properties, have recently become available to experimenters.

We would like to emphasize once again that most of the NS syntheses considered in the review are performed under soft chemistry conditions, actually, at room temperature. It is important that nanosheets are practically used as parts of materials for devices that function, as a rule, also at room temperature. Devices of this type include supercapacitors, batteries, electrochemical sensors, water and air treatment systems, *etc*. Evidently, this fact points to the possibility of significantly reducing not only the production cost of these nanomaterials, but also the burden on the environment.

Meanwhile, certain problems of NS synthesis under these conditions also should be mentioned. First of all, note that many compounds (in particular, compounds of most noble metals) with NS morphology have not yet been synthesized. The difficulty to specify exact thickness and lateral dimensions of NSs is also a relevant problem. Only a few methods of synthesis among those considered in the review make it possible to control these parameters to a certain extent. One of such methods is successive ionic layer deposition, which allows targeted and relatively easy control of NS size by specifying the number of treatment cycles of the substrate with the reactants. However, the experience showed that NSs formed in the early stages of this synthesis are fairly difficult to analyze because of their exceptionally small thickness; therefore, the information on the structural and chemical characteristics is still insufficient for experimenters. Another method of this type is the method based on fabrication of nanosheets on the surface of aqueous solutions of precursors under the action of gaseous reactants. The first stages of this synthesis give particularly NSs with the minimum thickness (see Section 5.3.2). However, in this case, there are problems of scalability of the synthesis of these NSs and manufacturing new functional nanomaterials based on them.

One more challenge that should be considered as important is to develop new approaches to convert single NSs into ordered arrays, including those with controlled morphology, for example, with a specified distance between the single NSs and definite spatial orientation of NSs with respect to the substrate. The design of new composite materials based on metal oxide and hydroxide NSs and joint arrays of these NSs with chalcogenide, noble metal, carbon material and other nanosheets are also important tasks. However, analysis of the current state of studies in this area is far beyond the scope of this review. We hope that the material presented in this publication will attract the attention of many specialists in various fields of chemistry, physics and materials science to this new and rapidly developing research area.

This review was prepared with the financial support of the Russian Science Foundation (Project No. 18-19-00370-П).

8. List of abbreviations and symbols

CBD — chemical bath deposition,
CMC — carboxymethylcellulose,
CTAB — cetyltrmethylammonium bromide,
DMAB — 4-dimethylaminobenzaldehyde,
EDA — ethylenediamine,

EDTA — ethylenediaminetetraacetate.
FTO — fluorine-doped tin oxide,
HER — hydrogen evolution reaction,
HMTA — hexamethylantetramine,
ITO — indium tin oxide,
LDH — layered double hydroxide
MOF — metal-organic framework,
NS — nanosheet,
OER — oxygen evolution reaction,
PAA — polyacrylic acid,
PDT — photodynamic therapy,
PTT — photothermal therapy,
PVP — polyvinylpyrrolidone,
PEG — polyethylene glycol,
ROS — reactive oxygen species,
SEM — scanning electron microscopy,
SILD — successive ionic layer deposition,
TEM — transmission electron microscopy,
TMA — tetramethylammonium,
XPS — X-ray photoelectron spectroscopy.

9. References

1. M.Nasilowski, B.Mahler, E.Lhuillier, S.Ithurria, B.Dubertret. *Chem. Rev.*, **116**, 10934 (2016); https://doi.org/10.1021/acs.chemrev.6b00164
2. T.-H.Gu, N.H.Kwon, K.-G.Lee, X.Jin, S.-J.Hwang. *Coord. Chem. Rev.*, **421**, 213439 (2020); https://doi.org/10.1016/j.ccr.2020.213439
3. M.Osada, T.Sasaki. *Adv. Mater.*, **24**, 210 (2012); https://doi.org/10.1002/adma.201103241
4. Y.Qi, M.A.Sadi, D.Hu, M.Zheng, Z.Wu, Y.Jiang, Y.P.Chen. *Adv. Mater.*, **2022**, 2205714 (2022); https://doi.org/10.1002/adma.202205714
5. X.Yu, S.Yun, J.S.Yeon, P.Bhattacharya, L.Wang, S.W. Lee, X.Hu, H.S.Park. *Adv. Energy Mater.*, **8**, 1702930 (2018); https://doi.org/10.1002/aenm.201702930
6. K.Khan, A.K.Tareen, M.Aslam, Y.Zhang, R. Wang, Z.Ouyang, Z.Gou, H.Zhang. *Nanoscale*, **11**, 21622 (2019); https://doi.org/10.1039/C9NR05919A
7. Y.Song, B.Xu, T.Liao, J.Guo, Y.Wu, Z.Sun. *Small*, **17**, 2002240 (2021); https://doi.org/10.1002/smll.202002240
8. A.D.Yapryntsev, A.E.Baranchikov, V.K.Ivanov. *Russ. Chem. Rev.*, **89**, 629 (2020); https://doi.org/10.1070/rcr4920
9. L.A.Aslanov, S.F.Dunaev. *Russ. Chem. Rev.*, **87**, 882 (2018); https://doi.org/10.1070/rcr4806
10. T.Taniguchi, L.Nurdiwijayanto, R.Ma, T.Sasaki. *Appl. Phys. Rev.*, **9**, 021313 (2022); https://doi.org/10.1063/5.0083109
11. I.A.Minich, O.I.Silyukov, S.A.Kurnosenko, V.V.Gak, V.D.Kalganov, P.D.Kolonitskiy, I.A.Zvereva. *Nanomaterials*, **11**, 2708 (2021); https://doi.org/10.3390/nano11102708
12. S.A.Kurnosenko, O.I.Silyukov, I.A.Minich, I.A.Zvereva. *Glass Phys. Chem.*, **47**, 372 (2021); https://doi.org/10.1134/S1087659621040131
13. R.Uppuluri, A.Sen Gupta, A.S.Rosas, T.E.Mallouk. *Chem. Soc. Rev.*, **47**, 2401 (2018); https://doi.org/10.1039/C7CS00290D
14. P.Xiong, R.Ma, G.Wang, T.Sasaki. *Energy Storage Mater.*, **19**, 281 (2019); https://doi.org/10.1016/j.ensm.2018.12.011
15. L.A.Aslanov, G.V.Fetisov, K.A.Paseshnichenko, S.F.Dunaev. *Coord. Chem. Rev.*, **352**, 220 (2017); https://doi.org/10.1016/j.ccr.2017.09.010
16. L.Aslanov, V.Zakharov, K.Paseshnichenko, A.Yatsenko, A.Orekhov, V.Tafeenko, V.Chernyshev. *Pure Appl. Chem.*, **90**, 833 (2018); https://doi.org/10.1515/pac-2017-1105
17. V.P.Tolstoy, N.I.Vladimirova, L.B.Gulina. *ACS Omega*, **4**, 22203 (2019); https://doi.org/10.1021/acsomega.9b03499
18. V.P.Tolstoy, L.B.Gulina, A.A.Golubeva, S.S.Ermakov, V.E.Gurenko, D.V.Navolotskaya, N.I.Vladimirova, A.V.Koroleva. *J. Solid State Electrochem.*, **23**, 573 (2019); https://doi.org/10.1007/s10008-018-04165-6
19. V.P.Tolstoi, L.B.Gulina. *Russ. J. Gen. Chem.*, **83**, 1635 (2013); https://doi.org/10.1134/S1070363213090016
20. V.I.Popkov, V.P.Tolstoy, V.G.Semenov. *J. Alloys Compd.*, **813**, 152179 (2020); https://doi.org/10.1016/j.jallcom.2019.152179
21. V.P.Tolstoy, L.I.Kuklo, L.B.Gulina. *J. Alloys Compd.*, **786**, 198 (2019); https://doi.org/10.1016/j.jallcom.2019.01.324
22. V.P.Tolstoy, A.A.Lobinsky, M.V.Kaneva. *J. Mol. Liq.*, **282**, 32 (2019); https://doi.org/10.1016/j.molliq.2019.02.067
23. A.A.Lobinsky, V.P.Tolstoy. *J. Solid State Chem.*, **270**, 156 (2019); https://doi.org/10.1016/j.jssc.2018.09.041
24. A.A.Lobinsky, V.P.Tolstoy. *RSC Adv.*, **8**, 29607 (2018); https://doi.org/10.1039/C8RA00671G
25. I.Kodintsev, V.Tolstoy, A.Lobinsky. *Mater. Lett.*, **196**, 54 (2017); https://doi.org/10.1016/j.matlet.2017.02.130
26. A.A.Lobinsky, V.P.Tolstoy, L.B.Gulina. *Mater. Res. Bull.*, **76**, 229 (2016); https://doi.org/10.1016/j.materresbull.2015.12.023
27. V.P.Tolstoy, A.A.Lobinsky, O.V.Levin, L.I.Kuklo. *Mater. Lett.*, **139**, 4 (2015); https://doi.org/10.1016/j.matlet.2014.09.134
28. A.A.Lobinsky, V.P.Tolstoy, L.B.Gulina. *Appl. Surf. Sci.*, **320**, 609 (2014); https://doi.org/10.1016/j.apsusc.2014.09.136
29. A.L.Ivanovskii. *Russ. Chem. Rev.*, **81**, 571 (2012); https://doi.org/10.1070/RC2012v081n07ABEH004302
30. N.Mahmood, I.A.De Castro, K.Pramoda, K.Khoshmanesh, S.K.Bhargava, K.Kalantar-Zadeh. *Energy Storage Mater.*, **16**, 455 (2019); https://doi.org/10.1016/j.ensm.2018.10.013
31. R.Ma, T.Sasaki. *Acc. Chem. Res.*, **48**, 136 (2015); https://doi.org/10.1021/ar500311w
32. H.Wang, J.Zhang, X.Hang, X.Zhang, J.Xie, B.Pan, Y.Xie. *Angew. Chem., Int. Ed.*, **54**, 1195 (2015); https://doi.org/10.1002/anie.201410031
33. J.Huang, J.Chen, T.Yao, J.He, S.Jiang, Z.Sun, Q.Liu, W.Cheng, F.Hu, Y.Jiang, Z.Pan, S.Wei. *Angew. Chem., Int. Ed.*, **54**, 8722 (2015); https://doi.org/10.1002/anie.201502836
34. P.Gao, P.Metz, T.Hey, Y.Gong, D.Liu, D.D.Edwards, J.Y.Howe, R.Huang, S.T.Misture. *Nature Commun.*, **8**, 14559 (2017); https://doi.org/10.1038/s41467-017-00705-2
35. S.Rong, K.Li, P.Zhang, F.Liu, J. Zhang. *Catal. Sci. Technol.*, **8**, 1799 (2018); https://doi.org/10.1039/C7CY02121F
36. G.Jia, M.Hupfer, M.Schulz, G.Schmidl, A.Dellith, M.Diegel, R.Müller, J.Dellith, F.Lindner, B.Dietzek-Ivanšić, J.Plentz. *Adv. Mater. Interfaces*, **9**, 2200936 (2022); https://doi.org/10.1002/admi.202200936
37. Z.Sun, T.Liao, Y.Dou, S.M.Hwang, M.S.Park, L.Jiang, J.H.Kim, S.X.Dou. *Nature Commun.*, **5**, 3813 (2014); https://doi.org/10.1038/ncomms5526
38. S.Wendt, P.T.Sprunger, E.Lira, G.K.H.Madsen, Z.Li, J.Hansen, J.Matthiesen, A.Blekinge-Rasmussen, E.Lægsgaard, B.Hammer, F.Besenbacher. *Science*, **320**, 1755 (2008); https://doi.org/10.1126/science.1159846
39. R.Suzuki, Y.Yamauchi, Y.Sugahara. *Dalton Trans.*, **51**, 13145 (2022); https://doi.org/10.1039/D2DT01557A
40. Z.Li, H.Mi, F.Guo, C.Ji, S.He, H.Li, J.Qiu. *Inorg. Chem.*, **60**, 12197 (2021); https://doi.org/10.1021/acs.inorgchem.1c01413
41. R.Elakkiya, S.Mathankumar, G.Maduraiveeran. *Mater. Chem. Phys.*, **269**, 124770 (2021); https://doi.org/10.1016/j.matchemphys.2021.124770
42. F.Feng, J.Wu, C.Wu, Y.Xie. *Small*, **11**, 654 (2015); https://doi.org/10.1002/smll.201402346
43. P.Sun, R.Ma, X.Bai, K.Wang, H.Zhu, T.Sasaki. *Sci. Adv.*, **3**, 1602629 (2017); https://doi.org/10.1126/sciadv.1602629
44. B.Mendoza-Sánchez, Y.Gogotsi. *Adv. Mater.*, **28**, 6104 (2016); https://doi.org/10.1002/adma.201506133

45. S.K.Radha, K.Crowley, B.A.Holler, X.P.A.Gao, W.R.L.Lambrecht, H.Volkova, M.-H.Berger, E.Pentzer, K.G.Pachuta, A.Sehirlioglu. *J. Appl. Phys.*, **129**, 220903 (2021); https://doi.org/10.1063/5.0051093
46. O.V.Almjasheva, V.I.Popkov, O.V.Proskurina, V.V.Gusarov. *Nanosyst. Phys. Chem. Math.*, **13**, 165 (2022); https://doi.org/10.17586/2220-8054-2022-13-2-164-180
47. X.Lu, H.Xue, H.Gong, M.Bai, D.Tang, R.Ma, T.Sasaki. *Nano-Micro Lett.*, **12**, 86 (2020); https://doi.org/10.1007/s40820-020-00454-w
48. J.Yu, Q.Wang, D.O'Hare, L.Sun. *Chem. Soc. Rev.*, **46**, 5950 (2017); https://doi.org/10.1039/C7CS00318H
49. B.Dong, Y.Ju, X.Huang, W.Li, Z.Ali, H.Yin, F.Sheng, Y.Hou. *Nanoscale*, **11**, 5141 (2019); https://doi.org/10.1039/C8NR09492F
50. G.Zhao, J.Li, L.Jiang, H.Dong, X.Wang, W.Hu. *Chem. Sci.*, **3**, 433 (2012); https://doi.org/10.1039/C1SC00722J
51. D.Zhang, Z.Fang, L.Wang, H.Yu, X.Lu, K.Song, J.Teng, W.Yang. *J. Adv. Ceram.*, **11**, 1187 (2022); https://doi.org/10.1007/s40145-022-0592-4
52. J.Yang, Z.Zeng, J. Kang, S.Betzler, C.Czarnik, X.Zhang, C.Ophus, C.Yu, K.Bustillo, M.Pan, J.Qiu, L.W.Wang, H.Zheng. *Nature Mater.*, **18**, 970 (2019); https://doi.org/10.1038/s41563-019-0415-3
53. I.Hussain, D.Mohapatra, G.Dhakal, C.Lamiel, S.G.Mohamed, M.S.Sayed, Y.R.Lee, J.Lee, M.Lee, J.J. Shim. *J. Energy Storage*, **32**, 101871 (2020); https://doi.org/10.1016/j.est.2020.101871
54. W.Wang, S.W.Chee, H.Yan, I.Erofeev, U. Mirsaidov. *Nano Lett*, **21**, 5977 (2021); https://doi.org/10.1021/acs.nanolett.1c00898
55. Q.Yang, Z.Lu, J.Liu, X.Lei, Z.Chang, L.Luo, X.Sun. *Prog. Nat. Sci.*, **23**, 351 (2013); https://doi.org/10.1002/pip.2437
56. T.L.Simonenko, V.M.Ivanova, N.P.Simonenko, E.P.Simonenko, V.G.Sevastyanov, N.T.Kuznetsov. *Russ. J. Inorg. Chem.*, **64**, 1753 (2019); https://doi.org/10.1134/S0036023619140080
57. T.L.Simonenko, V.A.Bocharova, P.Y.Gorobtsov, N.P.Simonenko, E.P.Simonenko, V.G.Sevastyanov, N.T.Kuznetsov. *Russ. J. Inorg. Chem.*, **65**, 1304 (2020); https://doi.org/10.1134/S0036023620090181
58. T.L.Simonenko, V.A.Bocharova, P.Y.Gorobtsov, N.P.Simonenko, A.G.Muradova, E.P.Simonenko, V.G.Sevastyanov, N.T.Kuznetsov. *Russ. J. Inorg. Chem.*, **65**, 1292 (2020); https://doi.org/10.1134/S0036023620090193
59. H.Xie, Z.Li, L.Cheng, A.A.Haidry, J.Tao, Y.Xu, K.Xu, J.Z.Ou. *iScience*, **25**, 103598 (2022); https://doi.org/10.1016/j.isci.2021.103598
60. S.Loy, J.Xiang, W.D.Yang, Y.F.Di, R.D.Zhao, F.F.Wu, D.M.Ma, M.T.Li, J.Li. *J. Alloys Compd.*, **922**, 166286 (2022); https://doi.org/10.1016/j.jallcom.2022.166286
61. K.Yan, M.Sheng, X.Sun, C.Song, Z.Cao, Y.Sun. *ACS Appl. Energy Mater.*, **2**, 1961 (2019); https://doi.org/10.1021/acsaem.8b02067
62. G.Xia, S.Wang. *Ceram. Int.*, **45**, 20810 (2019); https://doi.org/10.1016/j.ceramint.2019.07.068
63. L.Cuéllar-Herrera, E.Arce-Estrada, A.Romero-Serrano, J.Ortiz-Landeros, R.Cabrera-Sierra, C.Tirado-López, A.Hernández-Ramírez, J. López-Rodríguez. *J. Electron. Mater.*, **50**, 5577 (2021); https://doi.org/10.1007/s11664-021-09098-x
64. Y.Zhou, J.Li, Y.Yang, B.Luo, X.Zhang, E.Fong, W.Chu, K.Huang. *J. Alloys Compd.*, **788**, 1029 (2019); https://doi.org/10.1016/j.jallcom.2019.02.328
65. H.Lv, Q.Pan, Y.Song, X.X.Liu, T.Liu. *Nano-Micro Lett.*, **12**, 118 (2020); https://doi.org/10.1007/s40820-020-00451-z
66. E.M.Abebe, M.Ujihara. *ACS Omega*, **7**, 17161 (2022); https://doi.org/10.1021/acsomega.2c00826
67. M.J.Lawrence, A.Kolodziej, P.Rodriguez. *Curr. Opin. Electrochem.*, **10**, 7 (2018); https://doi.org/10.1016/j.coelec.2018.03.014
68. S.Pappu, K.Nanaji, S.Mandati, T.N.Rao, S.K.Martha, S.V.Bulusu. *Batter. Supercaps.*, **3**, 1209 (2020); https://doi.org/10.1002/batt.202000121
69. Z.Lu, L.Qian, Y.Tian, Y.Li, X.Sun, X.Duan. *Chem. Commun.*, **52**, 908 (2016); https://doi.org/10.1039/C5CC08845C
70. K.Ren, X.Wu, H.Zhang, J.G.Li. *Opt. Mater.*, **105**, 109884 (2020); https://doi.org/10.1016/j.optmat.2020.109884
71. Q.Liu, X.Chen, W.Hu, M.Zhang, L.Ding, M.Wang, Q.Qiao, S.Yang. *Solar RRL*, **3**, 1800299 (2019); https://doi.org/10.1002/solr.201800299
72. Z.Wang, Y.Xu, L.Tan, Y.Zhao, Y.F.Song. *Kexue Tongbao/ Chin. Sci. Bull.*, **65**, 547 (2020); https://doi.org/10.1360/TB-2019-0650
73. S.B.Khan, M.M.Rahman, H.M.Marwani, A.M.Asiri, K.A.Alamry. *Nanoscale Res. Lett.*, **8**, 1 (2013); https://doi.org/10.1186/1556-276X-8-377
74. J.S.Chen, J. Liu, S.Z.Qiao, R.Xu, X.W.Lou. *Chem. Commun.*, **47**, 10443 (2011); https://doi.org/10.1039/c1cc13929k
75. B.Su, M.Li, Z.Shi, Q.Lu. *Langmuir*, **25**, 3640 (2009); https://doi.org/10.1021/la803948m
76. K.Nejati, S.Davari, A.Akbari, K.Asadpour-Zeynali, Z.Rezvani. *Int. J. Hydrogen Energy*, **44**, 14842 (2019); https://doi.org/10.1016/j.ijhydene.2019.04.045
77. D.Tichit, G.Layrac, C.Gérardin. *Chem. Eng. J.*, **369**, 302 (2019); https://doi.org/10.1016/j.cej.2019.03.057
78. Y.Oaki, H.Imai. *Angew. Chem. Int. Ed.*, **46**, 4951 (2007); https://doi.org/10.1002/anie.200700244
79. J.Lim, J.M.Lee, B.Park, X.Jin, S.J.Hwang. *Nanoscale*, **9**, 792 (2017); https://doi.org/10.1039/C6NR08614D
80. L.Zhuang, L.Ge, Y.Yang, M.Li, Y.Jia, X.Yao, Z.Zhu. *Adv. Mater.*, **29**, 1606793 (2017); https://doi.org/10.1002/adma.201606793
81. J.S.Chen, Y.L.Tan, C.M.Li, Y.L.Cheah, D.Luan, S.Madhavi, F.Y.C.Boey, L.A.Archer, X.W.Lou. *J. Am. Chem. Soc.*, **132**, 6124 (2010); https://doi.org/10.1021/ja100102y
82. J.S.Chen, M.F.Ng, H.B.Wu, L.Zhang, X.W.Lou. *CrystEngComm*, **14**, 5133 (2012); https://doi.org/10.1039/c2ce25349f
83. G.E.Nyongombe, G.L.Kabongo, L.L.Noto, M.S.Dhlamini. *Int. J. Electrochem. Sci.*, **15**, 4494 (2020); https://doi.org/10.20964/2020.05.33
84. S.M.Pawar, B.S.Pawar, J.H.Kim, O.S.Joo, C.D.Lokhande. *Curr. Appl. Phys.*, **11**, 117 (2011); https://doi.org/10.1016/j.cap.2010.07.007
85. B.Cao, W.Cai, Y.Li, F.Sun, L.Zhang. *Nanotechnology*, **16**, 1734 (2005); https://doi.org/10.1088/0957-4484/16/9/054
86. E.Hosono, S.Fujihara, I.Honma, H.Zhou. *J. Mater. Chem.*, **15**, 1938 (2005); https://doi.org/10.1039/b418955h
87. C.W.Kung, C.Y.Lin, R.Vittal, K.C.Ho. *Sens. Actuators, B: Chem.*, **182**, 429 (2013); https://doi.org/10.1016/j.snb.2013.03.011
88. M.Wang, Q.Li, H.Yu, S.H.Hur, E.J.Kim. *J. Alloys Compd.*, **578**, 419 (2013); https://doi.org/10.1016/j.jallcom.2013.06.065
89. D.P.Dubal, R.Holze. *RSC Adv.*, **2**, 12096 (2012); https://doi.org/10.1039/c2ra21806b
90. D.P.Dubal, V.J.Fulari, C.D.Lokhande. *Microporous Mesoporous Mater.*, **151**, 511 (2012); https://doi.org/10.1016/j.micromeso.2011.08.034
91. D.P.Dubal, D.S.Dhawale, R.R.Salunkhe, V.S.Jamdade, C.D.Lokhande. *J. Alloys Compd.*, **492**, 26 (2010); https://doi.org/10.1016/j.jallcom.2009.11.149
92. D.P.Dubal, G.S.Gund, R.Holze, C.D.Lokhande. *J. Power Sources*, **242**, 687 (2013); https://doi.org/10.1016/j.jpowsour.2013.05.013

93. S.K.Shinde, H.M.Yadav, G.S.Ghodake, A.A.Kadam, V.S.Kumbhar, J.Yang, K.Hwang, A.D.Jagadale, S.Kumar, D.Y.Kim. *Colloids Surf., B: Biointerfaces*, **181**, 1004 (2019); https://doi.org/10.1016/j.colsurfb.2019.05.079
94. A.S.Patil, R.T.Patil, V.J.Fulari. *Mater. Today: Proc.*, **46**, 2340 (2021); https://doi.org/10.1016/j.matpr.2021.04.423
95. M.Park, E.Shin, J.Hong, H.Paik. *J. Korean Phys. Soc.*, **77**, 1248 (2020); https://doi.org/10.3938/jkps.77.1248
96. V.S.Bagal, G.P.Patil, A.B.Deore, P.K.Baviskar, S.R.Suryawanshi, M.A.More, P.G.Chavan. *Chem. Phys. Lett.*, **650**, 7 (2016); https://doi.org/10.1016/j.cplett.2016.02.052
97. C.T.Chang, C.Y.Lin. *RSC Adv.*, **6**, 67428 (2016); https://doi.org/10.1039/C6RA07267D
98. Y.C.Liang, Y.H.Chou. *RSC Adv.*, **10**, 45042 (2020); https://doi.org/10.1039/D0RA08746G
99. S.Chen, G.Yang, H.Zheng. *Electrochim. Acta*, **220**, 296 (2016); https://doi.org/10.1016/j.electacta.2016.10.119
100. V.T.Chebrolu, B.Balakrishnan, I.Cho, J.S.Bak, H.J.Kim. *Dalton Trans.*, **49**, 14432 (2020); https://doi.org/10.1039/D0DT00263A
101. S.M.Ali, E.H.Hussein, O.A.A.Dakhil. *Nano Futures*, **5**, 035001 (2021); https://doi.org/10.1088/2399-1984/ac1dba
102. Y.Zhao, C.J.Wang, W.Gao, B.Li, Q.Wang, L.Zheng, M.Wei, D.G.Evans, X.Duan, D.O'Hare. *J. Mater. Chem. B*, **1**, 5988 (2013); https://doi.org/10.1039/c3tb21059f
103. C.J.Wang, D.O'Hare. *J. Mater. Chem.*, **22**, 21125 (2012); https://doi.org/10.1039/c2jm34669a
104. Y.Ding, J.Xu, L.Chen, J.Yao, S.Dai, J.Wu, T.Hayat, A.Alsaedi. *J. Alloys Compd.*, **787**, 779 (2019); https://doi.org/10.1016/j.jallcom.2019.02.107
105. L.Wang, C.Song, Y.Shi, L.Dang, Y.Jin, H.Jiang, Q.Lu, F.Gao. *Chem. – Eur. J.*, **22**, 5575 (2016); https://doi.org/10.1002/chem.201504569
106. S.Liu, H.Jia, L.Han, J.Wang, P.Gao, D.Xu, J.Yang, S.Che. *Adv. Mater.*, **24**, 3201 (2012); https://doi.org/10.1002/adma.201201036
107. Y.Li, Y.Guo, R.Tan, P.Cui, Y.Li, W.Song. *Mater. Lett.*, **63**, 2085 (2009); https://doi.org/10.1016/j.matlet.2009.06.060
108. Q.Yang, Z.Lu, Z.Chang, W.Zhu, J. Sun, J. Liu, X.Sun, X.Duan. *RSC Adv.*, **2**, 1663 (2012); https://doi.org/10.1039/C1RA01008E
109. B.Singh, V.Polshettiwar. *Nanoscale*, **11**, 5365 (2019); https://doi.org/10.1039/C8NR10119A
110. H.Lutz, V.Jaeger, R.Berger, M.Bonn, J.Pfaendtner, T.Weidner. *Adv. Mater. Interfaces*, **2**, 1500282 (2015); https://doi.org/10.1002/admi.201500282
111. H.Chen, L.Xia, W.Fu, Z.Yang, Z.Li. *Chem. Commun.*, **49**, 1300 (2013); https://doi.org/10.1039/c2cc38293h
112. D.Yao, Y.Chen, R.Jin. *J. Mater. Chem. B*, **3**, 5786 (2015); https://doi.org/10.1039/C5TB00589B
113. K.S.Jang, J.D.Kim. *J. Nanosci. Nanotechnol.*, **11**, 4496 (2011); https://doi.org/10.1166/jnn.2011.3622
114. Z.Lu, J.Zhu, D.Sim, W.Zhou, W.Shi, H.H.Hng, Q.Yan. *Chem. Mater.*, **23**, 5293 (2011); https://doi.org/10.1021/cm202891p
115. H.Zhang, S.Liu. *J. Colloid Interface Sci.*, **485**, 159 (2017); https://doi.org/10.1016/j.jcis.2016.09.041
116. X.Zhang, Y.Zhao, S.Huang, Y.Wu, Z.Mao, X.Wang. *Nanotechnology*, **32**, 015502 (2021); https://doi.org/10.1088/1361-6528/ac238d
117. D.Chen, L.Peng, Y.Yuan, Y.Zhu, Z.Fang, C.Yan, G.Chen, R.Shahbazian-Yassar, J.Lu, K.Amine, G.Yu. *Nano Lett.*, **17**, 3907 (2017); https://doi.org/10.1021/acs.nanolett.7b01485
118. S.Takenaka, S.Uwai, S.Ida, H.Matsune, M.Kishida. *Chem. Lett.*, **42**, 1188 (2013); https://doi.org/10.1246/cl.130587
119. P.Wang, F.He, J.Wang, H.Yu, L.Zhao. *Appl. Surf. Sci.*, **358**, 175 (2015); https://doi.org/10.1016/j.apsusc.2015.06.102
120. H.Huang, G.Zhao, N.Zhang, K.Sun. *Nanoscale*, **11**, 16222 (2019); https://doi.org/10.1039/C9NR04937A
121. L.Peng, P.Xiong, L.Ma, Y.Yuan, Y.Zhu, D.Chen, X.Luo, J.Lu, K.Amine, G.Yu. *Nature Commun.*, **8**, 15139 (2017); https://doi.org/10.1038/ncomms15139
122. L.Peng, Z.Fang, J.Li, L.Wang, A.M.Bruck, Y.Zhu, Y.Zhang, K.J.Takeuchi, A.C.Marschilok, E.A.Stach, E.S.Takeuchi, G.Yu. *ACS Nano*, **12**, 820 (2018); https://doi.org/10.1021/acsnano.7b08186
123. S.M.Babulal, S.M.Chen, R.Palani, K.Venkatesh, A.S.Haidyrah, S.K.Ramaraj, C.C.Yang, C.Karuppiah. *Colloids Surf., A: Physicochem. Eng. Aspects*, **621**, 126600 (2021); https://doi.org/10.1016/j.colsurfa.2021.126600
124. Y.Qin, F.Chen, A.Halder, M.Zhang. *Chem. Eur.*, **5**, 2424 (2020); https://doi.org/10.1002/slct.201904511
125. M.Q.Yang, J.Dan, S.J. Pennycook, X.Lu, H.Zhu, Q.H.Xu, H.J.Fan, G.W.Ho. *Mater. Horizons*, **4**, 885 (2017); https://doi.org/10.1039/C7MH00314E
126. C.Xu, P.Qiu, H.Chen, F.Jiang, X.Wang. *Mater. Lett.*, **242**, 24 (2019); https://doi.org/10.1111/resp.13700_462
127. C.Zhao, C.Chen, F.Du, J. Wang. *RSC Adv.*, **5**, 38533 (2015); https://doi.org/10.1039/C5RA04571A
128. C.Kong, J.Lv, X.Hu, N.Zhao, K.Liu, X.Zhang, G.Meng, Z.Yang, S.Yang. *Mater. Lett.*, **219**, 134 (2018); https://doi.org/10.1016/j.matlet.2018.02.067
129. C.Kong, W.Lu, J.Zong, F.Pu, X.Hu, X.Zhang, Z.Yang, F.Wang, H.Jin. *J. Alloys Compd.*, **849**, 156635 (2020); https://doi.org/10.1016/j.jallcom.2020.156635
130. Y.Wang, Y.Sun, X.Zhang, Y.H.Wen, J.Guo. *RSC Adv.*, **6**, 51710 (2016); https://doi.org/10.1039/C6RA08534B
131. H.Xu, C.Wang, G.He, H.Chen, Y.Du. *Inorg. Chem.*, **61**, 14224 (2022); https://doi.org/10.1021/acs.inorgchem.2c02666
132. H.Yang, Y.Ma, Z.Ni, S.Zexiang, Y.Feng, T.Yu. *J. Nanosci. Nanotechnol.*, **9**, 1496 (2009); https://doi.org/10.1166/jnn.2009.C187
133. T.Ishizaki, S.Lee, K.Teshima. In *Magnesium Alloyss — Corrosion and Surface Treatments*. (Ed. F.Czerwinski). InTech, 2011. P. 261; https://doi.org/10.5772/1427
134. R.Hu, H.Wu, K.Hong. *J. Mater. Res.*, **24**, 187 (2009); https://doi.org/10.1557/JMR.2009.0026
135. A.C.Bouali, M.H.Iuzviuk, M.Serdechnova, K.A.Yasakau, D.Drozdenko, A.Lutz, K.Fekete, G.Dovzhenko, D.C.F.Wieland, H.Terryn, M.G.S.Ferreira, I.A.Zobkalo, M.L.Zheludkevich. *J. Phys. Chem. C*, **125**, 11687 (2021); https://doi.org/10.1021/acs.jpcc.1c02281
136. Z.Ren, J.Li, Y.Ren, S.Wang, Y.Qiu, J.Yu. *Sci. Rep.*, **6**, 20021 (2016); https://doi.org/10.1038/srep20021
137. A.Zavabeti, J.Z.Ou, B.J.Carey, N.Syed, R.Orrell-Trigg, E.L.H.Mayes, C.Xu, O.Kavehei, A.P.O'Mullane, R.B.Kaner, K.Kalantar-Zadeh, T.Daeneke. *Science*, **358**, 332 (2017); https://doi.org/10.1126/science.aao4249
138. F.Lawrenz, P.Lange, N.Severin, J.P.Rabe, C.A.Helm, S.Block. *Langmuir*, **31**, 5836 (2015); https://doi.org/10.1021/acs.langmuir.5b00871
139. P.Atkin, R.Orrell-Trigg, A.Zavabeti, N.Mahmood, M.R.Field, T.Daeneke, I.S.Cole, K.Kalantar-Zadeh. *Chem. Commun.*, **54**, 2102 (2018); https://doi.org/10.1039/C7CC09040D
140. F.Wu, C.Wang, M.H.Wu, K.Vinodgopal, G.P.Dai. *Materials*, **11**, 884 (2018); https://doi.org/10.3390/ma11060884
141. K.Vimalanathan, T.Palmer, Z.Gardner, I.Ling, S.Rahpeima, S.Elmas, J.R.Gascooke, C.T.Gibson, Q.Sun, J. Zou, M.R.Andersson, N.Darwish, C.L.Raston. *Nanoscale Adv.*, **3**, 5785 (2021); https://doi.org/10.1039/D1NA00598G
142. Y.Wang, M.Baharfar, J. Yang, M.Mayyas, M.B.Ghasemian, K.Kalantar-Zadeh. *Appl. Phys. Rev.*, **9**, 021306 (2022); https://doi.org/10.1063/5.0089232
143. M.Fang, D.Han, W.B.Xu, Y.Shen, Y.Lu, P.Cao, S.Han, W.Xu, D.Zhu, W.Liu, J.C.Ho. *Adv. Energy Mater.*, **10**, 2001059 (2020); https://doi.org/10.1002/aenm.202001059

144. C.Hou, M.Zhang, L.Zhang, Y.Tang, H.Wang, Q.Chi. *Chem. Mater.*, **29**, 1439 (2017); https://doi.org/10.1021/acs.chemmater.7b00188
145. Y.Masuda, K.Kato. *Cryst. Growth Des.*, **8**, 275 (2008); https://doi.org/10.1021/cg070345u
146. X.Hu, Y.Masuda, T.Ohji, K.Kato. *J. Cryst. Growth*, **311**, 482 (2009); https://doi.org/10.1016/j.jcrysgro.2008.09.031
147. F.Wang, Y.Yu, X.Yin, P.Tian, X.Wang. *J. Mater. Chem. A*, **5**, 9060 (2017); https://doi.org/10.1039/C7TA01857F
148. F.Wang, X.Yin, X.Wang. *Extrem. Mech. Lett.*, **7**, 64 (2016); https://doi.org/10.1016/j.eml.2016.01.003
149. X.Yin, Y.Shi, Y.Wei, Y.Joo, P.Gopalan, I.Szlufarska, X.Wang. *Langmuir*, **33**, 7708 (2017); https://doi.org/10.1021/acs.langmuir.7b01674
150. F.Wang, J.H.Seo, G.Luo, M.B.Starr, Z.Li, D.Geng, X.Yin, S.Wang, D.G.Fraser, D.Morgan, Z.Ma, X.Wang. *Nature Commun.*, **7**, 10444 (2016); https://doi.org/10.1038/ncomms12052
151. P.Tian, Y.Yu, X.Yin, X.Wang. *Nanoscale*, **10**, 5054 (2018); https://doi.org/10.1039/C7NR09042K
152. F.Wang, X.Wang. *Nanoscale*, **6**, 6398 (2014); https://doi.org/10.1039/c4nr00973h
153. H.Jin, C.Guo, X.Liu, J.Liu, A.Vasileff, Y.Jiao, Y.Zheng, S.-Z.Qiao. *Chem. Rev.*, **118**, 6337 (2018); https://doi.org/10.1021/acs.chemrev.7b00689
154. K.Akatsuka, M.A.Haga, Y.Ebina, M.Osada, K.Fukuda, T.Sasaki. *ACS Nano*, **3**, 1097 (2009); https://doi.org/10.1021/nn900104u
155. R.Ma, T.Sasaki. *Ann. Rev. Mater. Res.*, **45**, 111 (2015); https://doi.org/10.1146/annurev-matsci-070214-021202
156. S.H.Yu, H.Cölfen, J. Hartmann, M.Antonietti. *Adv. Funct. Mater.*, **12**, 541 (2002); https://doi.org/10.1002/1616-3028(20020805)12:8<541::AID-ADFM541>3.0.CO;2-3
157. H.Cölfen. *Top. Current Chem.*, **271**, 1 (2006); https://doi.org/10.1007/128_056
158. D.Kisailus, B.Schwenzer, J.Gomm, J.C.Weaver, D.E.Morse. *J. Am. Chem. Soc.*, **128**, 10276 (2006); https://doi.org/10.1021/ja062434l
159. Y.Oaki, S.Kajiyama, T.Nishimura, T.Kato. *J. Mater. Chem.*, **18**, 4140 (2008); https://doi.org/10.1039/b810399b
160. L.Liu, L.-Q.Yang, H.-W.Liang, H.-P.Cong, J. Jiang, S.-H.Yu. *ACS Nano*, **7**, 1368 (2013); https://doi.org/10.1021/nn305001r
161. V.P.Tolstoy, L.B.Gulina. *Langmuir*, **30**, 8366 (2014); https://doi.org/10.1021/la501204k
162. L.B.Gulina. Doctoral Thesis in Chemical Sciences, St. Petersburg State Technological Institute (Technical University), St. Petersburg, 2022
163. V.A.Drits, B.Lanson, A.C.Gaillot. *Am. Mineral.*, **92**, 771 (2007); https://doi.org/10.2138/am.2007.2207
164. V.P.Tolstoy, L.B.Gulina. *J. Nano Electron. Phys.*, **5**, 01003 (2013)
165. L.B.Gulina, V.P.Tolstoy. *Russ. J. Gen. Chem.*, **84**, 1472 (2014); https://doi.org/10.1134/S1070363214080039
166. V.V.Strykanova, L.B.Gulina, V.P.Tolstoy, E.V.Tolstobrov, D.V.Danilov, I.Skvortsova. *ACS Omega*, **5**, 15728 (2020); https://doi.org/10.1021/acsomega.0c02258
167. L.B.Gulina, V.P.Tolstoy, E.V.Tolstobrov. *Mendeleev Commun.*, **27**, 634 (2017); https://doi.org/10.1016/j.mencom.2017.11.033
168. L.B.Gulina, V.P.Tolstoy, I.A.Kasatkin, Y.V.Petrov. *J. Fluorine Chem.*, **180**, 117 (2015); https://doi.org/10.1016/j.jfluchem.2015.09.002
169. L.B.Gulina, V.P.Tolstoy, I.A.Kasatkin, S.A.Fateev. *J. Mater. Sci.*, **53**, 8161 (2018); https://doi.org/10.1007/s10853-018-2164-0
170. L.B.Gulina, P.O.Skripnyak, V.P.Tolstoy. *Mendeleev Commun.*, **33**, 124 (2023); https://doi.org/10.1016/j.mencom.2023.01.039
171. L.B.Gulina, V.P.Tolstoy, A.A.Solovev, V.E.Gurenko, G.Huang, Y.Mei. *Prog. Nat. Sci.*, **30**, 279 (2020); https://doi.org/10.1016/j.pnsc.2020.05.001
172. V.P.Tolstoy, N.I.Vladimirova, L.B.Gulina. *Mendeleev Commun.*, **29**, 713 (2019); https://doi.org/10.1016/j.mencom.2019.11.039
173. H.Brune, C.Romainczyk, H.Röder, K.Kern. *Nature (London)*, **369**, 469 (1994); https://doi.org/10.1038/369469a0
174. V.P.Tolstoi. *Russ. Chem. Rev.*, **62**, 237 (1993) ; https://doi.org/10.1070/RC1993v062n03ABEH000015
175. S.S.Ermakov, K.G.Nikolaev, V.P.Tolstoy. *Russ. Chem. Rev.*, **85**, 880 (2016); https://doi.org/10.1070/RCR4605
176. V.P.Tolstoy, A.A.Golubeva, E.O.Kolomina, D.V.Navolotskaya, S.S.Ermakov. *J. Anal. Chem.*, **77**, 257 (2022); https://doi.org/10.1134/S1061934822030108
177. S.P.Ratnayake, J.Ren, E.Colusso, M.Guglielmi, A.Martucci, E.Della Gaspera. *Small*, **17**, e2101666 (2021); https://doi.org/10.1002/smll.202101666
178. H.Soonmin. *Appl. Sci.*, **12**, 8184 (2022); https://doi.org/10.3390/app12168184
179. S.I.Sadovnikov. *Russ. Chem. Rev.*, **88**, 571 (2019); https://doi.org/10.1070/RCR4867
180. E.Guzmán, F.Ortega, R.G.Rubio. *Energies*, **15**, 3399 (2022); https://doi.org/10.3390/en15093399
181. L.P.Bogdanova, V.P.Tolstoi. *Prot. Met.*, **27**, 394 (1992); https://doi.org/10.1097/00004424-199205000-00015
182. N.S.Mohamed Mustakim, C.A.Ubani, S.Sepeai, N.Ahmad Ludin, M.A.Mat Teridi, M.A.Ibrahim. *Solar Energy*, **163**, 256 (2018); https://doi.org/10.1016/j.solener.2018.02.003
183. B.S.Zhuchkov, V.P.Tolstoy, I.V.Murin. *Solid State Ionics*, **101 – 103**, 165 (1997); https://doi.org/10.1016/S0167-2738(97)84026-X
184. G.Korotcenkov, L.B.Gulina, B.Cho, V.Brinzari, V.P.Tolstoy. *Pure Appl. Chem.*, **86**, 801 (2014); https://doi.org/10.1515/pac-2013-1102
185. M.Criado-Gonzalez, C.Mijangos, R.Hernández. *Polym.*, **13**, 2254 (2021); https://doi.org/10.3390/polym13142254
186. A.M.Díez-Pascual, A.Rahdar. *Nanomaterials*, **12**, 949 (2022); https://doi.org/10.3390/nano12060949
187. Y.Ko, S.Lee, C.H.Kwon, S.W.Lee, J.Cho. *Adv. Energy Mater.*, **11**, 2002969 (2021); https://doi.org/10.1002/aenm.202002969
188. V.I.Popkov, V.P.Tolstoy. *Surf. Coat. Technol.*, **409**, 126914 (2021); https://doi.org/10.1016/j.surfcoat.2021.126914
189. A.A.Lobinskii. Candidate Thesis in Chemical Sciences, St Petersburg State University, St Petersburg, 2016
190. A.A.Lobinsky, M.V.Kaneva, A.A.Lobinsky, M.V.Kaneva. *Nanosyst. Phys. Chem. Math.*, **12**, 182 (2021); https://doi.org/10.17586/2220-8054-2021-12-2-182-187
191. K.Wang, C.Shao, X.Li, F.Miao, N.Lu, Y.Liu. *Materials (Basel)*, **9**, 28787890 (2016); https://doi.org/10.3390/ma9020090
192. M.Li, L.Li, B.Li, L.Zhai, B.Wang. *Anal. Methods*, **13**, 1803 (2021); https://doi.org/10.1039/D1AY00021G
193. Y.L.Xie, L.F.Guo, C.J.Ben. *Int. J. Electrochem. Sci.*, **17**, 22022 (2022); https://doi.org/10.20964/2022.02.04
194. H.Jia, W.He, B.Zhang, L.Yao, X.Yang, Z.Zheng. *Appl. Surf. Sci.*, **441**, 832 (2018); https://doi.org/10.1016/j.apsusc.2018.02.030
195. G.P.Patil, P.K.Baviskar, V.S.Bagal, R.D.Ladhe, A.B.Deore, M.A.More, B.R.Sankapal, P.G.Chavan. *RSC Adv.*, **6**, 71958 (2016); https://doi.org/10.1039/C6RA16013A
196. S.K.Shinde, D.Y.Kim, G.S.Ghodake, N.C.Maile, A.A.Kadam, D.S.Lee, M.C.Rath, V.J.Fulari. *Ultrason. Sonochem.*, **40**, 314 (2018); https://doi.org/10.1016/j.ultsonch.2017.07.014
197. S.S.Raut, B.R.Sankapal. *J. Colloid Interface Sci.*, **487**, 201 (2017); https://doi.org/10.1016/j.jcis.2016.10.025

198. A.A.Lobinsky, V.I.Popkov. *Mater. Lett.*, **322**, 132472 (2022); https://doi.org/10.1016/j.matlet.2022.132472
199. M.A.Timmerman, R.Xia, P.T.P.Le, Y.Wang, J.E.ten Elshof. *Chem. – Eur. J.*, **26**, 9084 (2020); https://doi.org/10.1002/chem.201905735
200. Y.Zhou, H.Yin, S.Ai. *Coord. Chem. Rev.*, **447**, 214156 (2021); https://doi.org/10.1016/j.ccr.2021.214156
201. A.A.A.Ahmed. *Int. J. Nanosci.*, **19**, 1950039 (2020); https://doi.org/10.1142/S0219581X1950039X
202. X.Song, F.Yuan, L.M.Schoop. *Appl. Phys. Rev.*, **8**, 011312 (2021); https://doi.org/10.1063/5.0038644
203. H.-J.Kim, M.Osada, T.Sasaki. *Jpn. J. Appl. Phys.*, **55**, 1102A3 (2016); https://doi.org/10.7567/JJAP.55.1102A3
204. M.Safarpour, S.Arefi-Oskoui, A.Khataee. *J. Ind. Eng. Chem.*, **82**, 31 (2020); https://doi.org/10.1016/j.jiec.2019.11.002
205. A.A.Tsukanov, B.Turk, O.Vasiljeva, S.G.Psakhie. *Nanomaterials*, **12**, 650 (2022); https://doi.org/10.3390/nano12040650
206. A.A.Meleshko, A.G.Afinogenova, G.E.Afinogenov, A.A.Spiridonova, V.P.Tolstoy. *Rus. J. Infect. Immun.*, **10**, 639 (2020); https://doi.org/10.15789/2220-7619-AIA-1512
207. K.Kaur, S.Reddy, P.Barathe, V.Shriram, U.Anand, J.Prockow, V.Kumar. *Front. Microbiol.*, **12**, 747019 (2021); https://doi.org/10.3389/fmicb.2021.747019
208. L.Mei, S.Zhu, W.Yin, C.Chen, G.Nie, Z.Gu, Y.Zhao. *Theranostics*, **10**, 757 (2020); https://doi.org/10.7150/thno.39701
209. A.Ananth, S.Dharaneedharan, M.S.Gandhi, M.S.Heo, Y.S.Mok. *Chem. Eng. J.*, **223**, 729 (2013); https://doi.org/10.1016/j.cej.2013.03.045
210. F.Alimohammadi, M.Sharifian, N.H.Attanayake, A.C.Thenuwara, Y.Gogotsi, B.Anasori, D.R.Strongin. *Langmuir*, **34**, 7192 (2018); https://doi.org/10.1021/acs.langmuir.8b00262
211. R.Pachaiappan, S.Rajendran, P.L.Show, K.Manavalan, M.Naushad. *Chemosphere*, **272**, 128607 (2021); https://doi.org/10.1016/j.chemosphere.2020.128607
212. R.Davis Jr., R.A.Urbanowski Jr., A.K.Gaharwar. *Curr. Opin. Biomed. Eng.*, **20**, 100319 (2021); https://doi.org/10.1016/j.cobme.2021.100319
213. Y.Chen, C.Tan, H.Zhang, L.Wang. *Chem. Soc. Rev.*, **44**, 2681 (2015); https://doi.org/10.1039/C4CS00300D
214. A.Murali, G.Lokhande, K.A.Deo, A.Brokesh, A.K.Gaharwar. *Mater. Today*, **50**, 276 (2021); https://doi.org/10.1016/j.mattod.2021.04.020
215. Y.Yan, N.Jiang, X.Liu, J. Pan, M.Li, C.Wang, P.H.C.Camargo, J.Wang. *Front. Bioeng. Biotechnol.*, **9**, 788574 (2022); https://doi.org/10.3389/fbioe.2021.788574
216. G.Wang, W.Jiang, S.Mo, L.Xie, Q.Liao, L.Hu, Q.Ruan, K.Tang, B.Mehrjou, M.Liu, L.Tong, H.Wang, J.Zhuang, G.Wu, P.K.Chu. *Adv. Sci. (Weinh)*, **7**, 1902089 (2020); https://doi.org/10.1002/advs.201902089
217. D.Zhang, J.Zhou, F.Peng, J.Tan, X.Zhang, S.Qian, Y.Qiao, Y.Zhang, X.Liu. *J. Mater. Sci. Technol.*, **105**, 57 (2022); https://doi.org/10.1007/s10853-022-07754-z
218. S.Pavithra, B.Mohana, M.Mani, P.E.Saranya, R.Jayavel, D.Prabu, S.Kumaresan. *J. Inorg. Organomet. Polym. Mater.*, **31**, 1120 (2021); https://doi.org/10.1007/s10904-020-01772-7
219. C.Chen, Y.Wang, D.Zhang, J.Wang. *J. Ind. Eng. Chem.*, **105**, 291 (2022); https://doi.org/10.1016/j.jiec.2021.09.034
220. S.S.Timofeev, A.S.Lozhkomoev, S.O.Kazantsev, I.N.Tikhonova, M.I.Lerner. *Russ. J. Phys. Chem. A*, **95**, 1043 (2021); https://doi.org/10.1134/S0036024421050265
221. A.S.Lozhkomoev, O.V.Bakina, E.A.Glazkova, N.V.Svarovskaya, M.I.Lerner. *Russ. J. Phys. Chem. A*, **92**, 2530 (2018); https://doi.org/10.1134/S0036024418120270
222. V.Yousefi, V.Tarhriz, S.Eyvazi, A.Dilmaghani. *J. Nanobiotechnol.*, **18**, 155 (2020); https://doi.org/10.1186/s12951-020-00718-y
223. F.Chen, Q.Tang, T.Ma, B.Zhu, L.Wang, C.He, X.Luo, S.Cao, L.Ma, C.Cheng. *InfoMat.*, **4**, e12299 (2022); https://doi.org/10.1002/inf2.12299
224. J.Wang, Z.Liu. *TrAC Trends Anal. Chem.*, **133**, 116089 (2020); https://doi.org/10.1016/j.trac.2020.116089
225. A.P.Dral, J.E.ten Elshof. *Sens. Actuators, B*, **272**, 369 (2018); https://doi.org/10.1016/j.snb.2018.05.157
226. R.Kumar. *Nano-Micro Lett.*, **12**, 122 (2020); https://doi.org/10.1007/s40820-020-00462-w
227. M.L.M.Napi, S.M.Sultan, R.Ismail, K.W.How, M.K.Ahmad. *Materials*, **12**, 2985 (2019); https://doi.org/10.3390/ma12182985
228. Y.Chen, H.Cong, Y.Shen, B.Yu. *Nanotechnology*, **31**, 202001 (2020); https://doi.org/10.1088/1361-6528/ab6fe1
229. M.Wu, P.Hou, L.Dong, L.Cai, Z.Chen, M.Zhao, J.Li. *Int. J. Nanomed.*, **14**, 4781 (2019); https://doi.org/10.2147/IJN.S207666
230. H.Y.Xia, B.Y.Li, Y.Zhao, Y.H.Han, S.B.Wang, A.Z.Chen, R.K.Kankala. *Coord. Chem. Rev.*, **464**, 214540 (2022); https://doi.org/10.1016/j.ccr.2022.214540
231. M.Shen, W.Li, L.Chen, Y.Chen, S.Ren, D.Han. *Anal. Chim. Acta*, **1177**, 338787 (2021); https://doi.org/10.1016/j.aca.2021.338787
232. Z.Zhao, Y.Sun, J.Song, Y.Li, Y.Xie, H.Cui, W.Gong, J.Hu, Y.Chen. *Sens. Actuators, B*, **326**, 128811 (2021); https://doi.org/10.1016/j.snb.2020.128811
233. D.Song, L.Wang, B.Wang, J.Yu, Y.Li, Y.Qu, C.Duan, Y.Yang, X.Miao. *Int. J. Electrochem. Sci.*, **15**, 1949 (2020); https://doi.org/10.20964/2020.03.04
234. H.Li, Y.Wen, X.Zhu, J.Wang, L.Zhang, B.Sun. *ACS Sustain. Chem. Eng.*, **8**, 520 (2020); https://doi.org/10.1021/acssuschemeng.9b05987
235. J.Zhang, Y.Sun, X.Li, J.Xu. *Sci. Rep.*, **9**, 18121 (2019); https://doi.org/10.1038/s41598-019-49375-8
236. N.Nataraj, T.W.Chen, Z.W.Gan, S.M.Chen, B.S.Lou, M.A.Ali, F.M.Al-Hemaid. *Mater. Today Chem.*, **24**, 100768 (2022); https://doi.org/10.1016/j.mtchem.2021.100768
237. D.Jiang, C.Yang, Y.Fan, H.M.Polly Leung, I.Kiao, Y.Zhang, Z.Li, M.Yang. *Biosens. Bioelectron.*, **183**, 113214 (2021); https://doi.org/10.1016/j.bios.2021.113214
238. B.Wu, Z.Cheng, Y.Hou, Q.Chen, X.Wang, B.Qiao, D.Chen, J.Tu. *RSC Adv.*, **12**, 19495 (2022); https://doi.org/10.1039/D2RA03070E
239. Y.Ren, Y.Yan, H.Qi. *Adv. Colloid Interface Sci.*, **308**, 102753 (2022); https://doi.org/10.1016/j.cis.2022.102753
240. M.Wu, X.Niu, R.Zhang, Z.Ping Xu. *Adv. Drug Deliv. Rev.*, **187**, 114360 (2022); https://doi.org/10.1016/j.addr.2022.114360
241. J.Wen, K.Yang, J.Huang, S.Sun. *Mater. Des.*, **198**, 109298 (2021); https://doi.org/10.1016/j.matdes.2020.109298
242. M.J.Molaei. *J. Drug Deliv. Sci. Technol.*, **61**, 101830 (2021); https://doi.org/10.1016/j.jddst.2020.101830
243. L.Cheng, X.Wang, F.Gong, T.Liu, Z.Liu. *Adv. Mater.*, **32**, 1902333 (2020); https://doi.org/10.1002/adma.201902333
244. Z.Mohammadpour, K.Majidzadeh-A. *ACS Biomater. Sci. Eng.*, **6**, 1852 (2020); https://doi.org/10.1021/acsbiomaterials.9b01894
245. N.Alizadeh, A.Salimi. *J. Nanobiotechnol.*, **19**, 26 (2021); https://doi.org/10.1186/s12951-021-00771-1
246. T.A.Ranathunge, D.G.G.P.Karunaratne, R.M.G.Rajapakse, D.L.Watkins. *Nanomaterials*, **9**, 208 (2019); https://doi.org/10.3390/nano9020208
247. M.Raeisi, H.Q.Alijani, M.Peydayesh, M.Khatami, F.Bagheri Baravati, F.Borhani, M.Šlouf, S.Soltaninezhad. *Bioprocess Biosyst. Eng.*, **44**, 1423 (2021); https://doi.org/10.1007/s00449-021-02518-6
248. W.Shen, T.Hu, X.Liu, J.Zha, F.Meng, Z.Wu, Z.Cui, Y.Yang, H.Li, Q.Zhang, L.Gu, R.Liang, C.Tan. *Nature Commun.*, **13**, 3384 (2022); https://doi.org/10.1038/s41467-022-29831-2
249. Z.Dai, X.Xu, Z.Guo, K.Zheng, X.Z.Song, X.Qi, Z.Tan. *Mater. Sci. Eng. C*, **120**, 111666 (2021); https://doi.org/10.1016/j.msec.2020.111666

250. D.Jevapatarakul, J.T.-Thienprasert, S.Payungporn, T.Chavalit, A.Khamwut, N.P.T.-Thienprasert. *Biomed. Pharmacotherapy*, **130**, 110552 (2020); https://doi.org/10.1016/j.biopha.2020.110552
251. X.Ji, L.Ge, C.Liu, Z.Tang, Y.Xiao, W.Chen, Z.Lei, W.Gao, S.Blake, D.De, B.Shi, X.Zeng, N.Kong, X.Zhang, W.Tao. *Nature Commun.*, **12**, 1124 (2021); https://doi.org/10.1038/s41467-021-21436-5
252. L.Wang, B.Zhang, X.Yang, S.Guo, G.I.N.Waterhouse, G.Song, S.Guan, A.Liu, L.Cheng, S.Zhou. *Bioact. Mater.*, **20**, 126 (2023); https://doi.org/10.1016/j.bioactmat.2022.04.009
253. S.Wilhelm, A.J.Tavares, Q.Dai, S.Ohta, J.Audet, H.F.Dvorak, W.C.W.Chan. *Nature Rev. Mater.*, **1**, 16014 (2016); https://doi.org/10.1038/natrevmats.2016.74
254. G.Korotcenkov. *Nanomaterials*, **10**, 1 (2020); https://doi.org/10.3390/nano10071392
255. T.Li, W.Yin, S.Gao, Y.Sun, P.Xu, S.Wu, H.Kong, G.Yang, G.Wei. *Nanomaterials*, **12**, 982 (2022); https://doi.org/10.3390/nano12060982
256. R.Hinterding, A.Feldhoff. *Z.Phys. Chem.*, **233**, 117 (2019); https://doi.org/10.1515/zpch-2018-1125
257. S.A.Zakaria, S.H.Ahmadi, M.H.Amini. *Sens. Actuators, A*, **346**, 113827 (2022); https://doi.org/10.1016/j.sna.2022.113827
258. C.Zhao, H.Gong, G.Niu, F.Wang. *Sens. Actuators, B*, **324**, 128745 (2020); https://doi.org/10.1016/j.snb.2020.128745
259. R.B.Shinde, N.S.Padalkar, S.V.Sadavar, A.S.Patil, S.B.Kale, V.V.Magdum, Y.M.Chitare, S.P.Kulkarni, U.M.Patil, V.G.Parale, J.L.Gunjakar. *Mater. Today Chem.*, **24**, 100801 (2022); https://doi.org/10.1016/j.mtchem.2022.100801
260. Y.Han, Y.Liu, C.Su, X.Chen, B.Li, W.Jiang, M.Zeng, N.Hu, Y.Su, Z.Zhou, Z.G.Zhu, Z.Yang. *ACS Appl. Nano Mater.*, **4**, 1626 (2021); https://doi.org/10.1021/acsanm.0c03094
261. S.Zhang, P.Song, Y.Zheng, Y.Ding, Q.Wang. *J. Alloys Compd.*, **925**, 166663 (2022); https://doi.org/10.1016/j.jallcom.2022.166663
262. X.Li, H.Yang, X.Hu, Q.Wu, W.Xiong, Z.Qin, C.Xie, D.Zeng. *J. Hazard. Mater.*, **429**, 128270 (2022); https://doi.org/10.1016/j.jhazmat.2022.128270
263. W.Liu, D.Wei, X.Zhao, F.Xiao, C.Yang. *Appl. Surf. Sci.*, **602**, 154301 (2022); https://doi.org/10.1016/j.apsusc.2022.154301
264. M.Lv, S.Luo, Y.Tian, C.Lin, L.Jiang, L.Li, K.Shi. *New J. Chem.*, **46**, 11510 (2022); https://doi.org/10.1039/D2NJ01470J
265. T.Naseem, T.Durrani. *Environ. Chem. Ecotoxicol.*, **3**, 59 (2021); https://doi.org/10.1016/j.enceco.2020.12.001
266. D.Ściezyńska, D.Bury, P.Marcinowski, J. Bogacki, M.Jakubczak, A.Jastrzębska. *Catalysts*, **12**, 358 (2022); https://doi.org/10.3390/catal12040358
267. M.Shamsayei, Y.Yamini, H.Asiabi. *Appl. Clay Sci.*, **188**, 105540 (2020); https://doi.org/10.1016/j.clay.2020.105540
268. A.Nait-Merzoug, O.Guellati, S.Djaber, N.Habib, A.Harat, J.El-Haskouri, D.Begin, M.Guerioune. *Appl. Sci.*, **11**, 8899 (2021); https://doi.org/10.3390/app11198899
269. D.B.Jiang, C.Jing, Y.Yuan, L.Feng, X.Liu, F.Dong, B.Dong, Y.X.Zhang. *J. Colloid Interface Sci.*, **540**, 398 (2019); https://doi.org/10.1016/j.jcis.2019.01.022
270. S.Li, J.Chen, S.Hu, H.Wang, W.Jiang, X.Chen. *Chem. Eng. J.*, **402**, 126165 (2020); https://doi.org/10.1016/j.amc.2021.126165
271. Y.Wu, X.Li, H.Zhao, F.Yao, J.Cao, Z.Chen, F.Ma, D.Wang, Q.Yang. *Chemosphere*, **287**, 132061 (2022); https://doi.org/10.1016/j.chemosphere.2021.132061
272. S.P.Filippov, A.B.Yaroslavtsev. *Russ. Chem. Rev.*, **90**, 627 (2021); https://doi.org/10.1070/RCR5014
273. B.Zhou, Y.Yang, Z.Liu, N.Wu, Y.Yan, Z.Wenhua, H.He, J.Du, Y.Zhang, Y.Zhou, Z.Zou. *Nanoscale*, **14**, 7538 (2022); https://doi.org/10.1039/D2NR01131J
274. Z.Zhou, N.Sun, B.Wang, Z.Han, S.Cao, D.Hu, T.Zhu, Q.Shen, W.Wei. *ChemSusChem*, **13**, 360 (2020); https://doi.org/10.1002/cssc.201902828
275. A.Hanif, M.Sun, S.Shang, Y.Tian, A.C.K.Yip, Y.S.Ok, I.K.M.Yu, D.C.W.Tsang, Q.Gu, J.Shang. *J. Hazard. Mater.*, **374**, 365 (2019); https://doi.org/10.1016/j.jhazmat.2019.04.049
276. G.Wu, X.Wu, X.Zhu, J.Xu, N.Bao. *ACS Nano*, **16**, 10130 (2022); https://doi.org/10.1021/acsnano.2c02841
277. C.Wang, L.Zhang, Z.Zhang, R.Zhao, D.Zhao, R.Ma, L.Yin. *Prog. Mater. Sci.*, **118**, 100763 (2021); https://doi.org/10.1016/j.pmatsci.2020.100763
278. N.R.Chodankar, H.D.Pham, A.K.Nanjundan, J.F.S.Fernando, K.Jayaramulu, D.Golberg, Y.-K.Han, D.P.Dubal. *Small*, **16**, 2002806 (2020); https://doi.org/10.1002/smll.202002806
279. J.J.Zhou, Q.Li, C.Chen, Y.L.Li, K.Tao, L.Han. *Chem. Eng. J.*, **350**, 551 (2018); https://doi.org/10.1016/j.cej.2018.06.023
280. X.Yi, H.Sun, N.Robertson, C.Kirk. *Sustain. Energy Fuels*, **5**, 5236 (2021); https://doi.org/10.1039/D1SE01036K
281. Y.Zhu, C.Cao, S.Tao, W.Chu, Z.Wu, Y.Li. *Sci. Rep.*, **4**, 5787 (2014); https://doi.org/10.1038/srep05787
282. D.Su, X.Xie, S.Dou, G.Wang. *Sci. Rep.*, **4**, 5753 (2014); https://doi.org/10.1038/srep05753
283. Y.M.Volfkovich. *Russ. Chem. Rev.*, **91**, RCR5044 (2022); https://doi.org/10.1070/RCR5044
284. Y.Meng, D.Yu, Y.Teng, H.Qi, X.Liu, Y.Wu, X.Zhao, X.Liu. *J. Energy Storage*, **29**, 101195 (2020); https://doi.org/10.1016/j.est.2020.101195
285. M.Wang, Y.Feng, Y.Zhang, S.Li, M.Wu, L.Xue, J. Zhao, W.Zhang, M.Ge, Y.Lai, J. Mi. *Appl. Surf. Sci.*, **596**, 153582 (2022); https://doi.org/10.1016/j.apsusc.2022.153582
286. W.H.Low, P.S.Khiew, S.S.Lim, C.W.Siong, E.R.Ezeigwe. *J. Alloys Compd.*, **775**, 1324 (2019); https://doi.org/10.1016/j.jallcom.2018.10.102
287. F.Zhang, W.Zhang, D.Wexler, Z.Guo. *Adv. Mater.*, **34**, e2107965 (2022); https://doi.org/10.1002/adma.202107965
288. Y.Gao, Z.Pan, J.Sun, Z.Liu, J.Wang. *Nano-Micro Lett.*, **14**, 94 (2022); https://doi.org/10.1007/s40820-022-00844-2
289. J.Shin, J.Lee, Y.Park, J.W.Choi. *Chem. Sci.*, **11**, 2028 (2020); https://doi.org/10.1039/D0SC00022A
290. G.Zampardi, F.La Mantia. *Nature Commun.*, **13**, 687 (2022); https://doi.org/10.1038/s41467-022-28381-x
291. J.Li, W.Zhang, W.Zheng. *Energy Storage Mater.*, **53**, 646 (2022); https://doi.org/10.1016/j.ensm.2022.09.017
292. L.Wang, K.Takada, A.Kajiyama, M.Onoda, Y.Michiue, L.Zhang, M.Watanabe, T.Sasaki. *Chem. Mater.*, **15**, 4508 (2003); https://doi.org/10.1021/cm0217809
293. Y.Kadoma, Y.Uchimoto, M.Wakihara. *J. Phys. Chem. B*, **110**, 174 (2006); https://doi.org/10.1021/jp053854k
294. S.M.Xu, T.Pan, Y.B.Dou, H.Yan, S.T.Zhang, F.Y.Ning, W.Y.Shi, M.Wei. *J. Phys. Chem. C*, **119**, 18823 (2015); https://doi.org/10.1021/acs.jpcc.5b01819
295. M.Zhou, X.W.Lou, Y.Xie. *Nano Today*, **8**, 598 (2013); https://doi.org/10.1016/j.nantod.2013.12.002
296. F.Haque, T.Daeneke, K.Kalantar-zadeh, J.Z.Ou. *Nano-Micro Lett.*, **10**, 23 (2018); https://doi.org/10.1007/s40820-017-0176-y
297. H.Wang, T.You, W.Shi, J.Li, L.Guo. *J. Phys. Chem. C*, **116**, 6490 (2012); https://doi.org/10.1021/jp212303q
298. J.Ke, F.He, H.Wu, S.Lyu, J.Liu, B.Yang, Z.Li, Q.Zhang, J.Chen, L.Lei, Y.Hou, K.Ostrikov. *Nano-Micro Lett.*, **13**, 24 (2021); https://doi.org/10.1007/s40820-020-00545-8
299. W.Qian, S.Xu, X.Zhang, C.Li, W.Yang, C.R.Bowen, Y.Yang. *Nano-Micro Lett.*, **13**, 156 (2021); https://doi.org/10.1007/s40820-021-00607-5
300. H.Xu, S.Ouyang, P.Li, T.Kako, J. Ye. *ACS Appl. Mater. Interfaces*, **5**, 1348 (2013); https://doi.org/10.1021/am302631b
301. X.Chen, Y.Zhou, Q.Liu, Z.Li, J.Liu, Z.Zou. *ACS Appl. Mater. Interfaces*, **4**, 3372 (2012); https://doi.org/10.1021/am300661s
302. J.Huang, L.Xiao, X.Yang. *Mater. Res. Bull.*, **48**, 2782 (2013); https://doi.org/10.1016/j.materresbull.2013.04.022

303. F.Li, X.Liu, Q.Zhang, T.Kong, H.Jin. *Cryst. Res. Technol.*, **47**, 1140 (2012); https://doi.org/10.1002/crat.201200143
304. Y.Miao, H.Zhang, S.Yuan, Z.Jiao, X.Zhu. *J. Colloid Interface Sci.*, **462**, 9 (2016); https://doi.org/10.1016/j.jcis.2015.09.064
305. X.Zhao, F.Lou, M.Li, X.Lou, Z.Li, J.Zhou. *Ceram. Int.*, **40**, 5507 (2014); https://doi.org/10.1016/j.ceramint.2013.10.140
306. V.V.Kumar, K.Gayathri, S.P.Anthony. *Mater. Res. Bull.*, **76**, 147 (2016); https://doi.org/10.1016/j.materresbull.2015.12.016
307. T.Puangpetch, S.Chavadej, T.Sreethawong. *Powder Technol.*, **208**, 37 (2011); https://doi.org/10.1016/j.powtec.2010.11.039
308. X.Zou, Y.Zhang. *Chem. Soc. Rev.*, **44**, 5148 (2015); https://doi.org/10.1039/C4CS00448E
309. V.Tolstoy, M.Kaneva, N.Fedotova, A.Levshakova. *Ceram. Int.*, **46**, 20122 (2020); https://doi.org/10.1016/j.ceramint.2020.05.087
310. P.M.Bodhankar, P.B.Sarawade, G.Singh, A.Vinu, D.S.Dhawale. *J. Mater. Chem. A*, **9**, 3180 (2021); https://doi.org/10.1039/D0TA10712C
311. X.Xiong, Z.Cai, D.Zhou, G.Zhang, Q.Zhang, Y.Jia, X.Duan, Q.Xie, S.Lai, T.Xie, Y.Li, X.Sun, X.Duan. *Sci. China Mater.*, **61**, 939 (2018); https://doi.org/10.1007/s40843-017-9214-9
312. X.X.Jiang, J.Y.Xue, Z.Y.Zhao, C.Li, F.L.Li, C.Cao, Z.Niu, H.W.Gu, J.P.Lang. *RSC Adv.*, **10**, 12145 (2020); https://doi.org/10.1039/D0RA00845A
313. P.Li, X.Duan, Y.Kuang, Y.Li, G.Zhang, W.Liu, X.Sun. *Adv. Energy Mater.*, **8**, 1703341 (2018); https://doi.org/10.1002/aenm.201703341
314. Z.Cai, D.Zhou, M.Wang, S.M.Bak, Y.Wu, Z.Wu, Y.Tian, X.Xiong, Y.Li, W.Liu, S.Siahrostami, Y.Kuang, X.Q.Yang, H.Duan, Z.Feng, H.Wang, X.Sun. *Angew. Chem. Int. Ed.*, **57**, 9392 (2018); https://doi.org/10.1002/anie.201804881
315. D.Zhou, Z.Cai, Y.Jia, X.Xiong, Q.Xie, S.Wang, Y.Zhang, W.Liu, H.Duan, X.Sun. *Nanoscale Horiz.*, **3**, 532 (2018); https://doi.org/10.1039/C8NH00121A
316. X.Long, J.Li, S.Xiao, K.Yan, Z.Wang, H.Chen, S.Yang. *Angew. Chem. Int. Ed.*, **53**, 7584 (2014); https://doi.org/10.1002/anie.201402822
317. J.Li, R.Lian, J.Wang, S.He, S.P.Jiang, Z.Rui. *Electrochim. Acta*, **331**, 135395 (2020); https://doi.org/10.1016/j.electacta.2019.135395